Time-evolution of Partial Discharge Characteristics of XLPE MV Cable Termination Defects

Elizabeth NN Haikali

Student Number: 1055231

A dissertation submitted to the Faculty of Engineering and the Built Environment,

School of Electrical and Information Engineering,

University of the Witwatersrand, Johannesburg, in fulfilment of the requirements for

the degree of Master of Science in Engineering.

03 August 2018

Declaration of Authorship

I, Elizabeth NN Haikali, declare that this dissertation titled, *"Time-evolution of Partial Discharge Characteristics of XLPE MV Cable Termination Defects"* is my own unaided work, excluding where otherwise duly acknowledged. It is being submitted to the University of the Witwatersrand, Johannesburg, for the degree of Master of Science in Engineering. I also declare that this dissertation has not been submitted before to any other university for the award of any degree.

Signed: ____________________

Date: ____________________

Acknowledgement

Firstly I would like to acknowledge and thank GOD my creator for all that I am and have achieved thus far. Further I would like to thank my supervisor, Prof Cuthbert Nyamupangedengu for his commitment to support my development. I am thankful to NamPower (Ltd) who has covered all my tertiary costs since day 1 as an undergraduate up to my postgraduate level. Gratitude goes to my family, especially my beloved mother, for solely selflessly serving me and my siblings to have better opportunities than that which she had and at the same time instilling in us compassion towards humanity. I also acknowledge my late Father who passed not long after our re-union and the beginning of my masters, for cheering me on to embark on my masters, may his soul continue to rest in peace, I miss you deeply.

Abstract

Power cable terminations and joints experience high electrical stress due to the abrupt change in geometry of the cable; hence the insulation at these points is more prone to partial discharges and has been reported as the main root cause of power cable system failures. Electrical failure of the insulation is known to occur due to a phenomenon of Partial Discharges (PD). Modern practice (especially in higher voltage installations) entails installation of PD sensors at strategic locations during installation of electrical equipment such as cable joints and terminations. This enables continuous monitoring of PD events in the plant, and this is termed on-line PD diagnosis. However, with limited knowledge to interpret the meaning of certain PD changes during the service period, this practice remains limited. It is therefore the interest of the study to understand the time evolution behaviour of PD characteristics in order to discern the insulation condition or deteriorating stages.

The present study is on XLPE power cables, focusing on PD in artificial defects in the cable termination insulation that in most cases arise from poor workmanship. The power cables were subjected to accelerated ageing to emulate their ageing under service conditions. PD measurements were then conducted at periodic time intervals and characterized PD in terms of PD Inception Voltage (PDIV), maximum apparent PD magnitude (Q_{max}), Pulse Repetition Rate (PRR) and Phase-Resolved-Partial-Discharge-Pattern (PRPDP). The findings are that, Q_{max}, PRR and PDIV did not show any time-evolution trends unique to a defect, the general trends observed were that of a fairly constant PDIV with several fluctuations of a 5 kV band. Q_{max} showed a decreasing trend over ageing time. The PRR decreased overall, with a pick up increase near the end of the tests. Q_{max} and PRR were noted significantly fluctuative between 23% and 57% of the total ageing period, distinct characteristics were that, the tram line had the largest PRR which is expected since it is a flat cavity, and

the PRPDP appeared more skewed than other defects. The semicon feather had a PRPDP that seemed like a combination of a void discharge and corona discharge. The ring cut PRPDP was similar to that of the tram line except that it was not skewed. Furthermore, a capacitance PD model was constructed in Matlab® Simulink® to emulate experimental observed PD behaviour and therefore confirm the theory explaining the observed time-dependency of PD phenomena. Simulated void discharge PRPDP which corresponded with experimentally measured PRPDP were obtained for the unaged, moderately aged and severely aged cavity defect. The corona-surface discharge effect observed in the semicon PRPDP was also successfully emulated.

The study outcomes suggest that PD characteristics evolve over time, and that the behaviour of the observed trend is unique at different stages during ageing. The time evolution characteristics of PD are The PRPDP signatures did not change with time of ageing despite the variations in Q_{max} and PRR. This means that, defect signatures obtained prior ageing or in-service operation of the cables can still serve as a good reference of identifying the nature of the defect at different ageing stages except in the event of PD evanescence. From the simulations, it was derived that the PD region surface conductivity as well as the geometry of the defect are the main contributing factors to the unique signatures observed at different stages and per defect.

Contents

List of Figures

List of Tables

List of Acronyms and Abbreviations

$\mathbf{E}_o$	Applied electric field
$\mathbf{E}_{net}$	Total electric field across the PD site
$\mathbf{E}_{res(-)}$	Electric field due to residual charge from the negative half cycle
$\mathbf{E}_{res(+)}$	Electric field due to residual charge from the positive half cycle
HV	High Voltage
HFCT	High Frequency Current Transformer
MV	Medium Voltage
pC	pico Coulomb
PD	Partial Discharges
PDEV	Partial Discharge Extinction Voltage
PDIV	Partial Discharge Inception Voltage
PRR	Pulse Repetition Rate
PRPDP	Phase Resolved Partial Discharge Pattern
TEAM	Thermal Electrical Ambient Mechanical Stress
Q_{max}	Maximum Apparent Partial Discharge Magnitude
$\mathbf{U}_o$	Nominal phase voltage
UV	Ultra Violet rays
VHF	Very High Frequency

VLF Very Low Frequency

XLPE Cross Linked Polyethelyne

OIP Oil Impregnated Paper

HMWPE High Molecular Weight Polyethylene

EPR Ethylene Propylene Rubber

PVC Polyvinyl Chloride

TR-XLPE Tree-Retardant Crosslinked Polyethylene

List of Publications

1. E. Haikali, C. Nyamupangedengu, "Partial Discharges the 'Cancer' of Power Cables", in *ESI Africa Power Journal*, Issue 4, 2016, pp.16-21.

2. E. Haikali, C. Nyamupangedengu, "PD Evolution of Artificial Defects Introduced in MV XLPE Power Cable Terminations - Preliminary Results", in *Southern African Universities Power Engineering Conference Proceedings (SAUPEC 2018)*, Stellenbosch, January 2017, pp.141-146.

3. E. Haikali, C. Nyamupangedengu, "The Unique PD 'Signatures' of Artificial Installation Defects Introduced in MV XLPE Power Cable Terminations", in *Southern African Universities Power Engineering Conference Proceedings (SAUPEC 2017)*, Wits University, Johannesburg, January 2018, pp.198-203.

Chapter 1

INTRODUCTION

This chapter introduces the purpose of the study and research questions. A background review and a further emphasis are given on the relevance of the work at hand and the anticipated outcomes.

1.1 Background

Underground power cables are a preferred alternative for establishment of distribution networks as opposed to overhead power lines for various reasons. Overhead lines pose safety and environmental hazards especially in congested areas. According to the literature such as Bartnikas [1] and Thue [2], the main problems encountered that influence the evolution of power cable technology include the following: high dielectric losses, over-heating, partial discharges, water treeing and electrical treeing. This study looks into the problem of Partial Discharges (PD).

A PD is a discharge event that manifests as a micro-spark partially bridging the gap in between two electrodes. The sources of PD in the insulation are protrusions, air voids, impurities and non-uniformity in the insulation. A progressive discharge event may result in the degradation of the insulation and later a direct bridging of the electrodes that are supposed to be insulated from each other. A detailed review on PD diagnosis technology is presented in Chapter 2. PD diagnosis technology has been recognised as an effective insulation condition assessment method [3, 4]. Therefore, before dispatch from the manufacturer, power cables undergo factory acceptance tests to ensure that the cables meet the design requirements. Cables are subjected to test voltages that are above the operating level to simulate abnormal over voltage conditions. Medium Voltage (MV) cables that show PD activity above 5 pC at $1.73U_o$ are condemned according to the SANS 1339 standard [5].

1.2 Motivation of the Study

Despite the dispatch of high integrity cables from the factory, through transportation, handling and installation, these cables may lose a certain level of their integrity. An after-installation test is conducted prior to commissioning in order to test the workmanship. Most importantly in power cables, cable accessories are often constructed on site and are therefore known to be the weakest part of cable systems [6–8]. It has been reported in the literature that solid extruded insulated cables may pass the MV withstand test, despite showing significant PD activity [9]. However, this is an unacceptable condition as PDs lead to deterioration of the insulation and failure over time [10]. For this reason, the presence of PD in the insulation is undesirable and therefore PD diagnosis prominently forms part of power cable condition assessment.

Previously, PD assessment was conducted by well experienced personnel who would discern between different types of PD conditions. Diagnosis was then made in terms of the possible source simply by focusing on the PD pulse characteristics such as PD density, magnitude and phase angle of occurrence [10]. The PD recognition skill came with years of experience as personnel had more encounters with PDs; hence not sustainable for the next person to use. However, due to the importance of PD diagnosis, there has been significant work in the field. On-line monitoring of PD activity has become a common practice [11], but may not be fully used due to the shortfalls in the knowledge of how to co-relate PD signal evolution trends with defect ageing process. The extensive research work that has accumulated to-date in the PD knowledge domain has enhanced knowledge of PD mechanisms and unique PD signatures that would aid more personnel with diagnosis. The various findings in literature can then be grouped to create an extensive database for reference purposes when analysing PD patterns. The problem motivating this research is presented in the next section.

1.3 Problem Statement

There is a lack of knowledge in co-relating PD time-evolution behaviour to insulation degradation severity especially for specific typical MV XLPE cable termination installation defects. The consequences to this lack of knowledge include inadequately informed maintenance decisions especially those related to the on-line monitoring and condition-based maintenance philosophy. The problem can be tackled by conducting a study to answer the questions stated in the next section.

1.4 Research Questions

The work aims to answer the following questions.

- What are the time-evolution characteristics of PDs in typical installation defects in MV XLPE cable terminations?

- What is the explanation of the experimentally observed time-evolution behaviour of the PD and how can the mechanisms be validated through modelling?

1.5 Research Objectives

The study seeks for the understanding of the underlying PD mechanisms in specific types of power cable termination defects as a function of ageing time. An experimental method was designed that aged power cable terminations and monitored PD as it aged. In addition, a PD model was implemented in MATLAB® Simulink® to further analyse the factors influencing the experimentally observed PRPDP.

1.6 The Dissertation Structure

Chapter 2: This chapter presents a review of power cable technology, focusing on the different types of insulation and power cable structure development that led to extruded solid dielectric technology of interest. Thereafter, a brief discussion on the challenges faced with solid dielectric cables is presented.

Chapter 4: In this chapter, the laboratory experiment methodology of the study is presented. This includes the test circuits and procedures followed for the PD induced accelerated ageing and PD measurements conducted.

Chapter 5: The experimental results obtained are presented and discussed. The results are analysed focusing on the evolution trend of PDIV, Q_{max}, PRR and PRPDP. The observed effect of defect severity is also discussed here. Defect unique PRPDP are also analysed and presented in this chapter.

Chapter 6: Simulations are conducted to validate the phenomenological models used to explain the measured PD behaviour. Factors contributing to PD ageing are identified and an algorithm is developed and implemented in Matlab® to re-produce PRPDP similar to those obtained from experimental measurements.

Chapter 7: Finally the study findings are summarised, concluded and future recommendations for further work is presented.

1.7 Conclusion

In this chapter, the motivation of the study has been presented. A database of continuously monitored PD in different defect types would serve the purpose of supporting on-line condition monitoring of PD in electrical equipment. The benefit would be more informed maintenance decisions, and therefore effective utilization and sustainability of the modernized approach to electrical equipment condition monitoring. This benefit can translate into fewer unforeseen outages and reduced maintenance costs. The study is therefore interested in identifying evolution of PD parameter trends with ageing time, and to attempt to understand the underlying PD mechanism by making use of a PD model. The following chapter sets the scene by providing a background to the type of power cable of interest in the present study and the challenges faced amongst which PD is the main contributing factor to the failure of extruded solid dielectrics.

Chapter 2

ELECTRICAL CABLE INSULATION TECHNOLOGY - A LITERATURE REVIEW

The evolution in power cable technology is presented, and the main problems encountered that compromised performance and therefore led to better developments are highlighted. The insulation degradation phenomena of interest, that is Partial Discharges, is introduced.

2.1 Evolution of Power Cable Insulation Technologies

A typical conventional power system is comprised of the generating station(s), the transmission and distribution system. The generating station generates power using either steam turbines, hydro turbines or renewables. The transmission system then steps up the voltage to reduce losses and transmits power across long distances to load centres. The distribution system steps down the voltage to lower levels and connect the consumers. Following the invention of incandescent bulbs by Thomas Edison in the 1880's, there was a need to supply power to consumers who were mostly domestic households for lighting purposes [1]. This was initially carried out using overhead lines. However, due to the increasing number of connections as urbanisation grew, there was a congestion of overhead lines which posed a safety hazard to the public and disrupted the aesthetics. Underground cables were then introduced as an alternative means of transferring power to consumers with little or no environmental impacts as opposed to overhead lines. A brief investigation of the history of challenges encountered with power cables was conducted in order to understand the problems concerning power cables and the evolution trend.

The power cable technology was an advancement to the earlier low current communication cables used in telegraphy lines and wiring of mine blasting explosives [1,2]. The design modifications were mainly in the insulation thickness, the type and size of the conductor in order to accommodate more power transfer without overheating. One of the first power cables by Thomas Edison had a simple structure, basically a copper conductor enclosed in a duct with glass or porcelain insulating it from ground as shown in Figure 2.1. The rest of the space was filled up with bitumen as the insulation [2]. Several other insulation materials were later introduced such as gutta-percha, lead, vulcanised rubber, mineral oil impregnated paper, varnished cambric, gas and solid extruded dielectrics. The following power cable evolution history is discussed according to literature from Barnikas [1] and Thue [2].

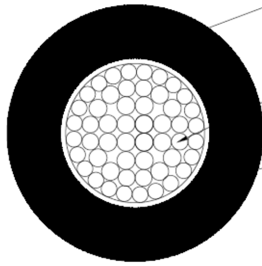

Figure 2.1: The first generation of power cables by Thomas Edison [1]

2.1.1 Oil Impregnated Paper Insulation

Gutta-percha insulated cables suffered failure in the 1840's due to oxidation and softening at high temperatures. Likewise, bituminous filled iron pipes proved costly and suffered high losses due to the poor heat capacity of bitumen. Oil Impregnated Paper (OIP) shown in Figure 2.2 were invented by Ferranti in the 1890's, their performance surpassed that of their predecessors. Several types of impregnants used were paraffin and resin based oil. Apart from their superiority, the insulation suffered ionization due to the non-uniform stress distribution in three core cables rated above 35 kV. This problem was addressed by wrapping a conductive tape around each conductor to create a smoother surface and establish a common potential between the cores. Another conductive belt was added to enhance cable cohesiveness and maintain individual core shields at the same potential to reduce leakage currents.

With further uprating of the cable ratings, the oil expanded and contracted with changes in cable loading. As a result, voids developed in the insulation, causing partial discharges that degraded the insulation. In response to this problem, lower viscosity oil was used as an impregnant and oil reservoir tanks were connected at cable ends to cater for conditions when the oil expanded or contracted. Further improvements included the use of oil pressure that is above atmospheric pressure to prevent moisture entrance and inception or ionization of voids. The pressure was maintained by oil pressurized tanks or gas tanks connected at cable ends.

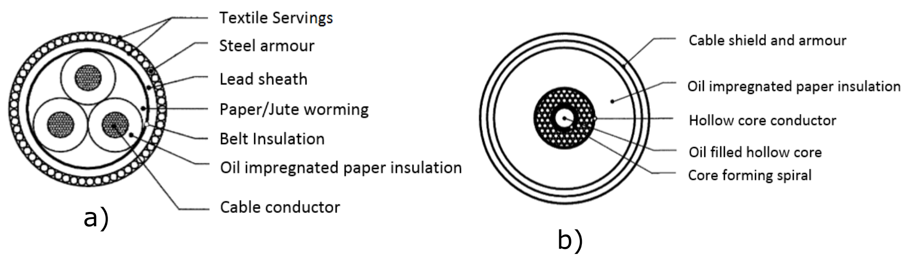

Figure 2.2: Oil Impregnated cables, a) belted cable, b) hollow conductor cable [1]

Due to overheating that resulted in high dielectric losses in OIP cables, hollow duct cores filled with pressurised oil were introduced. Forced cooling methods were used such as oil circulation to evenly distribute heat and avoid hot spots. Direct cooling methods were also used by circulating water in tubes located near the conductors. Despite these measures, high dielectric losses remained a challenge with impregnated paper cable insulation technology.

2.1.2 Rubber Insulated Cables

Distribution systems required cables to be flexible for ease in route manoeuvring; hence rubber was explored as an alternative insulation material in the 1950's. Butyl rubber was developed and gave good resistance to Partial Discharges (PD), chemical, oxidation and Ultra Violet rays (UV) penetration. However, a thicker insulation layer was required than that of OIP of the same rating. Butyl rubber also flowed at high operating temperature above 148 ^oC. Rubber cables were then restricted to applications where flexibility was a main requirement [1]. Varnished cambric cables were introduced in the early 1920's, however did not gain popularity due to the costly treatment process that removes moisture from the insulation. Later improvements to varnished cambric added asbestos shields. Nevertheless, OIP remained superior to other cable types.

2.1.3 Solid Dielectric Insulated Power Cables

Due to the high dielectric losses in the OIP, an alternative was to obtain an insulation material with lower dielectric losses. Polypropylene paper was an option, but due to its swelling and bending, it could not be impregnated successfully to prevent void formation. Pipe type cables were highly reliable at high operating voltages, but the system required more maintenance of the pressure and cooling system, and posed a hazard to the environment in case of a leakage. Most importantly, more specialised skills were required to properly splice and terminate the cables. The direct cooling method which helped decrease the dielectric losses meant that large amounts of water would be drained off in order to carry out repairs or maintenance. For these reasons, the search for a better insulation material continued, and this lead to the discovery of Polyethylene in the 1975 [1].

Solid extruded cables were made from low density linear polyethylene and were preferred over other insulation types due to their lower dielectric losses and lower capacitive charging currents than OIP. High Molecular Weight Polyethylene (HMWPE) had better behaviour at high temperature, good resistance to moisture, better electrical properties; hence used as a replacement for butyl rubber cables. Ethylene Propylene Rubber (EPR) was later manufactured in the 1960's, and behaved better than HMWPE in terms of mechanical strength, resistance to UV radiation and higher operating temperature ranges. The insulation temperature operating range was improved by curing

PE through vulcanization process giving birth to Cross Linked Polyethelyne (XLPE). XLPE was less flexible than EPR, but gave lower dielectric losses, higher operating temperature range and better resistance to discharges.

In the 1970's solid dielectric cables suffered a common failure caused by partial discharges, water and electrical treeing [1]. One of the factors identified to be the cause of void development in the insulation was the random change in cable temperature with load changes. More strict measures were employed in the manufacturing process to ensure that the insulation was free from impurities and the insulation was uniform by ensuring that the cross linking agent was evenly distributed during curing. Water trees were investigated and were understood to be enhanced by the presence of moisture or impurities in the insulation. The use of steam during curing was then stopped; a dry curing process was used instead. Additionally, metallic sheaths, neoprene jacket over EPR and Polyvinyl Chloride (PVC) over XLPE were introduced to prevent water from entering the insulation.

Other challenges experienced were failure in cable joints of the XLPE insulated cables. In response, improved uniform insulation shield that could be stripped off with ease were introduced for proper cable splicing and termination. These semi-conducting screens were simultaneously extruded together with the insulation on to the conductor core to minimize the chance of micro cavities. A tree retarding compound was added to XLPE producing Tree-Retardant Crosslinked Polyethylene (TR-XLPE). Figure 2.4 shows an XLPE cable whose PD behaviour due to installation defects will be investigated and discussed in the chapters to follow.

The evolution of power cable insulation and structure is summarised in Figure 2.3.

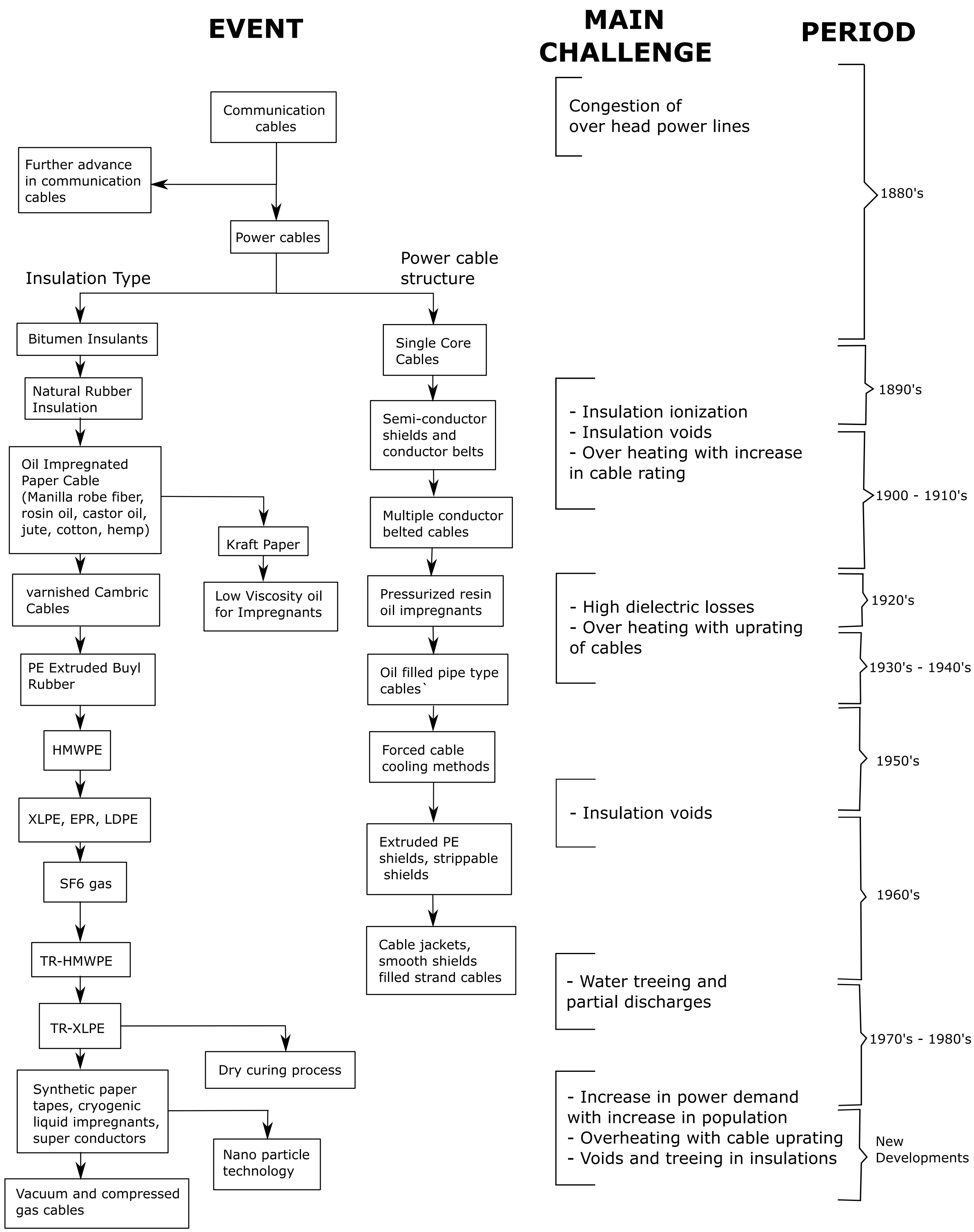

Figure 2.3: The Evolution of Power Cable Insulation and Structure

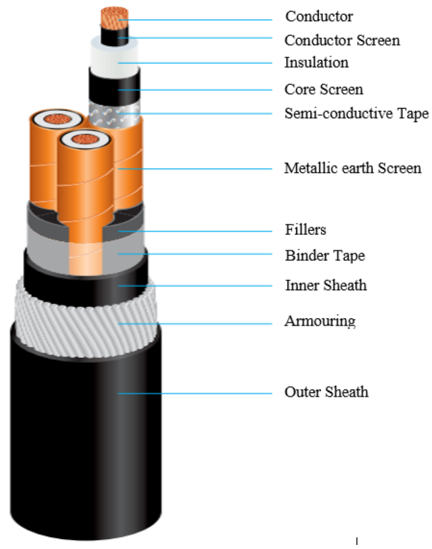

Figure 2.4: Structure of XLPE Cable
[12]

2.1.4 A Common Challenge with XLPE Power Cables

As discussed in the sections above, XLPE insulation eventually became the most preferred power cable insulation technology. However, high dielectric losses, insulation ionization, water and electrical treeing generally make up the biggest concern with the performance of all solid extruded insulated power cables. The challenges mentioned eventually line up to a common effect on the performance of the insulation. The significant presence of either reduces the electrical field strength of the insulation; hence the insulation breakdown strength is likely to be exceeded even at operating voltage. This manifests in a form of local insulation breakdown, or in a more severe condition, a power cable failure as the electrodes are short circuited. In this process the insulation affected looses its characteristics of an isolator, and becomes a conductive channel. The degradation of the XLPE due to these types of breakdowns form the basis of this work and it is discussed further in the next section.

2.2 Partial Discharges (PD)

Partial Discharges (PD) is defined as a breakdown of an insulation in a discharge event resulting in the partial bridging of the electrodes [13]. It is also defined by Stone in [14] as micro electrical sparks due to the arc breakdown of the gas in the void or in a region with a non-uniform electric field. In the presence of a seed electron, and if the electrical strength of the insulation region is exceeded, a partial discharge occurs. The seed electron can be generated from the ionization of the gas in the medium by natural background radiation (volume generation) or the liberation of electrons deposited on the insulation surface by the previous discharge (surface emission) [15]. However, since the power cable insulation is enclosed, the effect of the natural background radiation in providing the seed electron is less pronounced [16,17]. After repetitive continuous PD, the insulation breakdown strength may degrade and eventually insulation failure may occur which in cables is the bridging between cable cores or between a cable core and ground [4]. The typical causes of PD in power cables are identified as the presence of contaminants in the insulation, bad workmanship during cable accessory installation which includes cuts in the insulation and dirt contamination [4].

2.2.1 Types of PD

There are different forms of partial discharges based on the discharge location. Void PDs are partial discharges occurring within the insulation or at the insulation and electrode interface in air filled cavities or fissures. Cavities, impurities and gas bubbles are the common causes of void discharges [18]. Another form is surface discharges that occur on the outside surface of the insulation. Corona discharges are discharges that occur within an air medium not bounded by insulation. The conditions required for the discharge event and the discharge phenomena are similar for void, surface and corona discharges. Fortunately, for diagnostic purposes however, their characteristic behaviour tends to differ, due to the difference in the nature of the discharge site [19]. This allows for one to discern them for diagnosis purposes.

2.2.2 Effect of PD on Power Cable Insulation

When a seed electron is in the presence of an electric field exceeding the local breakdown strength of the local region, avalanches develop through impact ionization and photo-ionization. The avalanches generate hot energetic electrons, regarded as electrons with an energy level above 8 eV [20]. When these hot electrons bombard the solid insulation surface, the insulation C-H polymeric molecular bonds are broken down, resulting in chemical degradation of the insulation [21]. Additionally, free radicals are produced that further weaken the polymer C-H bonds. The discharge event gives off acidic by-products, which tend to react with the insulation, further breaking down the molecular bonds. The severity of the damage is influenced by the concentration of hot electrons in the avalanches, the concentration of the acid by-products and of the reactive species. The degradation of the insulation will be further discussed in more detail in chapter 4. The rate at which the insulation degrades is affected by several factors such as, dielectric temperature, conducting current density, cavity geometry and the dielectric properties [22].

The breakdown strength of the local region in the insulation then decreases, making it the weakest link in the insulation. Breakdown therefore occurs locally at the defected region, however with prolonged PD activity; the low breakdown strength region may extend to a critical length and eventually lead to electrode bridging. The extension of the insulation degradation region occurs in a manner known as electrical treeing. The time taken to initiate electrical treeing is generally significantly longer than the time from the point of treeing to when the insulation fails [22, 23]. The following section discusses the phenomena of electrical treeing.

2.2.2.1 Insulation Breakdown due to Electrical Treeing

An electrical tree is a tree shaped network made up of several connected air filled micro tunnels that progress swiftly into the insulation and eventually inducing failure [24]. Electrical treeing can be a result of persistent PD activity in a certain location which eventually causes the insulation surface to erode, forming pits. The pits have been observed as the origin of treeing, other causes of treeing in an insulation are projecting objects in the insulation or contaminants that create an enhanced electric field region. Electrical treeing evolves in three stages namely the inception, propagation and failure stages as discussed by Dissado in [25]. During inception, in the case of a protruding object in the insulation, the tip changes polarity with the AC applied voltage. This results in a cyclic push and pull force as the electrons and positive ions are attracted and repelled during the positive and negative half cycles respectively. The constant back and forth movement of hot electrons and positive ions cause collision between the charged particles and between the charged particles and the insulation. After a prolonged bombardment, the insulation C-H bonds get broken, and deform the insulation, forming a micro-void in the insulation [24]. The UV radiation given off by the charge recombination process may break the C-H bonds as well, although this concept is still under debate [25].

During the propagation stage, the formed micro-void will enlarge with further charged particle collisions. When it reaches a certain size sufficient to sustain PD, discharges begin to occur and further degradation due to the PD by-products. In return, the gap increases and extends further towards the opposite electrode [26]. The growing and extending pattern is said to be largely stochastic and partly deterministic, overall it is difficult to presume its growth. Electrical trees develop in different structure forms at this stage namely bush trees, branch trees or a combination of both bush and branch electrical trees.

After the tree extends to a critical length or width, local insulation breakdown may occur which may eventually cause global insulation failure. Studies have not yet determined the critical length or width that may prompt complete failure. Certain PD characteristics can be used to diagnose treeing in an insulation, such as the Phase Resolved Partial Discharge Pattern (PRPDP) as discussed in [26].

2.2.3 PD Trend Monitoring

Partial Discharges are a reliable indication of the condition of the equipment insulation. The PD phenomena is a complex function of several factors, such as the type of insulation, type of defect, operating condition, period in service, which all play a role in influencing the conditions required for a discharge event to occur. It has been established in the literature that PD ages in several stages. PD therefore evolves as the repetitive discharge events continue to occur in the same region, meaning the initial identification of PD might not be similar after it has been going on for a time period. The evolution of PD therefore makes PD diagnosis tricky which if not well understood might lead to wrong maintenance decisions and therefore costly unplanned outages. The next section reviews the literature on PD detection technology in terms of monitoring the changes in PD with ageing.

2.3 Electrical PD Detection Methods

There are two main conditions in which PD of a test object can be measured. PD can be tested when the equipment under test is isolated from the system and supplied with a test voltage and it is called off-line PD detection method. Otherwise, PD can be measured while the equipment under test is in operation, this is called on-line PD detection, and is popular mainly because it requires no down time. Off-line PD tests can be conducted at Very Low Frequency (VLF), power frequency, resonance frequency or with damped oscillating wave form. Conventional off-line tests make use of high-frequency capacitors (coupling capacitor) to pass the high frequency PD signal and block the nominal frequency (50 Hz). Off-line PD testing may pick up PD that is not detected by on-line testing specifically when the cable has not been in service or exposed to system transients and also due to reduced noise interferences [27].

On-line PD detection methods use a high frequency sensor such as a High Frequency Current Transformer (HFCT) or capacitive probe to tap the high frequency PD pulse from the cable and feed it through an amplifier to an analyser such as a spectrum analyser [7]. On-line PD testing can be implemented in the frequency domain; hence more flexibility in selection of a frequency band with minimal noise interference which is quite handy in field applications. Furthermore, on-line testing allows a long cable length to be tested in sections, reducing the attenuation effect on measured PD signal. Due to these advantages, on-line PD testing seem a more favourable and convenient approach to field testing of cables. With new developments in the PD field, on-line PD detection is introduced for equipment condition monitoring. PD detectors are permanently installed at strategic locations such as cable joints and cable splices to continuously monitor PD levels from commissioning to the end of the life time of the cable [28]. Continuous PD information will inform the maintenance crew about the status of the cable insulation, and possibly make it easier to trace a worsening condition of a cable. Knowledge of the status of the insulation condition would then aid with maintenance scheduling, reduce unnecessary down time and reduce wastage unlike before where cables were more likely to be replaced immediately whenever PD is detected since the progressiveness of the condition could not be traced or referenced back to anything. On-line PD monitoring will only be a success if the manner of PD evolution as the equipment continues to operate is known or understood, in order for the measurements to be interpreted for informed decisions. The present work therefore studies the evolution of PD in three common termination defects, tested at operating frequency (50 Hz). A database of such trends is critical for on-line PD detection method to fulfil its purpose.

2.4 Summary and Conclusion

This chapter reviewed the evolution of power cable insulation technology time-line since its invention. The insulation type most used in modern MV installations is XLPE; hence the focus of this study. One of the main challenges faced with XLPE and other solid extruded insulations is PD-induced degradation phenomena that were discussed in the chapter. The PD phenomenon is further discussed in the published paper found in B. PD changes with time of continued PD activity. On-line PD monitoring methods have been developed to capture PD continuously while the equipment is in service. The inadequate knowledge of time-dependent PD trends is a hindrance in unlocking full potential of the on-line PD monitoring technologies. The next chapter therefore presents the laboratory based experiment where accelerated PD induced ageing was conducted and PD parameters were monitored over a time period to obtain an evolution trend.

Chapter 3

The Experimental Investigation: Laboratory Tests

This chapter presents the experimental methodology approach to realize the study objectives mentioned in the previous chapter which is to obtain an understanding of the PD time-evolution behaviour in artificial defects. In order to maintain the test time within a practically reasonable duration, the PD ageing rate was accelerated. Accelerated ageing was achieved by applying stress factors such as voltage and frequency. The PD measurement method is also presented.

3.1 Experimental Methodology

The previous chapter introduced the insulation deterioration phenomena known as Partial Discharge. This chapter presents the cable test samples used, the approach implemented to accelerate the effect of the partial discharge phenomena on the degradation of the insulation. This was done in order to maintain the ageing time within a reasonable time frame yet following literature experimental based recommendations that do not introduce ageing phenomena different from that experienced during actual in service life of a power cable. The PD parameters were then measured periodically off-line during the PD induced ageing period.

3.1.1 Test Samples Preparation

Power cable defects can come about as a result of manufacturing flaws, rough transportation and handling, poor workmanship during installation and ageing due to operating conditions [29]. For transportation ease, only a certain length of a power cable can be rolled on to cable drums. On installation, many lengths of power cable lengths therefore are spliced to make up the required length. Furthermore, the cable termination end has to be connected to equipment. Due to the abrupt change in the surface geometry at the cable joints and terminations, the electrical field distribution is non-uniform at this point as shown in Figure 3.1. High potential gradients tangentially concentrate at the end point boundary interface of the semiconductor screen and the insulation layer [6]. In order to control the enhanced electrical stress to levels below insulation and air breakdown strength, stress cones or tubes made from high permittivity material are used [6]. Due to the concentrated electric field distortions at these points, and their high susceptibility to installation defects, cable joints and terminations are most prone to PDs and failure than the rest of the power cable [6–8].

The study focusses on three types of artificial defects that commonly occur due to poor workmanship on cable terminations during installation namely: semicon feather, tram line and ring cut in the XLPE as illustrated in Table 3.1. The samples were prepared in a previous study by Fynes-Clinton [30]. Before the defects were deliberately introduced on the cable ends, the cables and terminations underwent PD tests to ensure that they were free of PD at $2U_o$.

Table 3.1: Artificial Defects in cable terminations [31]

Defect Type	Description	Schematic
Semicon feather	The outer semi-conductor screen was not uniformly stripped from the XLPE surface, a triangular shape leaf of the screen as shown was left extending over part of the XLPE insulation creating a high field concentration point. The triangular semi-conductor screen feather dimensions on the two cores have a base of 10 mm, and a perpendicular height of 10 mm. The leaf was made longer on the third core for increased severity, with dimensions of 5 mm base, and 25 mm perpendicular height.	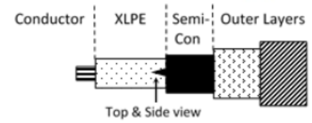 
Tram line cut	During installation, if ultimate care is not taken, especially if the semiconductor screen is stripped off with a sharp object, the XLPE insulation might suffer incisions. Such a kind of defect is represented by the tram line cut and the ring cut in the XLPE. For the tram line defect, the two cores are defected by a cut along the cable length of the dimensions (1 mm deep, 0.4 mm maximum thickness/width). The third core cut is 2 mm deep with a thickness of 0.8 mm.	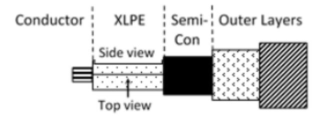 
Ring cut	The round circulating cut in the XLPE on the two cores was 1 mm deep and 0.6 mm thick. The third core cut was made 2 mm deep and 0.8 mm maximum thickness.	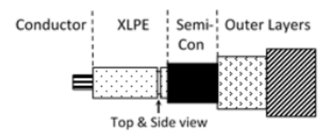 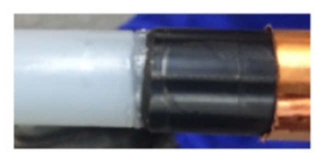

The tram line defect has a shape of a flat cavity because its longitudinal dimension is greater than the radial dimension with reference to the electrodes [32].

Three defected cables were used in the study, with one defect fabricated on one cable. On each cable length, two of the three sample cores were equally defected for reproducibility, meanwhile the defect on the third core was made more severe by increasing the defect dimensions as explained in Table 3.1. Due to their popularity in the industry, heat shrink terminations were used. The other end of each cable sample was terminated with defect-free heat shrink terminations.

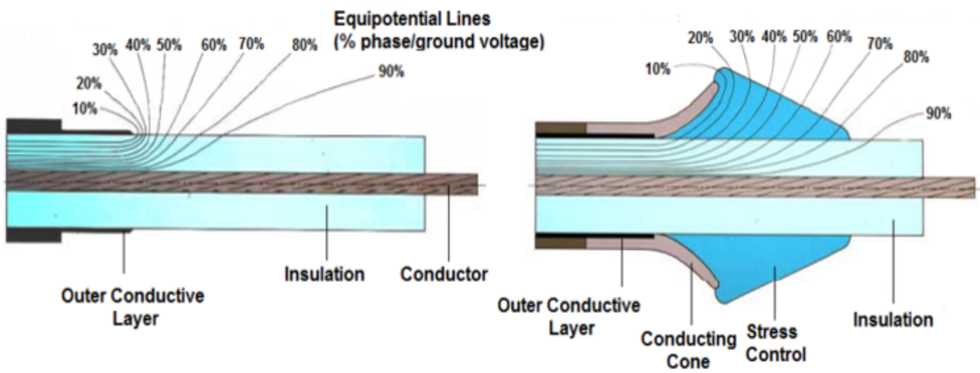

Figure 3.1: Electric Field at Cable Termination
[6]

3.1.2 Accelerated PD Induced Failure

In order to mimic long ageing periods when the cable is in service, the conditions exposed to the test samples were chosen to be similar to operating conditions. According to Mashikian and Szatkowski [33], some power cables indicating significant PD activy continued to serve for nearly 10 years, while some failed in a shorter time period in the order of months. Therefore it was necessary to accelerate the ageing period of the defects to reduce the testing time. Best practices found in literature were implemented to guard the testing conditions from diverting away from normal operating conditions.

Many stress factors influence the ageing of power cables in service. Munih et al. [34] defines them as Thermal Electrical Ambient Mechanical Stress (TEAM). To artificially accelerate ageing, a single stress or multiple stress can be used [35,36]. Electrical stress will be closely studied in the following section to define the stress values applicable to meet the study objectives.

3.1.2.1 Supply Voltage Frequency for Accelerated PD Ageing

Supply voltage frequency influences the rate at which ageing occurs [35, 37]. However Lyle et al. [38] does not encourage this practice ideally due to the undefined coefficient to be applied to the nominal frequency in order to obtain the correspondingly suitable test frequency. However, based on findings by Bartnikas *et al.* [37], ageing mechanisms at frequencies up to 1 kHz are similar to those at power frequency (50 Hz or 60 Hz). Mashikian and Szatkowski [33] observed a linear relationship between test frequency and insulation rate of degradation up to 600 Hz. Effects of frequency were also studied in [39, 40] where the PD pulse parameters of the voids did not respond to frequency changes. This means that to a certain level an elevated frequency above normal operating frequency does not change the PD mechanism, however it increases the ageing rate due to increased number of zero crossings of the applied voltage. With this understanding, frequency was one of the most reliable forms of accelerating PD ageing. Recommended frequency ranges from literature suggest ranges in 200 Hz to 400 Hz [35], or at worst any frequency below 1 kHz [37]. These frequency ranges were defined as frequencies at which the dissipation factor of the dielectric is not significantly enhanced which could otherwise prompt early thermal breakdown [41]. Therefore, the accelerated ageing frequency used in the present work was 350 Hz.

3.1.2.2 Supply Voltage Used as PD Accelerated Ageing Agent

Though frequency would ideally increase the PD-induced ageing rate despite all other parameters held constant within operating ranges, the ageing time would still take significantly longer [37]. For this reason in this work, voltage was chosen as an additional PD accelerated ageing stress factor. Higher voltage stress application can induce dielectric ageing mechanisms deviating from that at normal operating condition [37, 38]. Voltages in the range of $2.5U_o$ to $3U_o$ are recommended [37, 38, 42]. Where U_o is the operating voltage. This voltage range was arrived at by analysing the Weibull shape parameter for the test results done at $4U_o$, $3U_o$ and $2U_o$. The Weibull parameter appeared similar, depicting a similar failure mechanism. A summary of the ageing parameters used is presented in Table 3.2.

Table 3.2: Accelerated ageing conditions and tests

Test Parameter	**Parameter Value**
Accelerated Ageing Conditions	
Voltage	$2.5U_o$ (16.5 kV)
Frequency	350 Hz
Diagnostic Tests (were carried out every 8 hours)	
PD test	Conducted at Power Frequency (50 Hz)

3.1.2.3 The Accelerated Ageing Set-up and Procedure

The ageing test procedure is illustrated in Figure 3.2. To manage the testing time, maintain similar test conditions and time of ageing for all cables, all cable cores were connected in parallel. Figure 3.4 shows the test circuit used, with a Very High Frequency (VHF) voltage source, and a circuit breaker for protection in case of a core failure. The cores were stressed continuously for 8 hours; thereafter PD measurements were done off-line on each core, and then connected back for stressing.

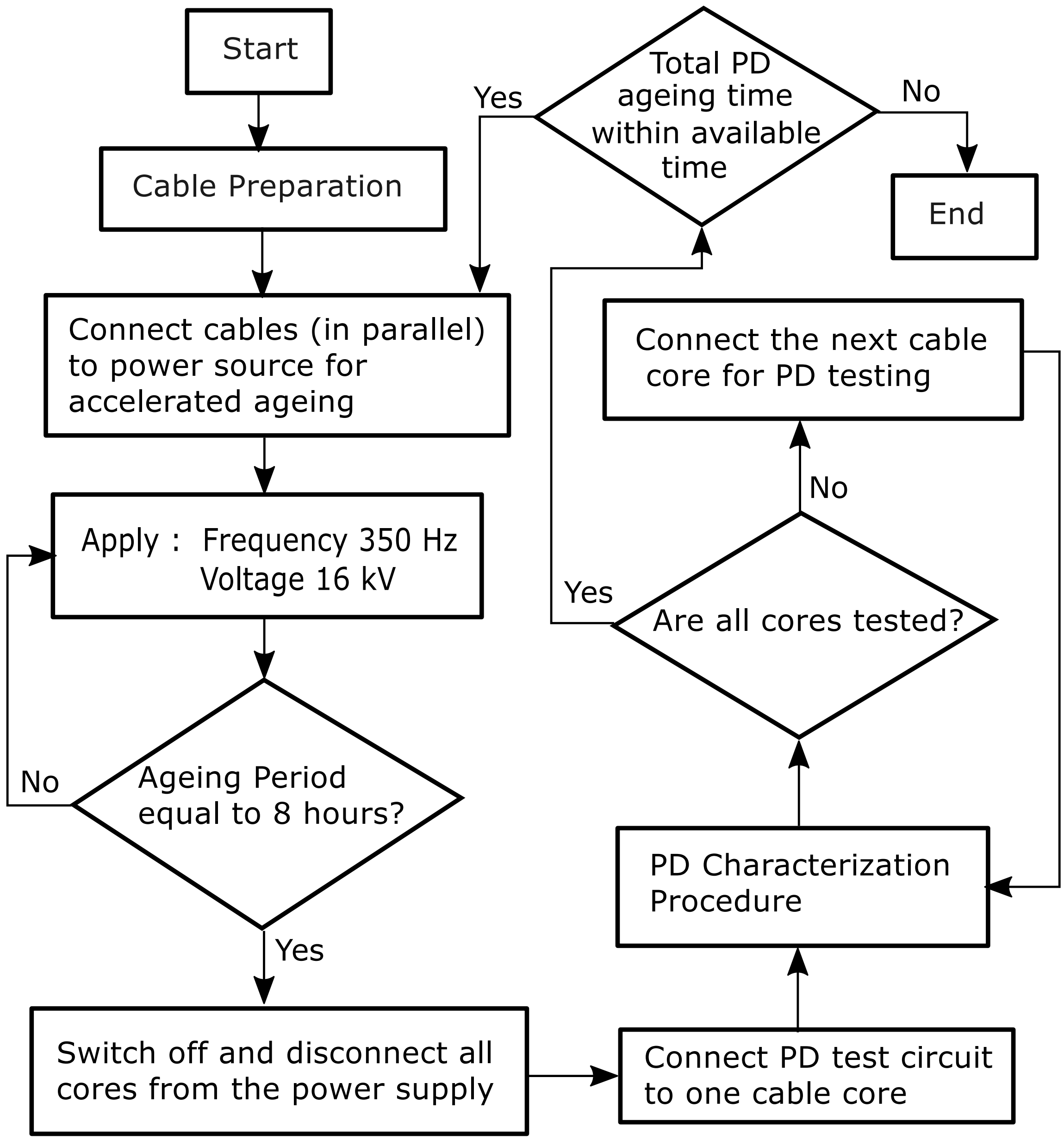

Figure 3.2: PD Induced Accelerated Ageing Process Flow

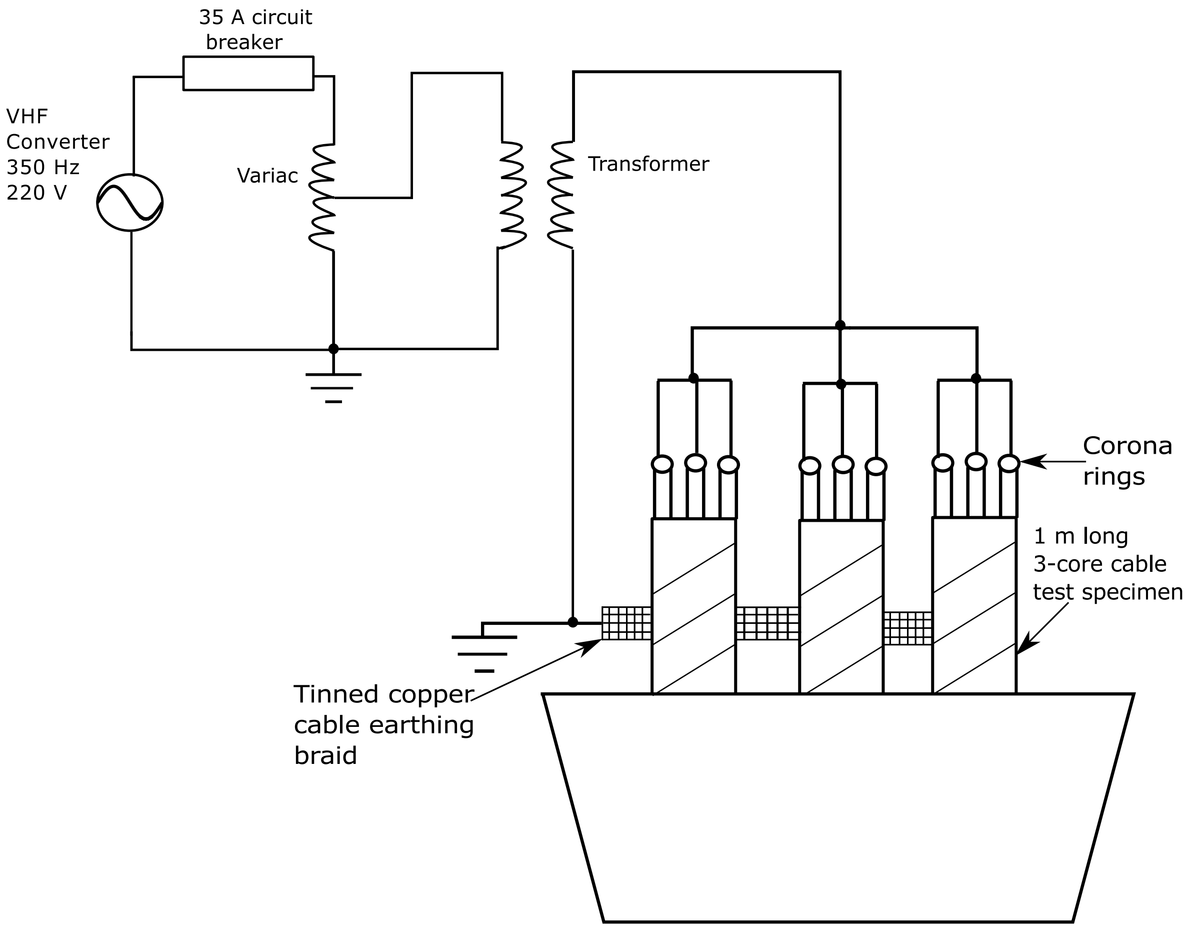

Figure 3.3: Accelerated PD-induced Ageing Circuit Configuration

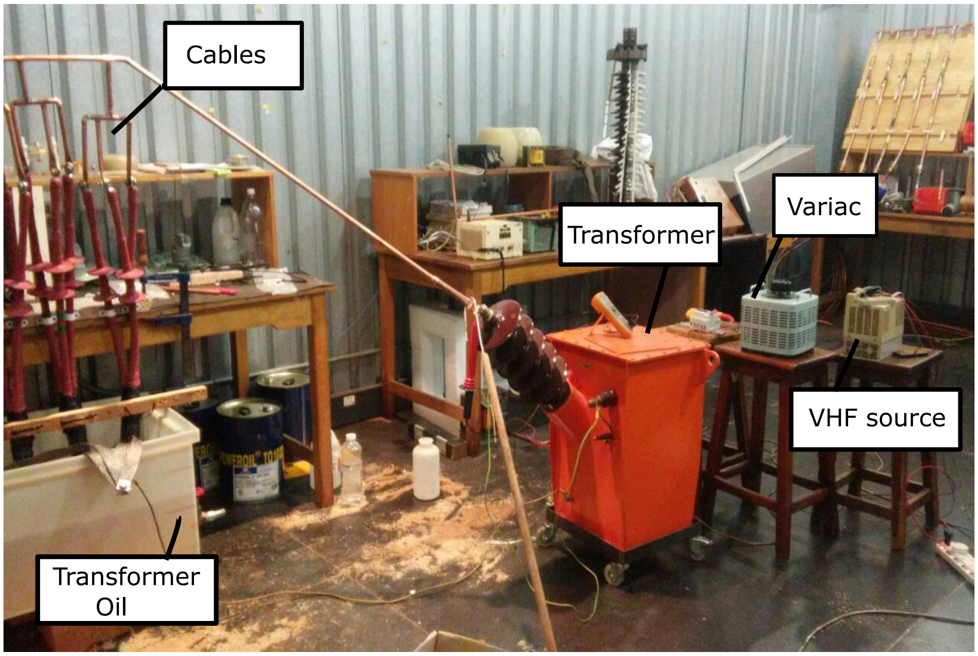

Figure 3.4: Accelerated Ageing Test Circuit Set Up

Figure 3.5: Accelerated Ageing Cable Set Up

Figure 3.6: Accelerated Ageing Test Circuit View

3.1.3 Partial Discharge Measurements

In order to monitor the PD characteristics with ageing time, PD measurements were conducted after a fixed time interval of 8 hours and then the test specimens put back into the voltage circuit for continued accelerated ageing. In practice, cable condition testing methods include insulation resistance (megger testing), polar index test and High Voltage (HV) withstand test [43]. These methods evaluate the resistance of the insulation, and low resistance is associated with a bad insulation condition. The disadvantages of these methods are their inability to detect PD activity at an early stage before catastrophic deterioration or damage [43]. PD tests can diagnose an earlier stage of insulation degradation, without stressing the insulation to an extent that could impend its failure. For these reasons, PD testing is one of the prominent cable insulation condition evaluation methods [44] and therefore also the chosen means of evaluating the cable condition in the present work. PD manifests itself in different ways that can be measured namely ultrasonic sound, heat, radiation from ionised particles, charge displacement and chemical reaction by-products. Electrical detection of PD focuses on measuring the charge displacement symptom of a PD event.

Figure 3.7 describes the PD test procedure used. The main PD characteristics measured are the Partial Discharge Inception Voltage (PDIV), Partial Discharge Extinction Voltage (PDEV), Phase Resolved Partial Discharge Pattern (PRPDP), Pulse Repetition Rate (PRR) and maximum apparent PD magnitudes (Q_{max}). The circuit in Figure 3.8 was used for the PD characterization based on the SANS 60270 standard [13], SANS 1339 [5], IEEE 400.3 [45].

Voltage was increased to 22.3 kV for 1 minute in order to re-ignite PD prior to measuring the apparent charge. The PRPDP was recorded at 22.3 kV and at 11 kV. Figure 3.8 shows the test circuit, with the coupling capacitor in parallel with the cable core to act as a high pass filter for the high frequency PD pulses. The volt drop due to the PD current was measured across a measuring impedance, fed into an amplifier and monitored using Power Diagnostix ICM Compact™. Each core was tested individually, while the rest of the cores were shorted to ground to avoid "cross talks". The testing period per core was limited to 15 minutes to ensure equal ageing time for all cores.

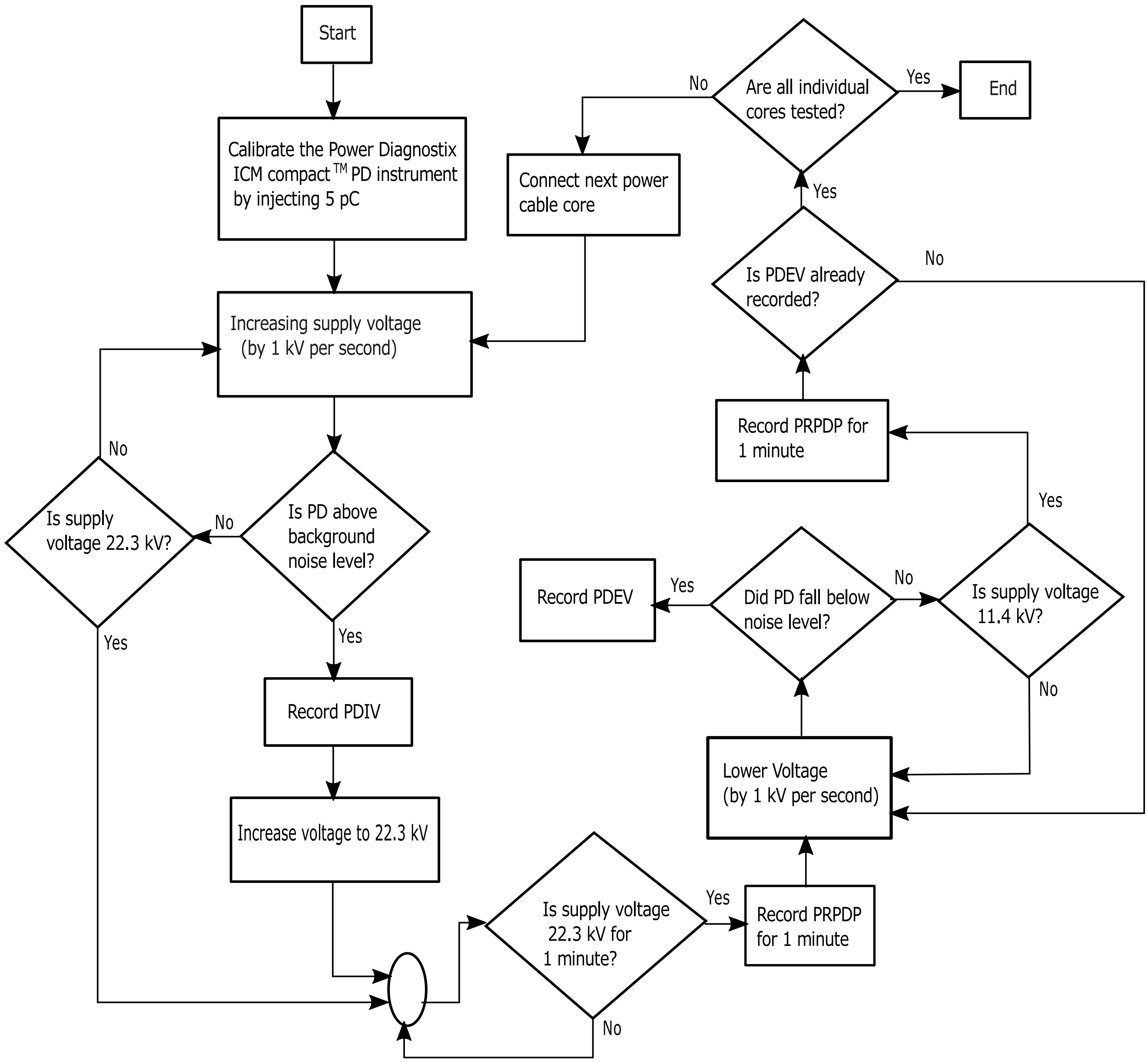

Figure 3.7: PD Measurement Procedure

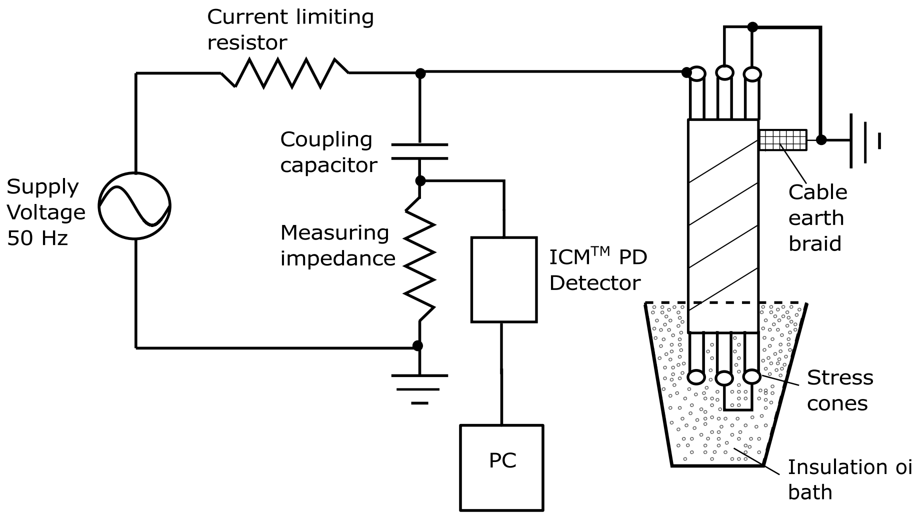

Figure 3.8: PD Measurement Circuit

3.2 Summary and Conclusion

In this chapter, the vulnerability of power cable joints and terminations to partial discharges has been discussed. Poor workmanship at these regions further contributes to the susceptibility to PD degradation. Further, the experimental method towards speeding up the insulation degradation has been presented. The 1 meter XLPE cable lengths with defects namely semicon, ring cut and tram line were aged at a high frequency of 350 Hz at 16 kV. The cable cores were all aged simultaneously in parallel connection. Off-line PD measurements were conducted periodically for each individual core at 50 Hz based on the IEC 60270 standard. The results of the measured PD will be presented, analysed and discussed in the following chapter.

Chapter 4

Experimental Results: PD parameters recorded periodically during accelerated ageing

This chapter presents the theory on the PD time-evolution behaviour over time drawn from literature in terms of influence of the discharge region environmental factors. It then presents the experimental results of PDIV, Q_{max}, PRR, PRPDP, and relates the observed behaviour to commonly accepted PD theory.

4.1 Introduction

This chapter presents the interpretation of the results which will look at the holistic overview of the PD mechanism, by closely analysing the Partial Discharge Inception Voltage (PDIV), maximum apparent PD magnitude (Q_{max}), Pulse Repetition Rate (PRR) and Phase Resolved Partial Discharge Pattern (PRPDP) behaviour over ageing time together and relating it to the PD mechanism theory. It has been observed that core 3 was in some cases more randomly different from the similar defected cores. However, the behaviour for core 3 somewhat relates to that of core 1 and 2 but with a time difference to it. Therefore, the results to be focused at in the discussion are the moving average of core 1 and 2 PD parameters.

4.2 The Monitored PD Characteristic Parameters (PDIV, PD magnitude, PRR, PRPDP

Changes that occur to the discharge environment or surface as PD continuously re-occur, consequently affect the two main factors that define whether a PD event occurs and that is the seed electron availability and the voltage build-up across the defect region. The said effect influences the measured PD characteristics that is PDIV, Q_{max}, PRR and PRPDP. In this manner, the measured PD parameters convey the ageing state of the defects.

4.2.1 Partial Discharge Inception Voltage (PDIV)

The Partial Discharge Voltage (PDIV) is the voltage at which the first partial discharges are noticed in a test object, occurring in a repetitive manner as the voltage is gradually increased from lower voltage level where no PD activity is observed [13]. The PDIV therefore gives indication of the lowest voltage level at which detectable PD starts to occur. A study by Pompili et al. [46] considered three approaches to determine PDIV in liquid insulation. Based on their results it was concluded that defining PDIV as the voltage where abrupt changes in Q_{max} is observed has more weight than other definitions in literature that base it on Q_{max} ranges and Pulse Repetition Rate (PRR) in a specified time of PD occurrence. Therefore, in the present work, the abrupt change in Q_{max} above background noise was used as an indication to note PDIV.

4.2.2 Maximum Apparent Partial Discharge Magnitude

The maximum apparent PD magnitude (Q_{max}) measured was not that of charge transferred across the discharge site, it was apparent, as it was the PD measured at the end of the cable, after the signal travels across the cable. This means that the measured charge is to some extent influenced by the type of test object in terms of attenuation. To reduce this effect, it is advised to make use of a coupling capacitor with a capacitance in the same range as the test object [47]. According to SANS IEC 60270, apparent charge is charge that would give the same reading when it is injected for a short time across the test object and when it is injected directly across the measuring module [13]. In this case, the maximum values of apparent PD charge magnitude were recorded.

4.2.3 Partial Discharge Pulse Repetition Rate (PRR)

According to IEC 60270, PD Pulse Repetition Rate (PRR) is the frequency of occurrence of PD pulses over a specified time period [13]. PRR gives an insight on the number of PD events, which is not evidently expressed by observing Q_{max} alone. The number of PD events has been observed to potentially indicate pitting in the insulation surface; hence aid in the insulation diagnosis, specifically the progression of the defect towards failure. This section discusses the observed PRR trends.

4.2.4 Phase Resolved Partial Discharge Pattern (PRPDP)

Phase-Resolved-Partial-Discharge-Pattern (PRPDP) refers to the PD pulse distributions such as Q_{max} or PRR plotted with respect to the phase angle at which they occur [48]. The time capture of the patterns reflect only the instance of PD pulse, while the PRPDP shows an accumulation of PD over a specific period such as 1 minute.

The PD measurements recorded at various intervals during the ageing period for each defect type are presented and discussed in the following sections.

4.3 PD Mechanisms Review

In order to interpret the experimental results based on known PD theory, the following section presents the time-evolution behaviour of PD observed in accordance with the literature. In order to "set the scene" for interpreting the PD measurement results presented later in this chapter, the various factors that can influence PD behaviour as a function of continuous ageing are reviewed in the next sections.

4.3.1 Parameters Influencing PD Time-Dependent Behaviour

The pre-liminary conditions for a PD event to take place are the presence of a free electron and an electric field equal to or above the inception field of the discharge region. Depending on the magnitude of the electric field, the free electron accelerates towards the anode and collides with gas molecules, resulting in impact ionization and a generation of free secondary electrons [16].

The cascade of collisions proceeds and eventually results in an exponential increase of electrons forming avalanches given by Equation 4.1. Where n_o represents the initial number of electrons, α is Townsend's first ionization coefficient which represents the number of new electrons generated during the electron travel from the cathode to the anode over distance d. A streamer discharge occurs when an avalanche grows to electron concentrations of greater than 10^8 [49].

$$N = n_o e^{\alpha d} \tag{4.1}$$

The two critical pre-liminary conditions for PD to take place, which is the availability of the seed electron and the possibility of the electric field strength in the discharge region exceeding the discharge region threshold are all influenced by many factors. It is understood from literature as presented in the following section that the dominant factors are namely surface conductivity, gas pressure, gas content, temperature, and surface homogeneity. PD ageing involves changes in these factors, which then give birth to new conditions in the discharge region as ageing progresses. These changes manifest in the form of changing PD characteristic parameters and in the present work the parameters under scrutiny were PDIV, Q_{max}, PRPDP and PRR with ageing. The effect of these factors are discussed in the next section.

4.3.1.1 Surface Conductivity

Surface conductivity of the discharge cavity walls has been measured by various researchers, both at unaged stage and progressively as PD induced ageing was conducted [50–52]. It has been noted that surface conductivity ranges from orders of 10^{-18} to 10^{-2} S [50, 53]. According to these researchers' reports, surface conductivity is lowest in un-aged insulation and sharply increases in the first hours of ageing. It has also been reported that surface conductivity eventually reaches a "threshold" and falls back to the initial conductivity after a long period of PD exposure. During initial PD activity, the increase in surface conductivity is due to a conductive liquid film layer that forms on the insulation surface. It has been identified as a layer since wiping of the surface at this stage restored the initial insulation conductivity [52]. The conductive layer has been characterized, it is suspected to be a result of a reaction between moisture (from humidity in the discharge region) and dissociated gaseous by-products of the discharge [15]. The effect of accumulated PD by-products explains the observed change in surface conductivity with increase in ageing time. Further effects resulting from the discharge by-products will be looked at.

Surface conductivity influences the charge decay constant. The more conductive the discharge area surface, the faster the charge will decay. This reduces the probability for a seed electron to be available to initiate collisions and also reduces the electric field intensity in the cavity. The statistical time lag for PD inception will therefore be longer. The statistical time lag is the time taken for a seed electron to be available after the electric field has exceeded the theoretical inception field of the void. The field therefore continues to increase above the theoretical inception field until a seed electron is available. The voltage difference between the theoretical inception voltage and the actual inception voltage is called gap over-voltage [54, 55].

The domino effect continues where gap over-voltages give rise to a phenomenon called cathode effect. The cathode effect is a phenomenon caused by an enhanced stress condition in a cavity. In the presence of an electric field, the available seed electron accelerates towards the anode. Along the way it collides with gas molecules causing ionization whereby more electrons and positive ions are generated. The accumulation of electrons forms avalanches; electrons being lighter and hence faster than positive ions, are swept away quickly by the anode. The positive ions accumulate and drift towards the cathode in a slower motion; hence a space charge is build-up near the cathode. The space charge field superimposes on the background field enhancing the stress level in the cavity. Under such an intense electric field, the positive ions emit photons that bombard the cathode, causing more electrons to be emitted from the cathode. The increase in electrons also means larger avalanches and generation of more secondary avalanches as a chain of collisions occur. The cavity consequently breaks down completely in a streamer discharge. Due to the build-up of high electric fields, discharges resulting from the cathode effect are characterised by large Q_{max}. The gap over-voltage and surface charge decay are illustrated in Figure 4.1.

The total electric field across the cavity (E_{net}) is the sum of the residual charge and that due to the externally applied voltage. The discharges cumulatively deposit electrons and positive ions at the opposite ends of the cavity [32]. The electric field due to this residual charge superimposes on the applied electrical field. As seen in Figure 4.1, $E_{res_{(-)}}$ is residual charge from the negative half cycle discharge events while $E_{res_{(+)}}$ is residual charge from the positive half cycle. The resultant electric field (E_{net}) in the cavity is the vector sum of all the component electric fields present in the cavity. However, at the zero crossing there is field enhancement of the net electric field across the cavity as the component electric fields are in phase and this explains why discharge pulses can appear on the zero crossing of the supply voltage waveform. The residual charge eventually decays due to diffusion of electrons into the insulation surface. Figure 4.1 is further explained in detail below with reference to the marked points on the applied electric field cycle.

Position A: This point represents the zero crossing region of the external applied voltage. As shown in Figure 4.1, E_{net} depends on the sum of E_o and E_{res}, and since E_o is zero, $E_{res_{(-)}}$ contributes solely to E_{net}. In cavities with no previous PD activity, there is no de-trappable charge on the cavity surface; hence PD is less likely to occur in this A region. However, with active cavities, provided that the charge decay constant of the previous discharge event is longer than the time taken to the succeeding point, then the influence of E_{res} on E_{net} is higher.

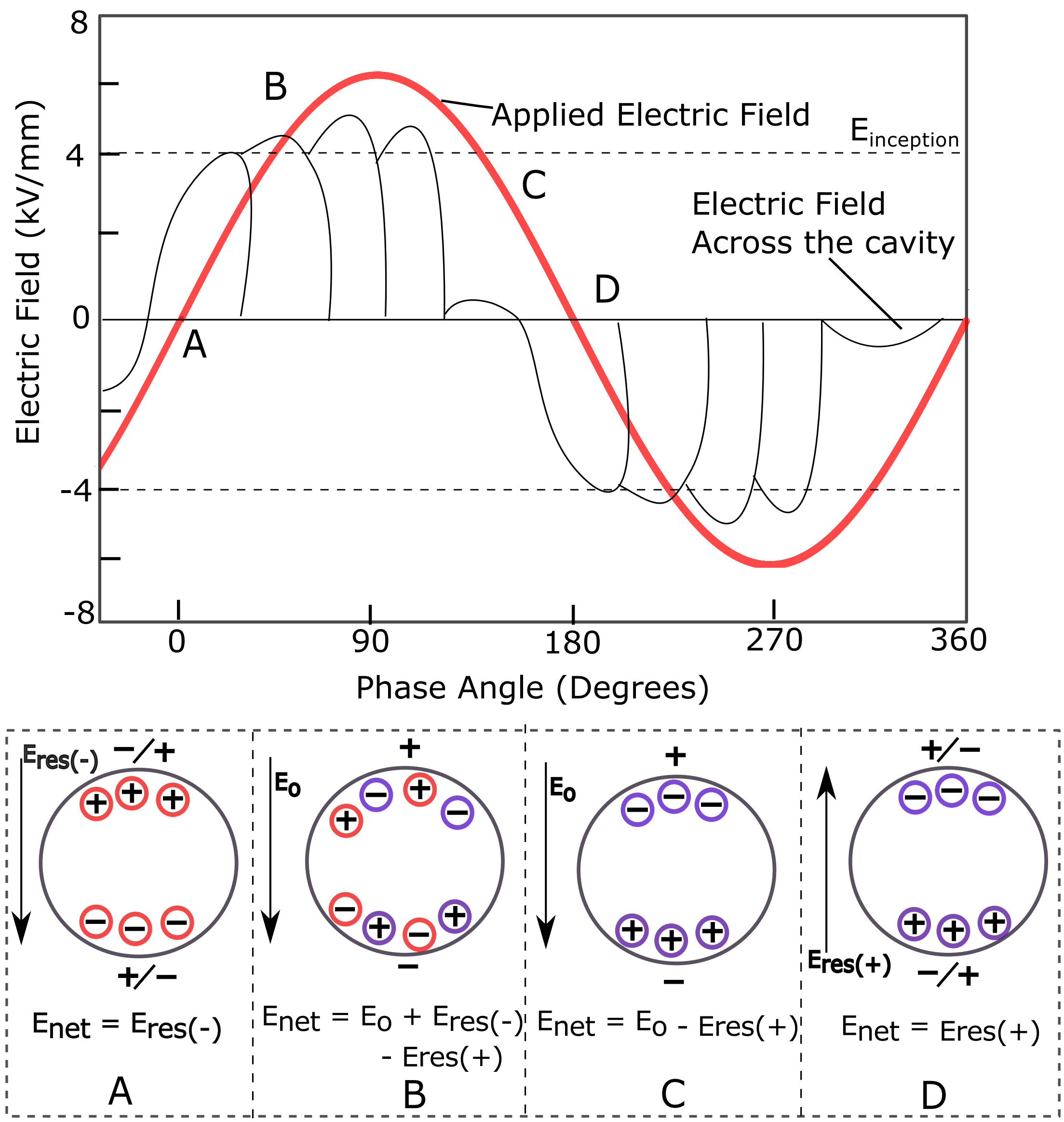

Figure 4.1: Electric field conditions in a cavity

[17]

Position B: This is the first quarter of the half cycle prior to the applied voltage peak (30 - 90 degrees). Due to the statistical time lag brought about by the delay in seed electron availability after the inception voltage is exceeded, over voltage conditions may occur. The intense electric fields across the discharge site then result in larger electron avalanches which manifest as larger PD magnitudes. This discharge part is often referred to as the "ear tip" part of the "rabbit ear"; the entire PRPDP takes the form of a "rabbit ear". $E_{res_{(-)}}$ enhances E_{net} while $E_{res_{(+)}}$ decreases E_{net}.

Position C: Between 90 - 135 degrees, $E_{res_{(+)}}$ opposes the applied electric field E_o, resulting in a reduced total electric field across the cavity, detected as lower PD magnitudes. This part is known to form the "body part" of the rabbit.

Position D: This represents the zero crossing region from the positive to the negative half cycle. The total electric field across the cavity is only due to that of the residual charge ($E_{res_{(+)}}$). Depending on the residual charge intensity, and seed electron availability PD may or may not occur.

4.3.1.2 Discharge Area Surface Morphology

Several researchers have studied the surface of an insulation that has been exposed to PD [15,22,51,52]. Initially, the insulation surface becomes covered with liquid droplets as discussed in the previous subsubsection 4.3.1.1. With an increase in ageing time, solid by-products begin to accumulate on the surface, possibly also a crystallization of the liquid droplets. These solid by-products were identified to contain a mixture of organic acids such as formic, acetic and carboxylic acids [15, 22, 51]. Van Brunt [56] suspected that PD avalanches react with gas molecules and produce free radicals or moieties such as ozone, oxygen ions and oxygen atoms as shown from Equation 4.2 to Equation 4.4. Moieties are micro units that form up a polymer and are therefore produced when the polymer chains such as the inter-chain or intra-chain bonds are broken down [20]. With long periods of PD ageing, the insulation surface becomes eroded with degradation pits possibly due to the avalanche electron impact on the surface as well as chemical attack of the insulation by the acid discharge by-products and free radicals. The etching away of the insulation is a permanent form of degradation to the insulation. This increases the surface roughness.

$$e + O_2 = O^-{}_2 + hv \tag{4.2}$$

$$e + O_2 = O^- + O^+ + e \tag{4.3}$$

$$e + O_2 = O^- + O \tag{4.4}$$

Surface morphology and conductivity are one of the main influencing factors for aged cavities [57]. Both surface conductivity and surface roughness change the physio-chemical structure of the discharge area surface as shown in Figure 4.2 where it is seen that the surface becomes more rough and eroded. The physiochemical changes of the surface influences the statistical time lag which eventually determines the actual breakdown strength of the void. Additionally, they influence the generation of avalanches by either providing electrons or by conducting the electrons away from the avalanches.

4.3.1.3 Gas Pressure and Volume in the Discharging Cavity

One of the chemical reactions during a discharge is the oxidation of the insulation. In this case, the insulation is a polymer, a chain of C-H bonds. One of the gaseous discharge by-products have been identified to contain Carbon and Oxygen moieties [15]. Gas pressure has been investigated by several researchers [50, 57, 58]. Most researchers have observed a decrease in gas pressure and volume initially as PD activity progressed. The decrement in gas pressure is suspected to be due to a high consumption rate of

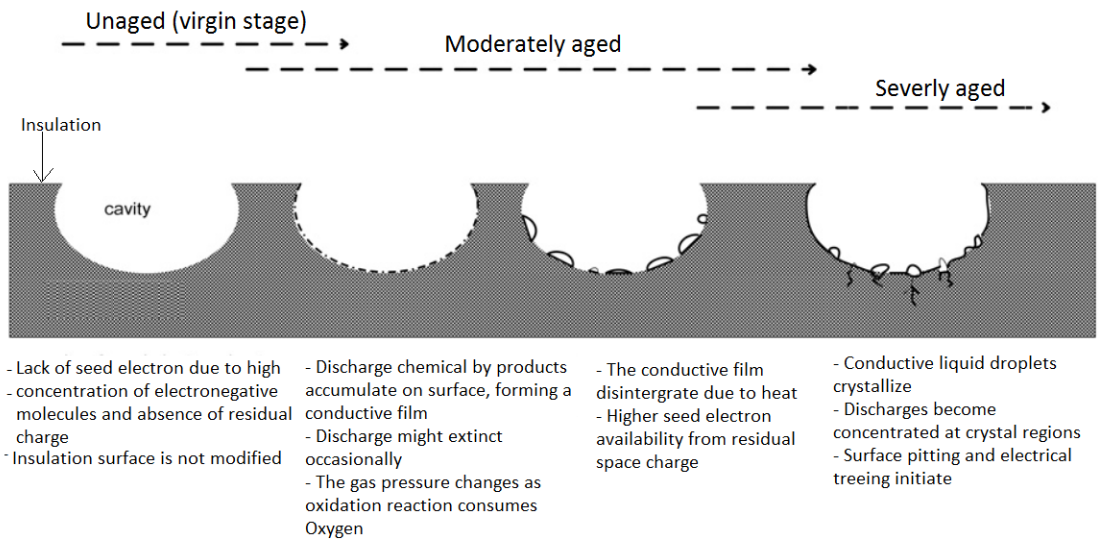

Figure 4.2: The physiochemical changes in the cavity with ageing [51]

oxygen in the oxidation reaction, faster than the rate at which the discharge gaseous by-products were generated. A later increment in gas pressure was attributed to the build-up of PD gaseous by-products and further dissociation, as well as a recovering oxygen specifically following a low PD activity period. It is suggested that un-vented void discharges such as those in the present work are more prone to be affected by changes in pressure, volume, temperature because they are 'non-breathing' [59].

The pressure in the void has been reported to be of less significance in influencing the discharge mechanism as a function of PD ageing [57]. However, Wang [57] established in his work that the PD ageing behaviour was related to the gas volume. A lower density of the gas reduces the effective ionization coefficient (α) indicated in Equation 4.1 [50,57].

4.3.1.4 Gas Content in the Discharge Cavity

The gas content in a discharging cavity matters as it can provide potential for impact ionization to create avalanches that may amount to electrons sufficient to support a discharge. Electron affinity is one of the main properties that have a direct impact on the discharge. Electronegative gasses may “consume” (attach) electrons and therefore reduce avalanches, or even worst case, make it difficult for a seed electron to be free to initiate collisions. A significant presence of electronegative gasses also lead to a gap over voltage effect for the first discharges, thereafter, the residual charge supplies the seed electrons and therefore reduces the statistical time lag.

4.4 Semicon Feather Defect PD Evolution Behaviour: Measured Results and Discussion

4.4.1 Measured Results

Figure 4.3 shows the PD parameters measured during accelerated PD induced ageing of the semicon defect. In addition, Figure 4.4 shows typical PRPDP at various ageing stages.

Stage 1: covers the first 100 ageing hours. In this stage, PDIV increased by 48%. The maximum apparent PD magnitude (Q_{max}) increased as well by 56%, while the PRR dropped by 20%. The lowest PDIV and the largest Q_{max} were recorded in this stage. The PRPDP shown in Figure 4.4 a) shows rabbit ear like PD with a full “body part” (a thick base).

Stage 2: begins from 100 to 180 hours. PDIV decreased by 10%, while Q_{max} dropped by 77%. The PRR increased by 43%. Q_{max} drop in this stage was significant though not the highest recorded. The PRPDP has a sign of longer rabbit ear tips with a thinner base.

Stage 3: starts from 200 hours to 250 hours, PDIV decreased by 33%. Within this time range, Q_{max} increased by 60%. The PRR dropped slightly by just 13%. The largest PDIV drop was recorded in this stage. The PRPDP appear more similar to that observed in Stage 1 except that the "rabbit ear" shows increased width.

Stage 4: is categorised as the fourth stage ranging from 250 to 400 hours, PDIV remained constant at 16 kV. Q_{max} in this stage fluctuated with a 25% margin around the range of 400 pC. The PRR fluctuated as well with 33% about 1500 counts, and later increased by 50% towards 400 hours. This was the period with the most fluctuation in PD parameters, also with the highest PRR. The PRPDP shows almost more distinctive "rabbit ears".

Stage 5: from 400 hours onwards, PDIV began to rise gradually by 48%, then dropped by 28% around 660 hours but eventually increased by 40%. Meanwhile, Q_{max} decreased by 25% by 500 hours and continuously dropped by 90%. An interesting point was the sudden increase in Q_{max} corresponding to the PDIV drop at 660 hours. PRR on the other hand decreased by 37%, then increased by 500% with fluctuations of 13% margin and eventually decreased by 33% at 800 hours, however began rising back with 40% at the end of the test. This stage had the largest though gradual increase in PRR and simultaneously the largest drop in Q_{max}. The PRPDP appears more of a hump ("turtle shape") commonly reported in literature [60] and PD appears bushy.

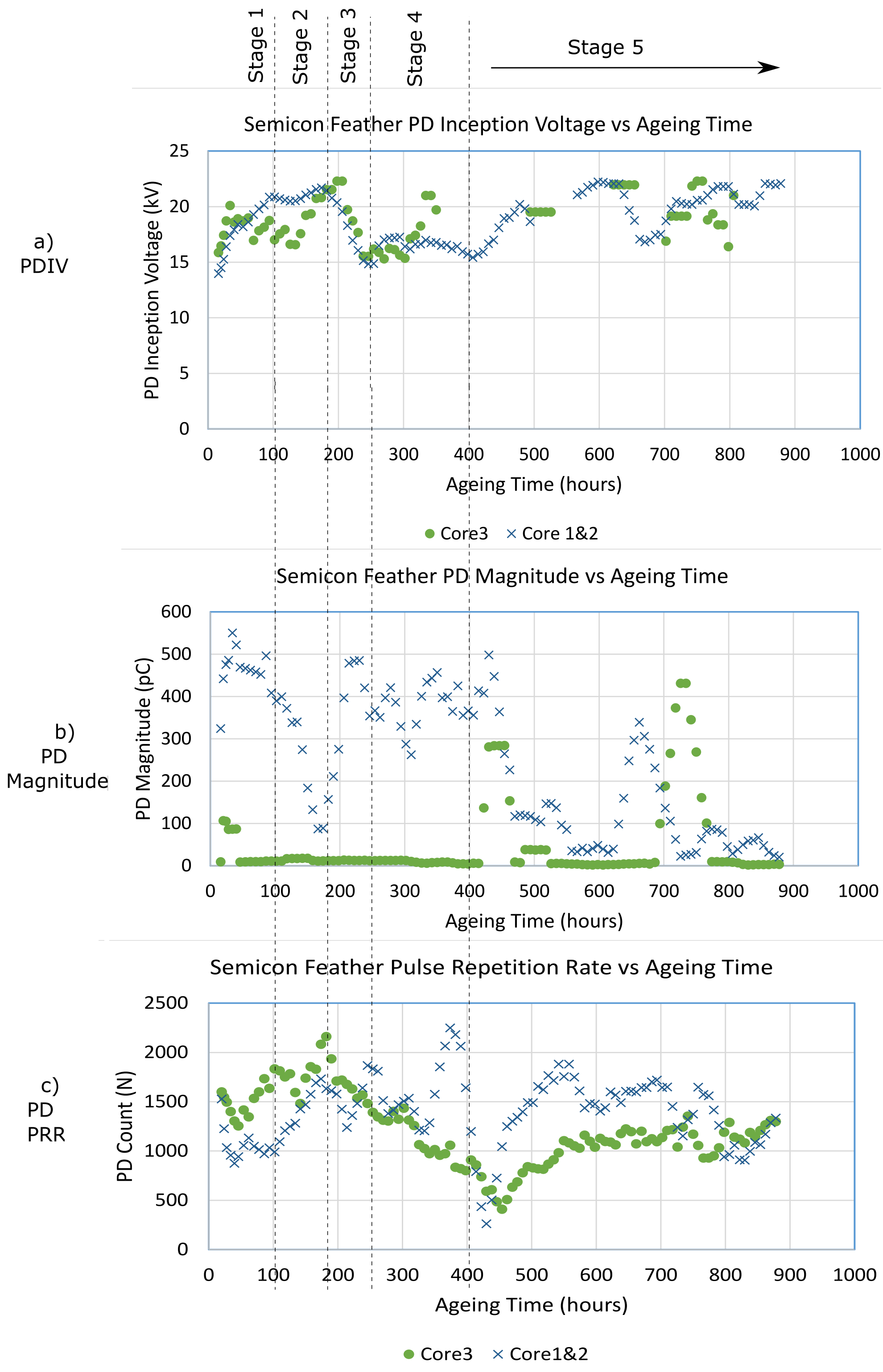

Figure 4.3: PD Characteristics of the semicon defect. a) PDIV, b) PD magnitude, c) Pulse Repetition Rate

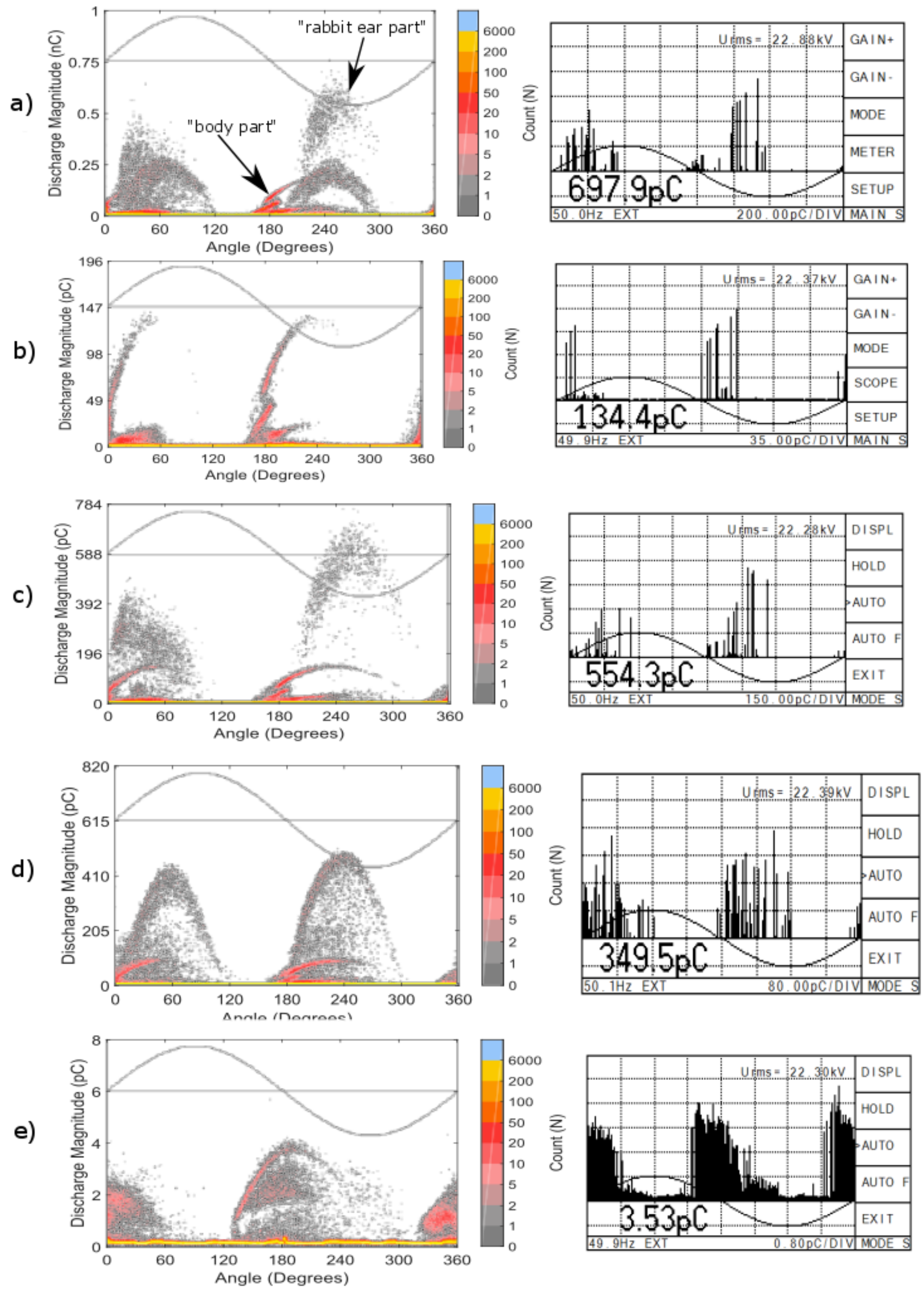

Figure 4.4: PRPDP of the semicon feather defect after the following ageing hours respectively from top: a) Stage 1, b) Stage 2, c) Stage 3, d) Stage 4, e) Stage 5

Overall, it is observed that the PDIV was fairly constant, with fluctuations of 7 kV at most throughout the ageing time. For the semicon feather defect, the general trend identified from the beginning of the test to the end is one with a decreasing Q_{max} and an increasing PRR. Q_{max} and PRR behaviour between 250 and 400 hours fluctuated the most, and thereafter, significantly decreased and increased respectively. The initially spotted signature of "rabbit ears" with a body part and a corona like pattern to them remained visible through the ageing stage, with a decreasing corona like effect on it.

4.4.2 Semicon Feather Defect Ageing Behaviour Explained

Stage 1: a simultaneous increase in PDIV (48%) and maximum apparent PD magnitude (Q_{max}) (56%) and a decrease in PRR (20%) dominated the initial ageing trend. This behaviour is similar to findings from [19, 22, 50, 59, 61–64]. The increase in PDIV is attributed to the conditions of a virgin insulation surface. At the early ageing phase, the defect insulation surface ionization co-efficient is higher [17], which means it is more difficult to de-trap electrons from the insulation bulk. Furthermore, the oxygen concentration is high at this stage, reducing the mobility of free electrons. These conditions in turn translated into a longer wait time for a seed electron to be availed, the consequence being larger gap over voltages as discussed in the previous sections. The symptoms of large gap over voltages are higher PDIV and larger Q_{max}. Considering that the statistical time lag is longer for PD events, it is suspected that inherently the number of discharges per cycle become fewer as there is less time reserved for more discharge events to occur in a half cycle; hence the observed decrement in PRR. Figure 4.4 b) shows the PRPDP indicating the gap over voltage effect. The first discharges in a half cycle occur at a larger inception voltage; hence the larger magnitudes. The succeeding discharges benefit seed electrons from the initial discharge; hence occur at a lower voltage and consequently are of lower magnitudes. This behaviour has been reported by other researchers [22,50,61]. The PRPDP shows peaks that are concentrated on the rising edge of the applied voltage cycle, a sign of gap-over voltage condition. The appearance of "thin rabbit ear tips" and a "thicker body part" is an indication of existence of PD of different magnitudes, small Q_{max} pulses make up the "thicker body part", meanwhile the larger PD pulses make up the "rabbit ear tips".

Stage 2, Stage 3 and Stage 4: as the residual charge from previous discharges build-up on the insulation surface, it becomes a rich source of harvest of seed electrons. This consequently reduces the statistical time lag; hence the reduction in PDIV. Q_{max} decrease as well due to the reduction or absence of gap over voltages. Provided that the inception field is exceeded, the seed electron is the only limiting factor to the frequency of the discharge events. A generous availability of seed electrons therefore encourage more discharge events to occur; hence the increase in PRR with 43%. The highest PRR and Q_{max} fluctuations were also noted in this period. The explanation for the fluctuations is speculated to be an indication of instability in the discharge area environment. A change in electronegative gas composition would change the dynamics of electronic avalanche development differently depending on the conductivity of the cavity surface. A high content of electronegative gasses in a discharge area with a longer charge decay time (less conductive) would reduce the size of avalanches but not necessarily reduce the number of PD events. However, a high content of electronegative gasses in a discharge area with a shorter charge decay time (more conductive) may reduce the PRR. Though PDIV is lower and correspondingly Q_{max} too, the gap over-voltage effect is most evident in the PRPDP, by the peak on the applied voltage waveform rising edge. PD covers a smaller degree phase, an indication of increased surface conductivity.

Stage 5: the surface conductivity is speculated to be the dominantly influencing factor at the initial hours of this phase. The PRR decreased and Q_{max} decreased while PDIV increased simultaneously. One of the mechanism suspected to support this behaviour is, significant increase in surface conductivity. Such an increase would reduce electron mobility on the surface by decreasing the time decay constant of residual charge. A high surface conductivity makes it difficult to hold voltage across the defect. The gap over voltage phenomena will therefore re-occur due to the increased delay of the free electron availability.

Additionally, the cavity surface will conduct away electrons that would otherwise contribute to generating larger avalanches; hence the decrease in Q_{max}. Another potential factor with similar adverse effects is the effective ionization coefficient of the gas in the defect region which is dependent on the gas composition, pressure and temperature [59]. With increase in pressure, the ionization coefficient decreases according to Paschen's law [49]; hence smaller avalanches. Due to this, after the PDIV increased, significant PD ceased to occur between 500 and 600 hours.

General diagnosis of the discharge nature in [19] recommended that if after a long ageing time then there are no incidences of complete PD evanescence, then the defect is highly likely to be a surface discharging site. In the present study, this has been the observation with the semicon feather defect which, based on the nature of the defect as described in Table 3.1, has a surface discharge component. There is no direct incision or groove made in the insulation, and the defect is therefore more of a lamination that extends over the XLPE insulation. It is suspected that the discharge behaves like a surface discharge.

Finally, the further decrease in Q_{max} to single digit pC and an increase in PRR observed at the test termination as shown in Figure 4.4 e) is similar to that of bush electrical trees which could be an indication of a imminent failure. Localised field enhancement arround crystals deposited on the cavity surface cause discharges to occur at lower PDIV [48, 51, 59]. Morshuis [59] refferred the high repetition rates of severely aged defects to "corona like". Contrary, Temmen [51] gave the insight that with an increased surface conductivity at the severely aged stage, the existence of multiple discharge sites is also limited as the entire surface is likely to be at the same potential. At the crystal tips, a generous amount of electrons are injected that support the initiation of electrical trees and possibly their progression. The resultant surface pits act as multiple discharge sites with localised PDIV (lower) that discharge simultaneously; hence the higher PRR.

Wang [22] observed that defects with no traces of PD by-products on their surface showed rabbit-like patterns, while those with large amount of by-products showed turtle-like patterns. The transition from rabbit ear like to turtle like occurred with the increased change in PD by-product accumulation on the defect surface. Therefore, the observed increase in the rabbit ear bluntness and bushy appearance can be attributed to a sign of increase in by product build-up on the discharge area surface.

Other workers reported large PDs prior to breakdown [65–67]. In his study, Tokunanga [65] found that near breakdown, Q_{max} increased by nearly 3 times of initial PD which he suspected to be a sign of treeing. However in the present study for the semicon, Q_{max} was lower at 878 hours which was the last set of tests done. After exhaustive accelerated ageing of the cores, it still could not be concluded how far off the cores were from breakdown.

Qureshi [67] aged 15 kV rated XLPE cable joints and observed that the cores with the lower PDIV failed first before the others, and in his case, PDIV decreased with ageing time almost by 60%. The findings from Qureshi are similar to that from Pihera et al. [68]. However, during the 800 hours of ageing at elevated supply voltage and frequency, none of the cores in the present study broke down.

4.5 Ring Cut Defect PD Evolution Behaviour Measured and Observed

Figure 4.5 and Figure 4.6 shows the ring cut defect experimental results which are analyzed below.

Stage 1: within the first 50 hours; PDIV increased by 12%, while maximum apparent PD magnitude (Q_{max}) increased as well by 50%. The PRR on the other hand decreased by 24%. The PRPD appears that of equal "rabbit ear", no distinct "body part" shown in Figure 4.6 as in the case of the semicon.

Stage 2: from 50 hours to 120 hours, PDIV increased by 25% but Q_{max} decreased by 55%. PRR in this time frame fluctuated though overall increased by 42%. The PRPDP appear more blunt and bulky, with significant PD at the zero crossing of the applied voltage wave form.

Stage 3: observation was that the PDIV remained constant at 20 kV from 120 to 300 hours. Q_{max} on the other hand started out constant at 200 pC, fluctuated by 100% margin. PRR in this range fluctuated with 16% about 1500 counts. The PRPDP appears similar to the previous stage (2) though with reduced tip bluntness.

Stage 4: from 300 hours, remained constant at 20 kV with minor fluctuations of 15% till 500 hours. Q_{max} fluctuated, however overall decreased gradually by 99% at 500 hours. PRR on the other hand, remained somewhat constant at 900 counts with slight decrements of 11% at 500 hours. The largest decrement in Q_{max} was noted in this stage. Full symmetrical "rabbit ears" are noted on the PRPDP.

Stage 5: from 500 hours onwards, PDIV decreased by 20% and thereafter increased by 25%. Within this range, Q_{max} remained below 10 pC. The PRR increased by 63%, after which it continued increasing by another 27%. Eventually PRR decreased as from

800 hours by 60%. PRR increased with the largest margin in this stage. The PRPDP appears like a hump.

Overall, PDIV was constant over ageing time, with a 5 kV band fluctuation once in a while. Q_{max} followed a decreasing trend to 2% of the initial value, while PRR also decreased to 50% of the initial PRR. Stage 3 and stage 4 were both characterized by the most fluctuations in Q_{max} and PRR.

Similar to the semicon defect, the last stage observed in the ring cut was the longest, with least fluctuative behaviour in PD characteristic quantities.

4.5.1 Ring Cut Defect Ageing Behaviour Explained

The ring cut behaviour was found quite similar to the semicon feather defect, both started out with "rabbit-ears" though no noticed "body part" in the PRPDP, PD seemed a continuous shape of gradual even shape. Several mechanisms are suspected to co-exist at any given time in a defect discharge region, related to changes in the surface conductivity, residual charge, gas pressure, gas content and temperature [19]. This explains the observation in this study, where different Q_{max} are recorded at different ageing times, which can be attributed to the consistently changing PD environment. The semicon defect is therefore suspected to support more mechanisms simultaneously, than the ring cut, due to the absence of the "body part" in the ring cut PRPDP.

However, for the ring cut the PRPDP were less shifted towards the voltage peak, unlike the semicon and were symmetrical in terms of magnitude and shape. Other exceptional differences are that the PD parameter changes of the ring cut were not as abrupt and random as the semicon. PIV and Q_{max} changed more gradually and with lower magnitudes less than 30%.

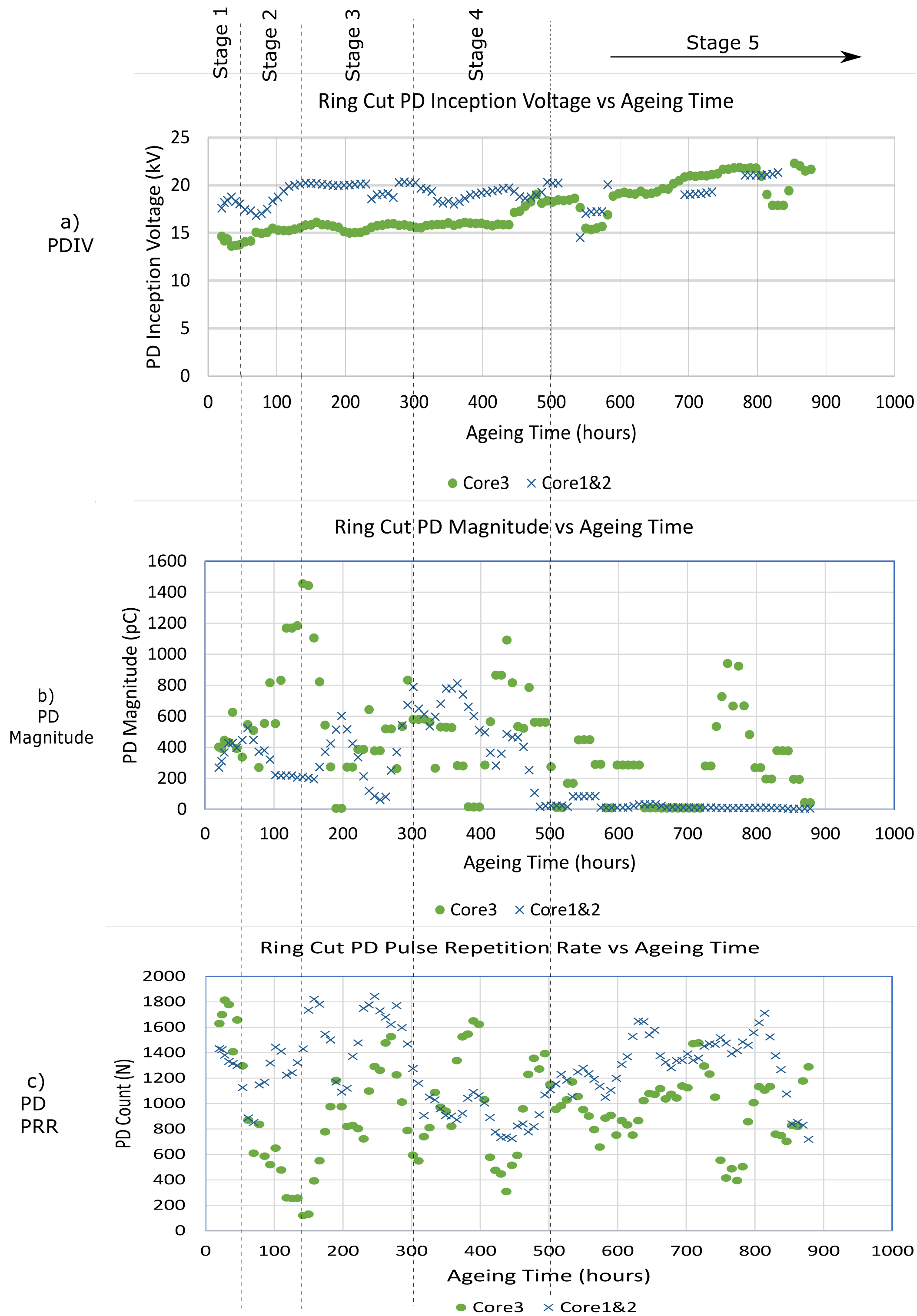

Figure 4.5: PD Characteristics of the ring cut defect. a) PDIV, b) PD magnitude, c) Pulse Repetition Rate

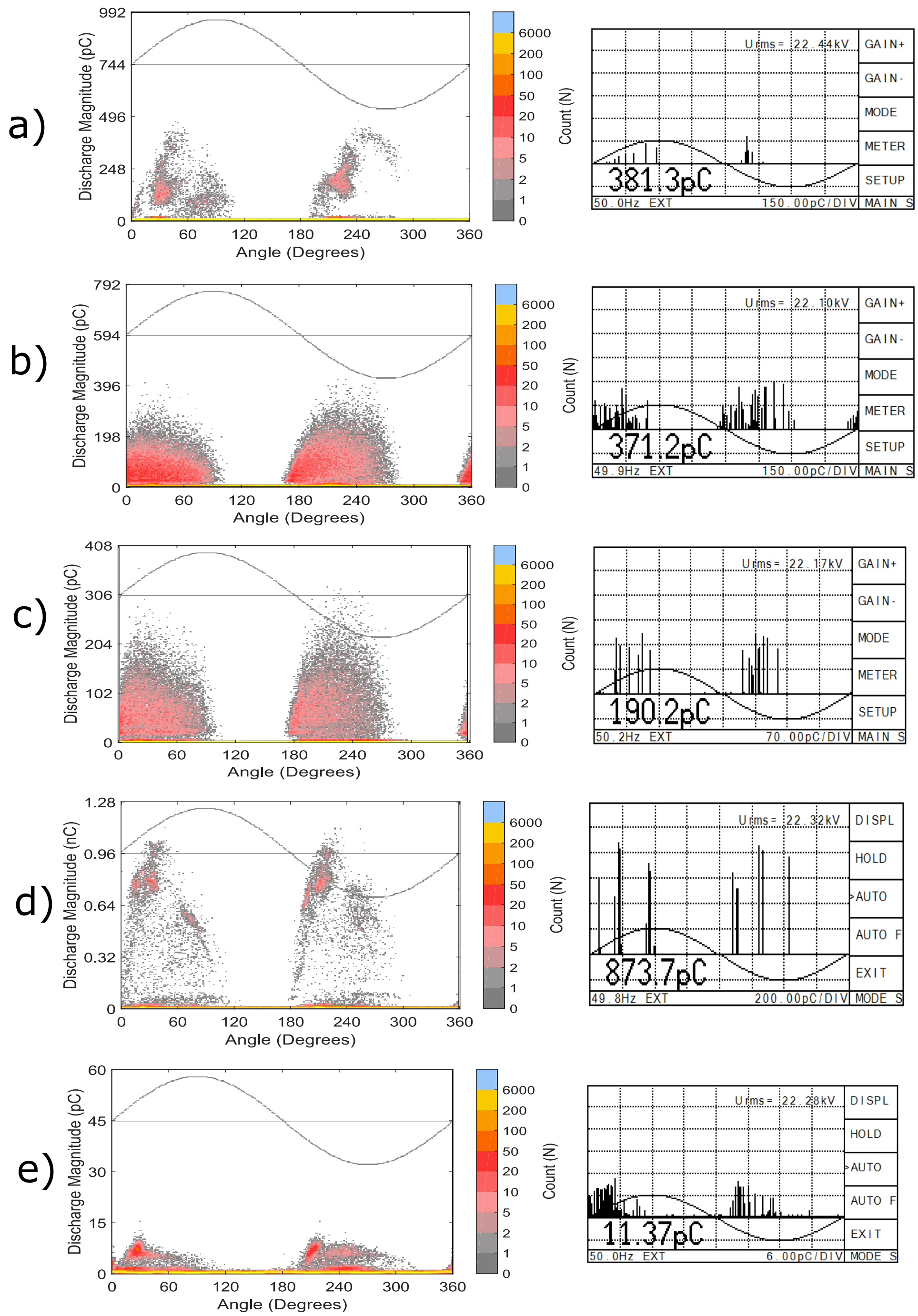

Figure 4.6: PRPDP of the ring cut defect after the following ageing hours respectively from top: a) Stage 1, b) Stage 2, c) Stage 3, d) Stage 4, e) Stage 5

However, the ring cut had longer periods in comparison to the semicon where in some cases pulsating PD was observed, and in most cases could not be detected above a noise floor of 0.2 pC. Findings from Nyamupangedengu [19] suggest that if after ageing time there are incidences of complete PD evanescence, then the defect is likely to be a cavity. With regard to the time period that the mentioned behaviour needs to be observed for the judgement to hold is still an area of research to be deliberated at. The PRPDP shows prominent PD at the zero crossing of the applied voltage waveform. This is attributed to the trench nature of the ring cut, which provides a convenient area for retaining residual charge.

As mentioned for the ring cut, high PRR of pulsating PD that could not be detected above a noise floor of 0.2 pC. In the literature, small pulsating PD has been given various names such as Swarming Pulsive Micro-Discharges (SPMD) or glow discharges [15, 62, 69]. It is not established whether this is a delayed effect of a drop in surface conductivity or an indication of crystal formation on the insulation surface. Both could possibly support such behaviour as discussed in subsection 4.4.2. In stage 5, small magnitude that was of a pulsating nature has been observed for the ring cut.

4.6 Tram Line Defect PD Evolution Behaviour: Measured and Observed

Figure 4.7 and Figure 4.8 present PD characteristic results of the tram line defect obtained during PD induced ageing.

Stage 1: in the initial 100 hours; PDIV increased by 78%, Q_{max} decreased by 50% and remained fairly constant. PRR on the other hand decreased by 14%. The PRPDP appear like "chipped rabbit ears", with inhomogeneous shape. PD covered the zero crossing region.

Stage 2: from 100 hours to 200 hours, PDIV remained fairly constant at 22.3 kV. Q_{max} was initially constant at 100 pC and dropped to below 100 pC. PRR remained constant at 1800 counts. PRPDP appeared like that of the ring cut, however skew.

Stage 3: observation was from 200 hours to 400 hours. PDIV remained constant at 22.3 kV, no significant Q_{max} were observed on the PRPDP (a typical of this is shown in Figure 4.8) at some points. Q_{max} in this range was low with incremental fluctuations of 100 pC. Despite the absence of significant Q_{max}s, the PRR increased from by 40% at 300 hours, then dropped back by 35% at 400 hours. The “rabbit ears” reduced, with a hump like structure appearance.

Stage 4: covers a period from 400 hours to 500 hours, PDIV decreased by 15%, while Q_{max} increased by 500% and dropped back to below 100 pC, also had no significant Q_{max} in this range several times. PRR increased with 133%. The “rabbit ears” re-appeared, covering a smaller phase angle.

Stage 5: from 500 hours till end of ageing, PDIV decreased with 33% then significant PD disappeared. Q_{max} remained constant below 100 pC. PRR remained fairly constant at with a slight increment of 4% at the end of the test. PD was highly pulsating. The PRPDP appear with what seem like hollowness within the “rabbit ears”.

Generally, the largest increase in PDIV was observed in stage 1. The PDIV over time decreased, with several moments of what partly seemed like PD evanescence. Both Q_{max} and PRR decreased over time.

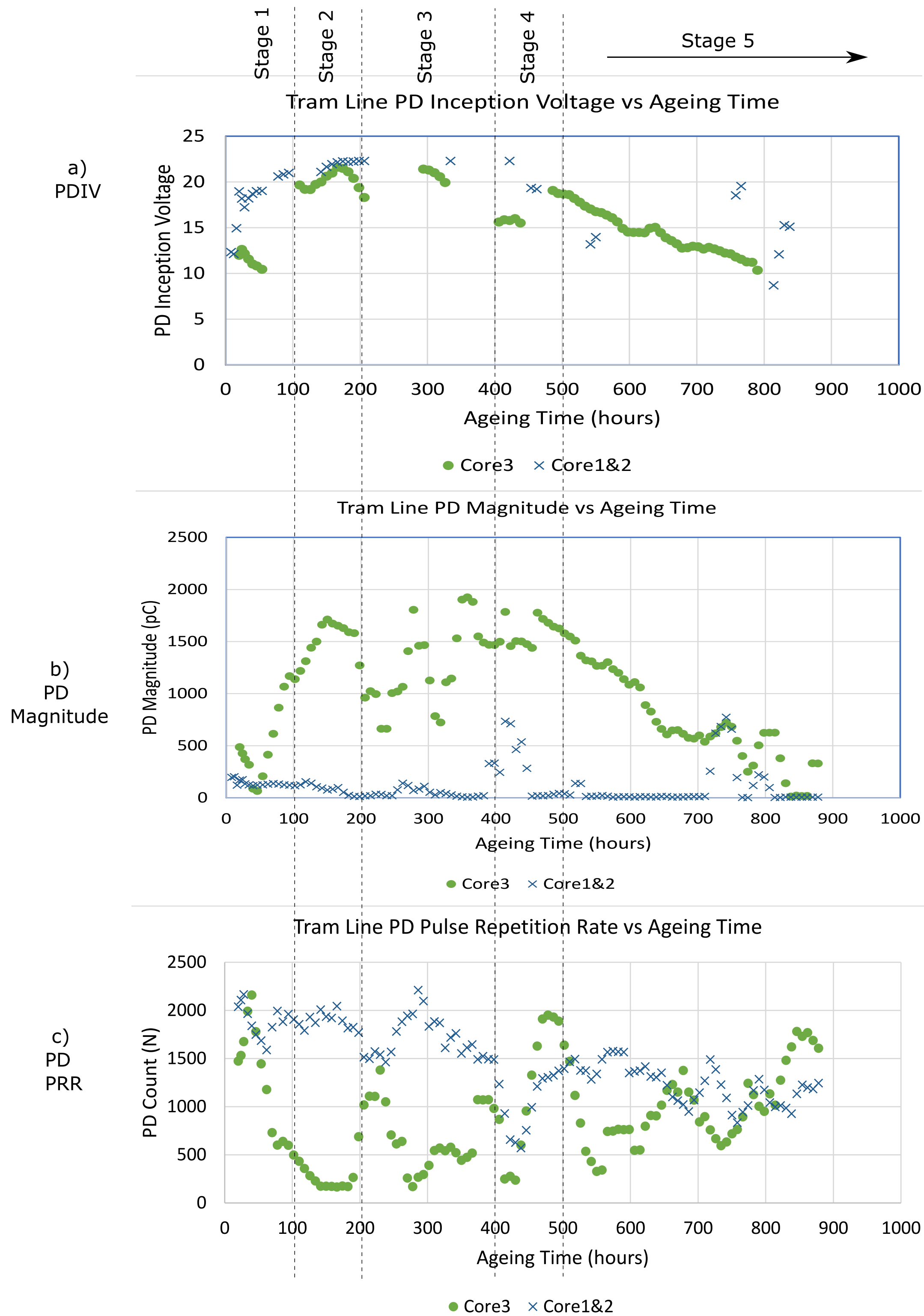

Figure 4.7: PD Characteristics of the tram line defect. a) PDIV, b) PD magnitude, c) Pulse Repetition Rate

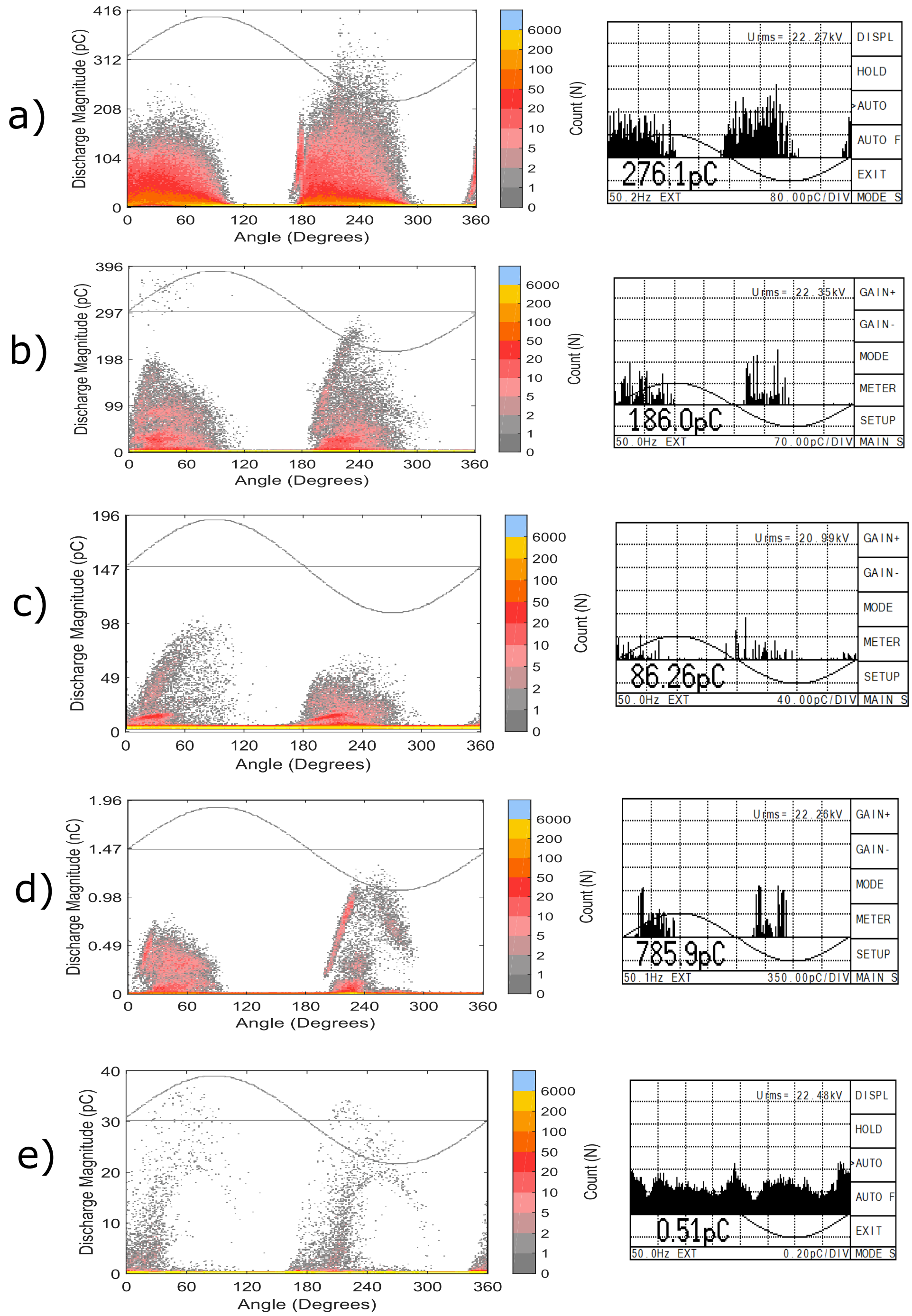

Figure 4.8: PRPDP of the tram line defect after the following ageing hours respectively from top: a) Stage 1, b) Stage 2, c) Stage 3, d) Stage 4, e) Stage 5

4.6.1 Tram Line Defect Ageing Behaviour Discussion

A cavity is narrow if the height perpendicular to the electrode is larger than the width of the cavity parallel to the electrode. In the present study, the tram line could therefore be regarded as equivalent to a flat cavity, while the ring cut was more spherical type [32]. Morshuis [59] observed that spherical cavities discharge one discharge at a time, resulting in fewer PD counts within a given time frame as opposed to flat cavities which tend to have multiple discharges. This observation is confirmed from the behaviour that the tram line had the highest PRR since it forms a longer trench in the XLPE, giving a larger surface area for PD to occur. The tram line had smaller Q_{max} in comparison to the ring cut and what appeared almost like PD evanescence. This is assumed to be due to the fact that the tram line is made along the cable length, away from the sensitive semicon end region. This could mean therefore that the tram line was exposed to less field intensity. However, the PRR recorded is higher than the ring cut.

The observed prolonged period of PD evanescence raised concern regarding the deterioration of the tram line defect. Danikas [70] through x-ray photoelectron spectroscopy has observed that the changes in insulation that occur when visible detected PD ignite are quite similar to those that occur at voltages below PDIV, an observation supported also by Danikas [70]. The degradation is attributed to small current that may be induced by voltage falling below PDIV, causing small impulsive PD or pre-discharge rather to occur. The small pulsating PD may be difficult to detect with conventional instruments (which is assumed to be the case with the tram line) yet causes similar though slower degradation as PD above noted PDIV. This observation could potentially suggest that PDIV is not a full indication of ongoing PD activity.

4.7 Comments on the Effect of the Increased Defect Severity

A common observation across all defects and all cores was that, the largest defect had the least PDIV. This is consistent with expectations since larger defect geometry enhances the electric field more, as there is a larger region with a lower relative permittivity than that of the surrounding bulk insulation. Air which tends to fill voids in solid dielectrics has a relative permittivity of 1 as opposed to that of XLPE which is 2.25. The larger the void, the more enhanced is the electric field. The voltage required to breakdown the defect region is therefore relatively smaller. This observation is similar to the findings observed by Illias [71]. According to Illias, larger cavities had a lower PDIV while smaller cavities especially those smaller than 0.1 mm had larger PDIV. This was assumed to be due to the larger air volume present in larger cavities that increases the probability of existence of a seed electron. Bahder [72] also observed that the smaller the cavity diameter, the higher the PDIV. Flat cavities, that is those cavities with the surface parallel to the electrode larger than the width of the cavity, had higher PDIV.

In terms of defect size, Core 3 (in all defect types) had the largest Q_{max}. Illias [71] had similar observations in his study of cavity size and temperature effect on PD. He found that larger cavities had larger charge magnitudes than smaller cavities. An additional observation was that most severe semicon core experienced the longest period of PD evanescence. It is assumed that perhaps the semicon tip was eroded away by the discharge.

Further observations show that the most severe core across all defect had a lower PRR than the other cores. Illias [71] found that the larger cavities had correspondingly smaller number of PD pulses . Larger cavities are associated with faster charge decay, leaving less time for the harvest of a seed electron. In the same manner, residual voltage has more limited time to superimpose for the breakdown voltage to be exceeded. Consequently, fewer PD pulses occurs in larger cavities. This explains why core 3 (with the most severe defect) had the least PRR in all cases of the semicon, the ring cut and the tram line cavities.

4.8 Defect Type Dependent PRPDP

Typical occurring PRPDP for each defect are shown in Figure 4.9. The observed PRPDP appearance is related to the nature of the specific defects as discussed below.

With reference to Figure 4.9 a), the semicon had a “right ear” (in the 2nd half cycle) that was more pronounced than the ’left ear’ (in the 1st half cycle). This is because of the change in cathode-anode role during the positive half cycle and the negative half cycle. During the negative half cycle, with reference to the discharge area, the insulation takes the role of the cathode. The insulation is a richer source of electrons than the ground metallic electrode which forms part of the opposite interface [73]. Therefore, larger PD magnitudes (Q_{max}) were observed in the negative half cycle. Positive PD covers between 0 degree to 120 degree of the phase angle while negative PD covers between 180 degrees and 300 degrees. As mentioned earlier, the semicon PRPDP gives an indication of the presence of “corona-like” [26, 74] and a “cavity-like” defect [8, 74, 75], a combination behaviour reported in literature for interface defects [8,76]. This is because of PD that concentrates at the applied voltage waveform peak. Considering the role of residual charge, it seems there is no out of phase residual charge to counteract the electric field in the defect region. Further explanation of the unique PRPDP is attributed to the nature of the semicon feather defect. The semicon feather consists of a feather tip which is sharp and protruding over the XLPE. This tip is suspected to be the contributor of the corona like PRPDP, due to the ionization of the gas or insulation surface at the tip region.

The typical ring cut PRPDP is shown in Figure 4.9 b). The PRPDP is that of a "rabbit-ear", however without a well defined "body-part" to it, a typical behaviour of void discharges [8, 74, 75]. The ring cut is a trench in the XLPE near the region where the semicon layer ends. This trench therefore provides a suitable space for retaining residual charge. The effect of residual charge is the presence of "rabbit ears". The ring cut PRPDP covers between 0 degrees to 100 degrees in the positive half cycle, and in the negative half cycle occurs between 190 degrees and 270 degrees.

The tram line PRPDP is represented in Figure 4.9 c), where the PRPDP appears "rabbit ear" too, however more similar to the ring cut. The PRPDP also appear more skew, a feature that is reported in literature for partial discharge occurring on the insulation along the cable length [77]. Positive PD occur between 0 and 110 degrees, and negative PD occurs between 180 and 280 degrees.

The PRPDP obtained in this study correspond to those reported by Arnold *et al.* [78] from his experimental results where he examined distinguishable features of different types of discharges.

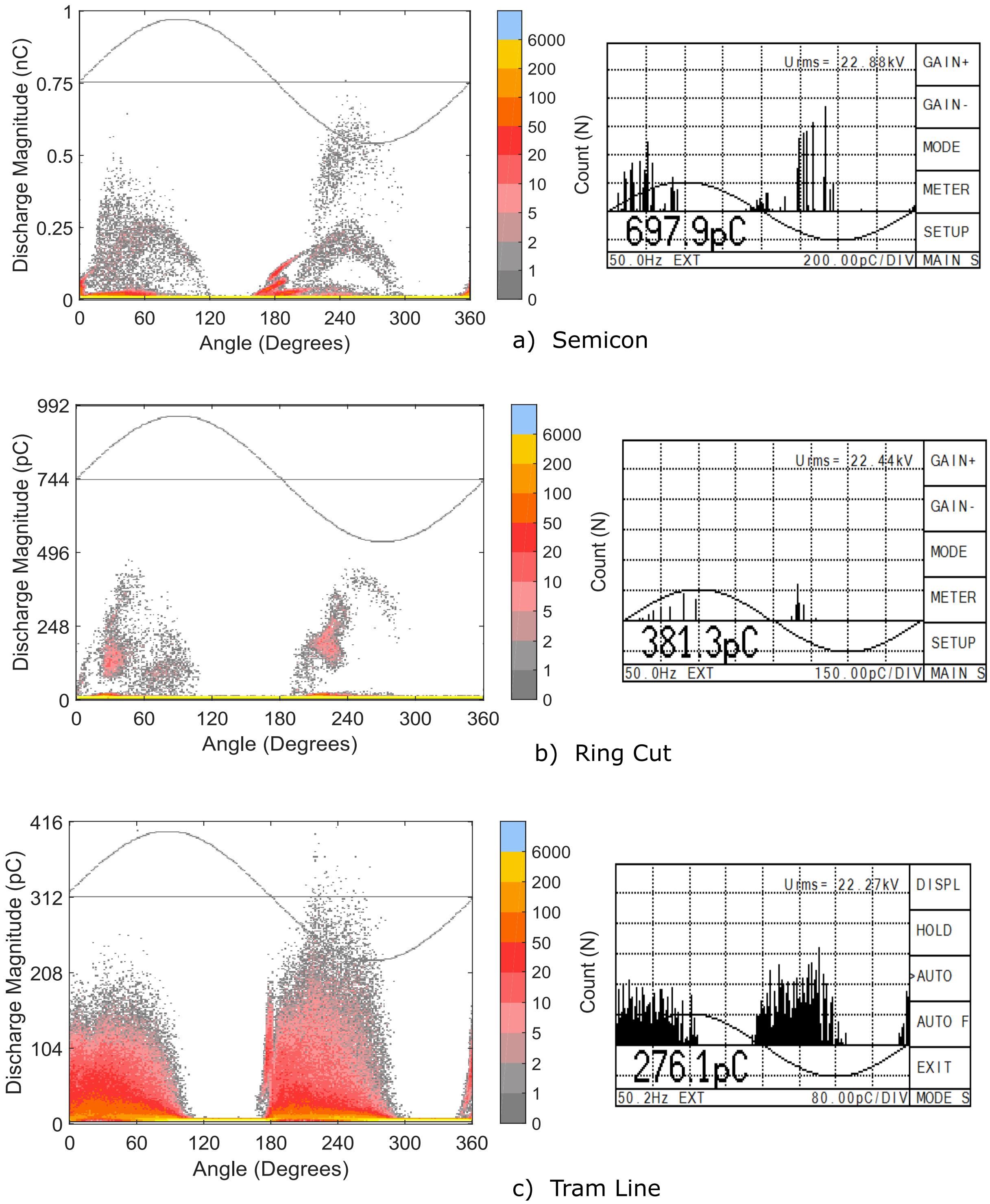

Figure 4.9: Similar occurring PRPDP for: a) Semicon feather PRPDP, b) Ring cut PRPDP and c) Tram line PRPDP, respectively from top

4.9 Summary and Conclusion

Accelerated ageing was conducted on uniquely defected cable terminations over a total of 878 hours. Although the accelerated PD ageing was done at 350 Hz, PD measurements were conducted at power frequency and the PD parameters investigated were the PDIV, the maximum apparent PD magnitude (Q_{max}), the PD PRR, and the PRPDP. A summarised table with PD parameter averages for each stage per defect is also found in A. With increase in ageing time, a behaviour trend categorized in 5 stages has been observed for the semicon, tram line and ring cut PD defects. The middle stages mainly 2, 3 and 4 had the most fluctuations of the PD parameters. PD measurements in this time frame could be misleading if only one reading is taken without further continuous monitoring and trending. On-line PD testing for continuous PD monitoring would therefore be an effective tool to pick up a more accurate PD reference point. The PDIV was fairly constant for all defects, with a gradual decrease only for the tram line defect. Q_{max} decreased with time for all defects, with the least values observed in the tram line. The PRR also decreased overall with time however with sudden increases near the end of the tests. The PRPDP evolved in between "rabbit ear" and "turtle" like appearing shapes. However, the patterns were distinct for each defect and were time-invariant through the ageing time. The pre-liminary results of the study were presented as a paper at a peer reviewed conference as found in B and F.

A model for the PD ageing phenomena is developed and discussed in the next chapter. The simulations further validate the mechanisms presented in explaining the observed changes in PD characteristics.

Chapter 5

PD Simulations to Validate Interpretations of the Observed PD Time Evolution Behaviour

Modelling and simulation of PD enables a confirmation of the theory used to explain the experimental findings, the conditions for a discharge event to occur are defined, the dielectric properties, the defect geometry and defect conditions. This chapter discusses the method used in determining model parameters and model structure. It then presents modelling changing PD phenomena resembling ageing PD in comparison to measured results and discusses results obtained from the model.

5.1 Insulation Models

Insulation models are used to establish an understanding of the physiochemical process in an insulation. These models are useful in the design and development of the insulation. Macroscopic models, also known as physical ageing models, focus on modelling ageing by expressing the growth of the damage leading to failure [23]. The presence of micro-defects in the insulation is considered as a catalyst leading to the electrical and mechanical degradation of the insulation. Macroscopic PD models convert the behaviour of the PD phenomenon to analytical terms or mathematical expressions, combining them to form an integrated model. Generally, PD models fall under any of the three types of models depending on phenomenon of interest namely: PD event model, PD aging and degradation model, and breakdown model [17]. The PD event models are the Perdersen, the Niemeyer model and the capacitive model. The Perdesen model forms the basis of the induced charge concept developed by Niemeyer [17]. Additionally, the capacitance model is based on the Perdesen model. The Perdesen model is built on the fundamental concept that when a discharge event occurs, the residual space charge deposited on the cavity surface wall makes the cavity a dipole. These dipoles in return induce charge on the electrodes. The total induced charge is therefore the difference between the electrode measured charge before a discharge event and that after the discharge event and is therefore termed apparent charge.

The Percolation model falls under the breakdown model. The Space Charge Dissado-Mazzanti-Montanari model, the Field Limited Space Charge and the electro dynamic stress model all belong to the PD ageing degradation category. The present study focuses on developing a PD event model based on the 3-capacitance model. The 3-capacitance model has been widely implemented in literature as discussed in subsection 5.2.1 and was chosen in the present work for modifications to simulate PD defect ageing mechanisms. The simulation results were then compared with the measured results as presented in this chapter.

5.2 The Capacitive PD Model Background

5.2.1 The History of the Capacitance Model

The lumped capacitance "ABC" PD model simulates electric fields within the void and in the void vicinity. The capacitance model was first introduced by Gemant and Philippoff in 1932 [79]. The void was taken as a capacitor, and the discharge event regarded as the instantaneous discharging of the capacitor. Since then, several works have been carried out to improve on the model. Whitehead [79] further improved the model, by adding a device that can be electronically controlled (thyristor) instead of the spark gap previously used to simulate a discharge arc. Paolleti and Golubev [43] further added a shunt conductance that represents the rest of the healthy insulation and another also for the void itself.

However, there has been criticism towards the shortfalls of the capacitive model, mainly stating that it is an inadequate representation of the void, that does not meet fundamental principles of electric, electrostatic and conduction field theories [80]. The argument is that representing a void with a capacitance is not accurate as the void walls are not at an equal potential. It has been further stated that, the Laplacian field based equation that relates charge to be directly proportional to the potential difference across the void does not apply after a PD event due to the presence of a Poissonian field of the residual space charge on the cavity wall. Additionally, the void capacitance is said to change during the discharge process which is not reflected in the capacitance model. These arguments were then later addressed by Achillides, Georghious and Kyriakides [79].

Dielectrics store electrical energy in a form of bound charges that do not contribute to the conductivity of the material [79]. Achillides et al. [79] then proved through mathematical expressions that the capacitance indeed increases with increase in the PD transient events. With regard to the presence of the Poissonian field, it was argued that only a vacuum can meet the expectation of not being under an external field. The dielectric interface between the void and the surrounding dielectric is said to have a tangential electric field of zero, meaning the surfaces of the cavity are at an equal potential.

The 3-capacitor PD model has been used in several studies in the literature involving parallel electrode systems as well as coaxial electrodes such as power cables to explore various PD characteristics and how they are affected by test conditions or changes in the defect regions. The classical capacitance model does not incorporate the physical phenomena internally in the dielectrics, but instead focuses more on attempting to reproduce the PD signals based on observed parameters from experiments and other supported literature [81]. A number of studies have been conducted where the lumped capacitance model approach was used to simulate PD activity.

Agoris et al. [81] have applied the capacitance model to model multiple cavities in a dielectric. By closely monitoring the voltage variations in each individual cavity, the found that PD in a cavity causes transient over-voltages in other cavities within its vicinity; hence triggers break down in other cavities. This is an interesting finding, that also demonstrates the benefits of a lumped capacitance model in helping with analysing local individual behaviour of cavities which is difficult by laboratory experiments.

Nikolay [82] *et al.* implemented the capacitive model in which he successfully explored different PD test circuit arrangements to determine the influence of modelling

PD in different PD measuring circuit layouts. In their study, they found that measuring PD across a measuring impedance connected to the coupling capacitor is not as effective as connecting the measuring impedance in series to the component representing the void. This informed the study to consider the effect of the test circuit in the model and where the PD signal was measured from.

Toader *et al.* [83] used the capacitive model to evaluate apparent charge and PD energy. They established that the cavity volume is directly proportional to the apparent Q_{max}. This is the observation in this study, the most severe defect shows the largest apparent Q_{max} across all defects.

Gowda *et al.* [84] implemented the capacitance model to evaluate the effect of different void geometries in the insulation and effect of applied voltage. They confirmed that an increase in applied voltage results in an increase in PD pulse repetitions.

Haghjoo *et al.* [85] further developed a comprehensive 3-capacitor PD model to investigate the effect of cavity size and cavity position on PD characteristic parameters such as PDIV, maximum apparent PD charge and PRR. In their study, they improved the model by including the effect of the void position with reference to the outer surface of the cable. They also introduced a field enhancement factor which is due to the electric field lines congestion as they transition between different mediums (across the cavity into the healthy insulation) [85].

Jaarsveldt [86] applied the comprehensive 3-capacitor model to simulate various cavity sizes and their influence on PD magnitude and PRR. He reported an increase in PD magnitude with an increase in cavity volume.

The simulation results regarding cavity size and location; applied voltage source amplitude; applied voltage source frequency; insulation temperature were in agreement with published experimental findings in [27, 32, 83, 87–89]. These comparisons have provided evidence of the viability to use the improved capacitance model for PD modelling. It is for this reason that the model was adopted for use in the present work in an effort to reproduce the measured time dependent PD behaviour. The next section presents the fundamental basis on which the capacitance model is implemented.

5.3 The Capacitance Model Equivalent Circuit

The model developed in this work is aimed at confirming through validation the understanding of the influence of the cavity environment that is responsible for the PD behaviour identified in the experimental results. This is achieved by implementing a comprehensive three capacitor model also known as the improved "abc" model whose equivalent circuit is shown in Figure 5.2. The main parameters of the model are defect geometries, bulk dielectric and surface parameters. As discussed earlier, the comprehensive model is an improved version of the basic model. The features that were improved are the replacement of the spark gap with a controlled device (switch) and the introduction of the probability function which is a function of de-trappable electrons to represent the stochastic availability of the seed electron. Additional improvements include the shunt conductance to represent the void wall conductance, the insulation in the same sector as the void and the rest of the healthy insulation, and also the use of the void position within the insulation in defining the void geometry. The comprehensive model also takes into account the field enhancement in the void due to the presence of the void in the insulation. This section gives a detailed overview of the circuit layout and define circuit parameters.

The model is implemented in MATLAB® Simulink® using the Simscape library, making use of the ode45 (Trapezoidal) simulation solver with a non-adaptive algorithm configuration.

5.3.1 PD Equivalent Circuit Model Parameters

If the test object is a power cable, the magnified geometrical set-up is as shown in Figure 5.1. Figure 5.2 shows insulation with a cavity defect connected across a voltage source and the equivalent RLC circuit. The capacitance and resistance parameters are derived from the void and insulation geometries and material properties of the insulation and the air trapped in the void.

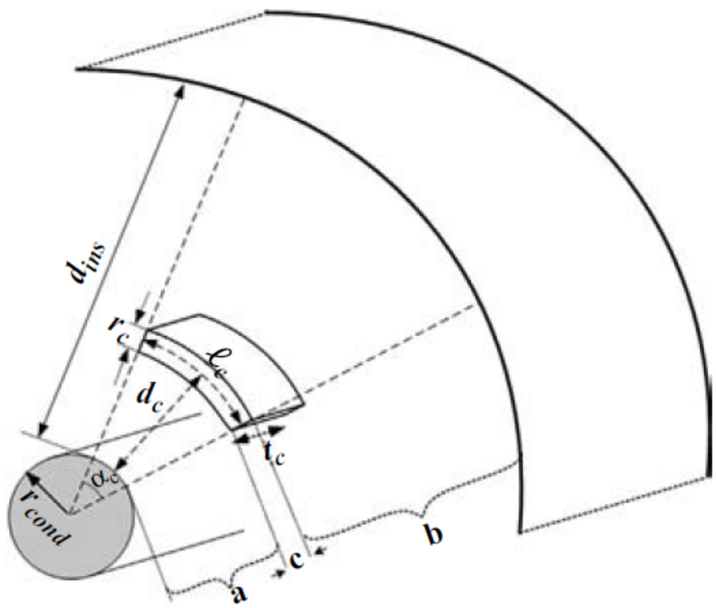

Figure 5.1: Cross section of a power cable containing a dielectric bound void [85]

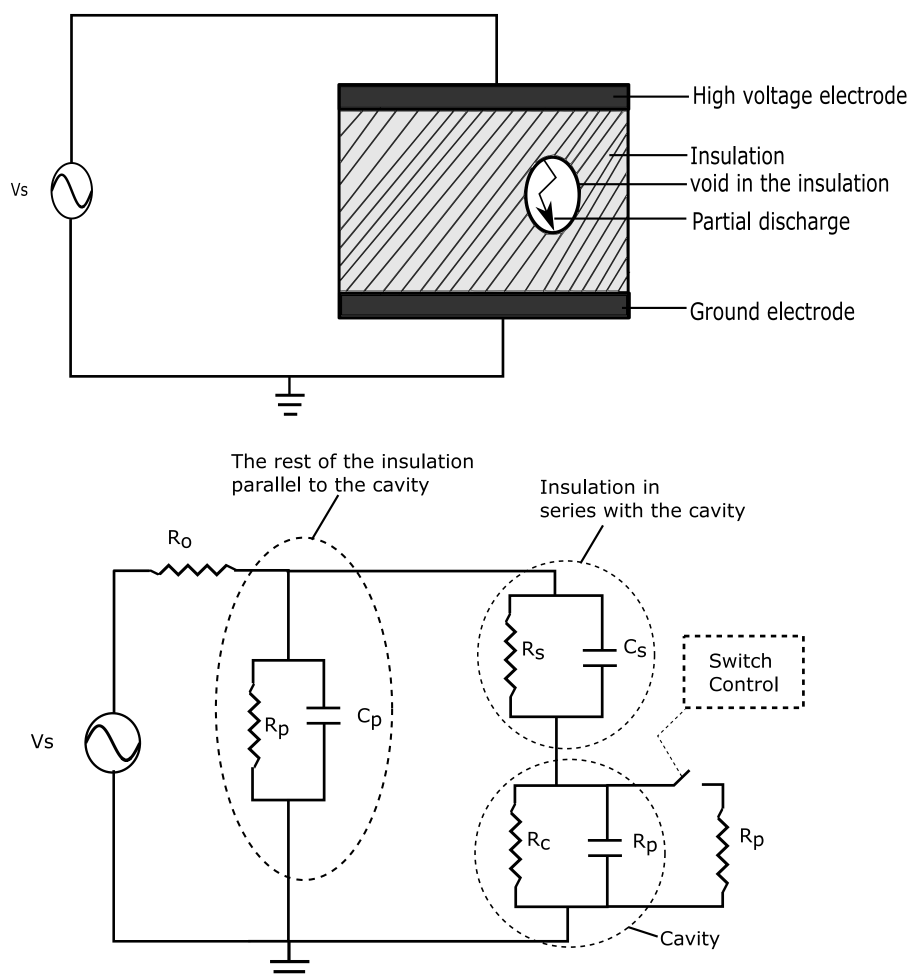

Figure 5.2: Capacitive circuit model for the insulation with a void

5.3.1.1 Calculating Parameters for Resistive and Capacitive Circuit Components

The equations used to derive the circuit parameters of the model are adopted from Hadhjoo *et al.* [85].

According to Gauss' law, the voltage between surfaces of concentric cylinders can be determined if each radius is known. Power cables have a coaxial geometry and insulation layers are concentric relative to the core center. Voltage between arbitrary different layer points of radius r_1 and r_2 in the insulation can therefore be determined by Equation 5.1. In which q denotes the charge present on the conductor surface per unit length of the conductor. The permittivity of the insulation material is given by e_{ins} and $D(r)$ is the electric flux density.

$$\Delta V|_{r_1}^{r_2} = \int_{r_1}^{r_2} \frac{D(r)}{\varepsilon_{ins}} = \frac{q}{2\pi\varepsilon_{ins}} ln(\frac{r_2}{r_1}) \tag{5.1}$$

The capacitance of the dielectric lying in between any two cylindrical surfaces can therefore be defined when the arc angle is given by α_c as shown in Equation 5.2.

$$C_{sector} = \frac{q_{sector}}{\Delta V|_{r_1}^{r_2}} = \frac{q(\alpha_c/2\pi}{\Delta V|_{r_1}^{r_2}} = \frac{\alpha_c \varepsilon_{ins}}{ln(\frac{r_2}{r_1})} \tag{5.2}$$

According to Figure 5.1 , the arc angle α_c is defined in Equation 5.3, which is the ratio of the arc length and the arc radius in radians.

$$\alpha_c = \frac{l_c}{(r_{cond} + d_c)} \tag{5.3}$$

For a given cavity width of t_c, the capacitance of region a and region b shown in Figure 5.1 is given by Equation 5.4 and Equation 5.5 respectively.

$$C_a = \frac{\varepsilon_{ins}}{ln(r_{cond} + d_c - \frac{r_c}{2})/r_{cond}} \cdot \frac{l_c}{r_{cond} + d_c} \cdot t_c \tag{5.4}$$

$$C_b = \frac{\varepsilon_{ins}}{ln(r_{cond} + d_{ins})/(r_{cond} + d_{ins} + \frac{r_c}{2})} \cdot \frac{l_c}{r_{cond} + d_c} \cdot t_c \tag{5.5}$$

Both region a and b are in series with the void, the total capacitance C_s of these two regions can therefore be represented by Equation 5.6.

$$C_S = \frac{C_a C_b}{C_a + C_b} \tag{5.6}$$

The embedded void capacitance t_c is given by Equation 5.7. The void medium is filled with air; hence the permittivity used is that of free space e_o.

$$C_c = \frac{\varepsilon_o}{ln(\frac{r_{cond}+d_c+\frac{r_c}{2}}{r_{cond}})} \cdot \frac{L_c}{r_{cond} + d_c} \cdot t_c \tag{5.7}$$

Meanwhile, the capacitance C_p of the rest of the healthy insulation is given by Equation 5.8. The full length of the cable is L.

$$C_p = \frac{2\pi\varepsilon_{ins}}{ln(\frac{r_{cond}+d_{ins}}{r_{cond}})} \cdot L \tag{5.8}$$

The resistance of the corresponding insulation regions is calculated by referring to the current density (J) and the electric flux density across the region denoted by D. σ_{ins} represents the insulation conductance. The current density $J(r_2)$ is expressed at level r_2 as in Equation 5.9.

$$J(r_2) = \frac{\sigma_{ins}}{\varepsilon_{ins}} D(r_2) \tag{5.9}$$

Using the current density, the current can be defined for a specified region depending on the arc angle, the arc length and the radius of the cylindrical surface.

$$I(r_2) = J(r_2)\alpha_c r_2 t_c \tag{5.10}$$

The resistance of the specified region will therefore be a ratio of Equation 5.1 and Equation 5.10 according to Ohm's law.

$$R|_{r_1}^{r_2} = \frac{\Delta V|_{r_1}^{r_2}}{I(r_2)} = \frac{1}{\alpha_c} \cdot \frac{1}{\sigma_{ins} t_c} ln \frac{r_2}{r_1} \tag{5.11}$$

According to Equation 5.11 , the resistance values for region a and b in Figure 5.1 are determined by Equation 5.12 and Equation 5.13.

$$R_a = \frac{1}{\sigma_{ins}} \frac{r_{cond} + d_c}{l_c t_c} ln(\frac{r_{cond} + d_c - \frac{r_c}{2}}{r_{cond}}) \tag{5.12}$$

$$R_b = \frac{1}{\sigma_{ins}} \frac{r_{cond} + d_c}{l_c t_c} ln(\frac{r_{cond} + d_{ins}}{r_{cond} + d_c + \frac{r_c}{2}}) \tag{5.13}$$

The combined resistance of region a and b is therefore given by.

$$R_s = R_a + R_b \tag{5.14}$$

The resistance of the void is determined in a similar way, except that the conductance used is that of the void surface and not of the bulk insulation material.

$$R_c = \frac{1}{\sigma_c} \frac{r_{cond} + d_c}{l_c + t_c} ln(\frac{r_{cond} + d_c + \frac{r_c}{2}}{r_{cond} + d_c - \frac{r_c}{2}}) \tag{5.15}$$

The resistance of the rest of the healthy insulation is given by.

$$R_p = \frac{1}{2\pi L \sigma_{ins}} ln(\frac{r_{cond} + d_i ns}{r_{cond}}) \tag{5.16}$$

The presence of the void in the insulation distorts the electric field distribution which inherently affects the capacitance and resistance parameters of the insulation in the same sector. The capacitance and resistance equations (Equation 5.6, Equation 5.7, Equation 5.14) hold true only when the electric field in the insulation is homogeneous. The electric field has been observed to be amplified by a factor defined by Equation 5.19:

$$K_{ef} = \frac{\varepsilon_r}{\varepsilon_r + 2(1 - \varepsilon_r) l_c t_c r_c A} \tag{5.17}$$

The area of the void is denoted by A, and for a spherical void with a radius a, it is given by:

$$A = \frac{1}{48a^3} \tag{5.18}$$

The enhancement factor is then simplified to be expressed as in Equation 5.19.

$$K_{ef} = \frac{3\varepsilon_r}{1 + 2\varepsilon_r} \tag{5.19}$$

The enhancement factor is applied to the calculated parameters in Equation 5.20, Equation 5.21 and Equation 5.22.

In the cavity, the electric field and therefore the capacitance is increased by the K_{ef} factor as shown in Equation 5.20.

$$C_c^{cor} = \frac{\varepsilon_r C_c}{K_{ef}} \tag{5.20}$$

In the insulation that is in series with the cavity, the electric field intensity and capacitance is reduced by the K_{ef} factor as shown in Equation 5.21.

$$C_s^{cor} = K_{ef} C_s \tag{5.21}$$

The resistance of the insulation in series with the void is increased by the K_{ef} factor as shown in Equation 5.22.

$$R_s^{cor} = \frac{R_s}{K_{ef}} \tag{5.22}$$

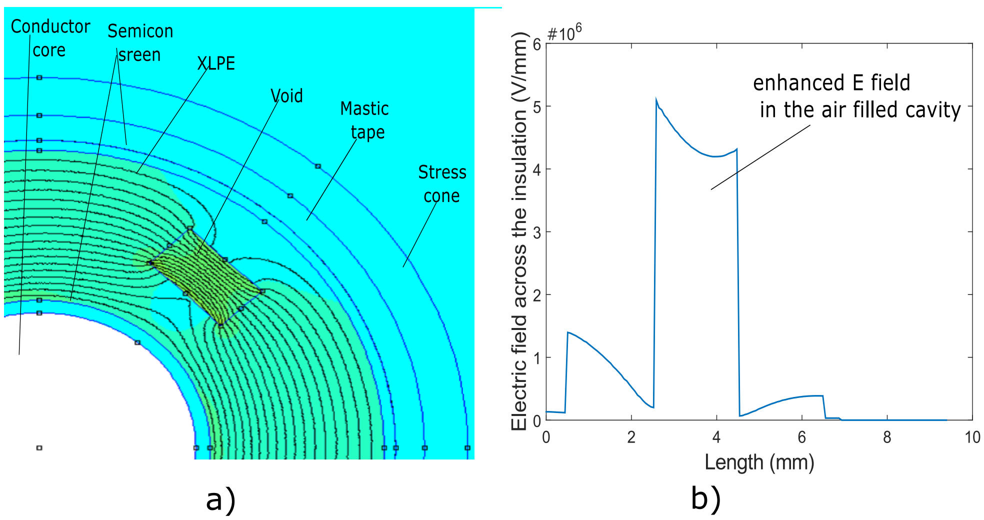

Figure 5.3: FEM simulation of a cavity in an insulation a) Electric field lines in an insulation containing a defect, b) Electric field intensity plots across the cable core

The electric field distribution as shown in Figure 5.3 from the FEM simulations show that the void is “squeezed” by the incoming electric field that end at the void interface with the insulation. From the void and insulation boundary to the region in the same sector, the electric fields deflect, consequently bulging the base of the insulation near the void. The resistance is therefore decreased as it is inversely related to surface area. Meanwhile, the capacitance of the same sector is enhanced.

5.3.1.2 Circuit Component Values as Implemented in Simulink®

The formulas furnished in the previous section were used to compute circuit parameters for each defect studied in the present work. The obtained values are shown in Table 5.1 and implemented in the Matlab® Simulink® model shown in Figure 5.4.

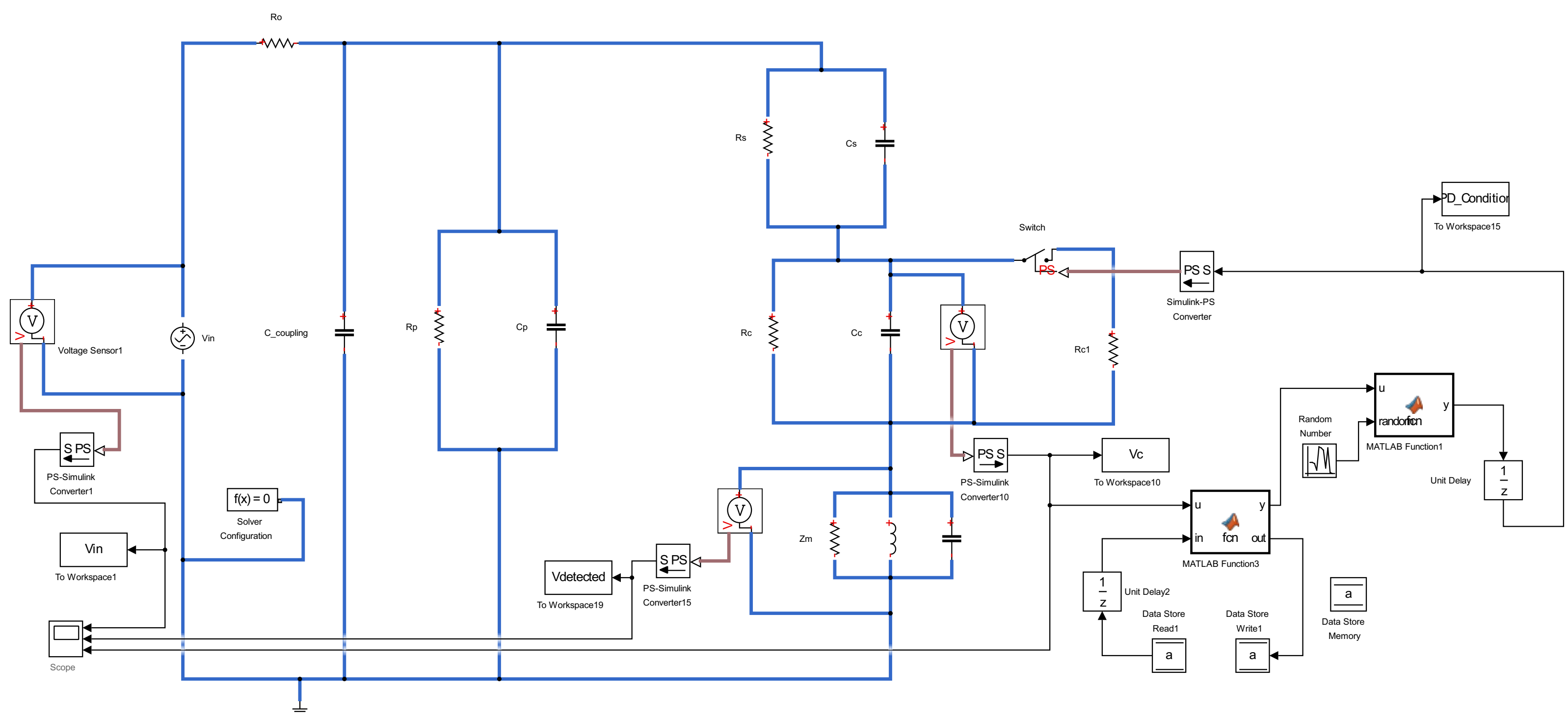

Figure 5.4: 3-Capacitance Model Layout Configuration in Simulink® [90]

Table 5.1: Defect dimensions and circuit component values

Defect Type	**Semicon Core 1 & 2**	**Semicon Core 3**	**Tram Line Core 1 & 2**	**Tram Line Core 3**	**Ring Cut Core 1 & 2**	**Ring Cut Core 3**
Defect Parameters (m)						
d_c	4.60E-3	4.60E-3	3.90E-3	3.60E-3	4.10E-3	3.60E-3
r_c	1.50E-3	1.50E-3	1.40E-3	2E-3	1E-3	2E-3
t_c	1E-3	5E-3	20E-3	20E-3	0.60E-3	0.60E-4
l_c	2.61E-4	3.66E-4	5.92E-6	1.09E-5	25.80E-3	22.60E-3
d_{insu}	4.60E-3	4.60E-3	4.60E-3	4.60E-3	4.60E-3	4.60E-3
r_{cond}	3.30E-3	3.30E-3	3.30E-3	3.30E-3	3.30E-3	3.30E-3
Circuit Components (ohm) , (F)						
R_c	5.77E10	8.21E10	1.19E12	9.20E11	6.48E9	1.48E10
R_s^{cor}	2.68E19	3.71E19	5.85E20	2.60E20	3.86E18	3.61E18
R_p	1.97E15	1.97E15	1.97E15	1.97E15	1.97E15	1.97E15
C_c^{cor}	3.70E-14	2.57E-14	1.97E-15	2.53E-15	2.77E-13	1.35E-13
C_s^{cor}	1.25E-14	9.02E-15	5.71E-16	1.29E-15	8.66E-14	1.29E-13
C_p	1.70E-10	1.70E-10	1.70E-10	1.70E-10	1.70E-10	1.70E-10

5.3.2 PD Phenomena Mechanisms Implemented in the Simulation Model

In the simulated PD mechanism, the PD event inception and extinction are represented respectively by the closing and opening of the switch in Figure 5.2. Some conditions need to be met in order for the said action to take place as presented in Figure 5.5 showing the flow chart of the PD event simulation algorithm. The PD inception and PD extinction process code is presented in the Appendix B as adopted from Jaarsveldt [90].

5.3.2.1 PD Inception (Switch Closing Mode)

The switch enters a closing mode, when the conditions for a discharge event to occur are met. This entails, that there is a seed electron available to start the avalanche development. The availability of the seed electron is a stochastic event that depends on various factors such as the number of de-trappable electrons on the cavity surface, which also depends on the charge decay constant. In order to simulate this event in the model, a random number is generated at every time instant to represent the seed electron unpredictable nature. In addition to the presence of a seed electron, the voltage across the void needs to exceed the breakdown strength of the void. This occurs when the seed electron is accelerated in a field sufficient for collisions that support avalanche development. When the avalanche reaches 10^8 electrons then it transitions from Townsend to streamer type of discharge. This occurs at a critical voltage known as the Partial Discharge Inception Voltage (PDIV).

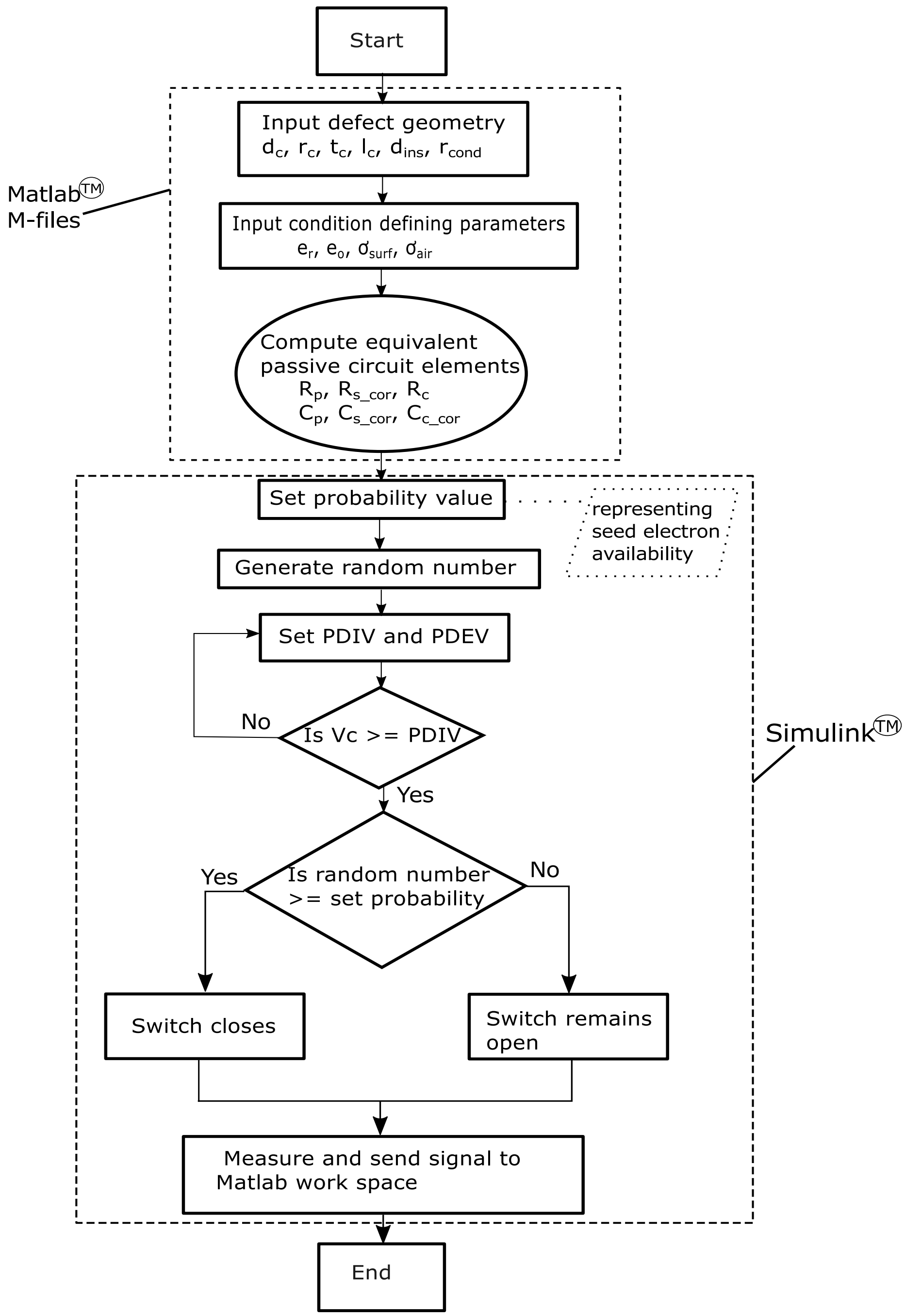

Figure 5.5: Process flow of the PD model simulation algorithm. The Simulink® part of the algorithm is implemented using the circuit shown in Figure 5.4.

The PDIV and PDEV were calculated through an iterative process to determine the voltage level that initiated PD with the computed circuit components corresponding to each defect.

5.3.2.2 PD Extinction (Switch Opening Mode)

The switch opens when the voltage across the void falls below a certain level causing PD extinction (the electron avalanche stops). The PDEV was maintained at 20 percent below PDIV. This decision is informed by the literature where it is known that PDEV is usually 20-50% of PDIV [32], and in the experimental results obtained in this study.

5.4 Simulating Defect Ageing in Comparison to Measured Results

The model output is in the form of a PD voltage signal. This section presents the obtained simulation results and compares them with the experimental results presented in chapter 3. Close similarities were observed between the two. The main parameters identified to change with PD ageing are the cavity or discharge area surface conductivity, gas content and pressure, temperature, statistical time lag and consequently breakdown voltage [15, 22]. Cavity defects under study are un-vented types of defects; hence are more sensitive to changes in internal gas content and pressure. According to Equation 5.23 the breakdown voltage depends on pressure and temperature. Therefore, the effect of temperature and pressure to the PD phenomenon is assumed to be accounted for in the algorithm by manually altering the breakdown voltage. The surface conductivity of an insulation ranges from orders of 10^{-15} S at virgin stage, to orders of 10^{-6} S for severely aged [50–52]. The interest of the study was to represent these parameters in the simulation, vary them based on the PD phenomenon behaviour explained in literature and monitor their influence to the PD voltage signal to determine any similarity with experimental results obtained.

$$V_b = \frac{\delta}{k_h}(2.1\sqrt{r_c} + 2.42r_c) \tag{5.23}$$

Where the humidity correctional factor is given by k_h while correctional factor accounting for temperature and pressure is given by δ (Equation 5.24).

$$\delta = 295\frac{p}{T} \tag{5.24}$$

In this case, p serves as the pressure of the gas enclosed within the void and T is the absolute internal temperature of the void. In order for a breakdown to occur, the voltage across the void V_c needs to exceed the breakdown voltage V_b.

5.4.1 Cavity PD Simulation Results

The simulation results for cavity type of defects (tram line and ring cut) were inherently similar, depicting similar mechanisms. Therefore, only one set of cavity simulation results are presented and discussed. In addition to that, the semicon feather defect PRPDP also showed cavity PD features simultaneously with a corona like features. The cavity portion of the PRPDP is discussed first in the next section.

5.4.1.1 Simulated Unaged Cavity Defect PD

Prior to defect ageing, that is long term exposure to PD, the cavity surface conductivity is initially low which means a long decay time constant. This means that residual charge is retained on the discharge surface area and provides the free electron. In the process oxygen is consumed by the discharge at a high rate. These conditions cause PD to occur at a lower PDIV; hence lower PD magnitudes initially as well. Therefore, the PDIV and PD magnitude starts out small initially followed by the increased observed in this study. To model this initial state, the void resistivity was set to the order of 10^{12} ohm, and the PDIV set to 8 kV, while PDEV set to 6 kV. Figure 5.6 shows the simulation results of the unaged stage as well as typical experimental PRPDP results. In both cases, the PRR is high, with PD covering the zero crossing. The PRPDP in each half cycle consists of PD with nearly the same magnitudes.

5.4.1.2 Simulated Moderately Aged Cavity Defect PD

At the end of unaged stage the conductivity increases as the discharge by-products accumulate on the surface (conductive liquid film layer). The breakdown voltage also increases and reaches a stable level. Therefore, at the moderately aged stage, the surface conductivity is higher, the breakdown voltage and PD magnitude are also higher. Due to increased surface conductivity, the charge decays quickly on the discharge surface area; hence the first discharge in each half cycle has a delay in seed electron availability. Therefore, there is a gap-over voltage at the beginning of each half cycle (the rising edge). This reduces the available time in a half cycle for multiple discharge events to occur. Consequently, the PD repetition rates begin to decrease at this point. It is reported and also observed in the present work that the PRPDP appears transitioning from turtle like to rabbit ear like.

a)
(Simulated)

b)
(Simulated)

c)
(Measured)

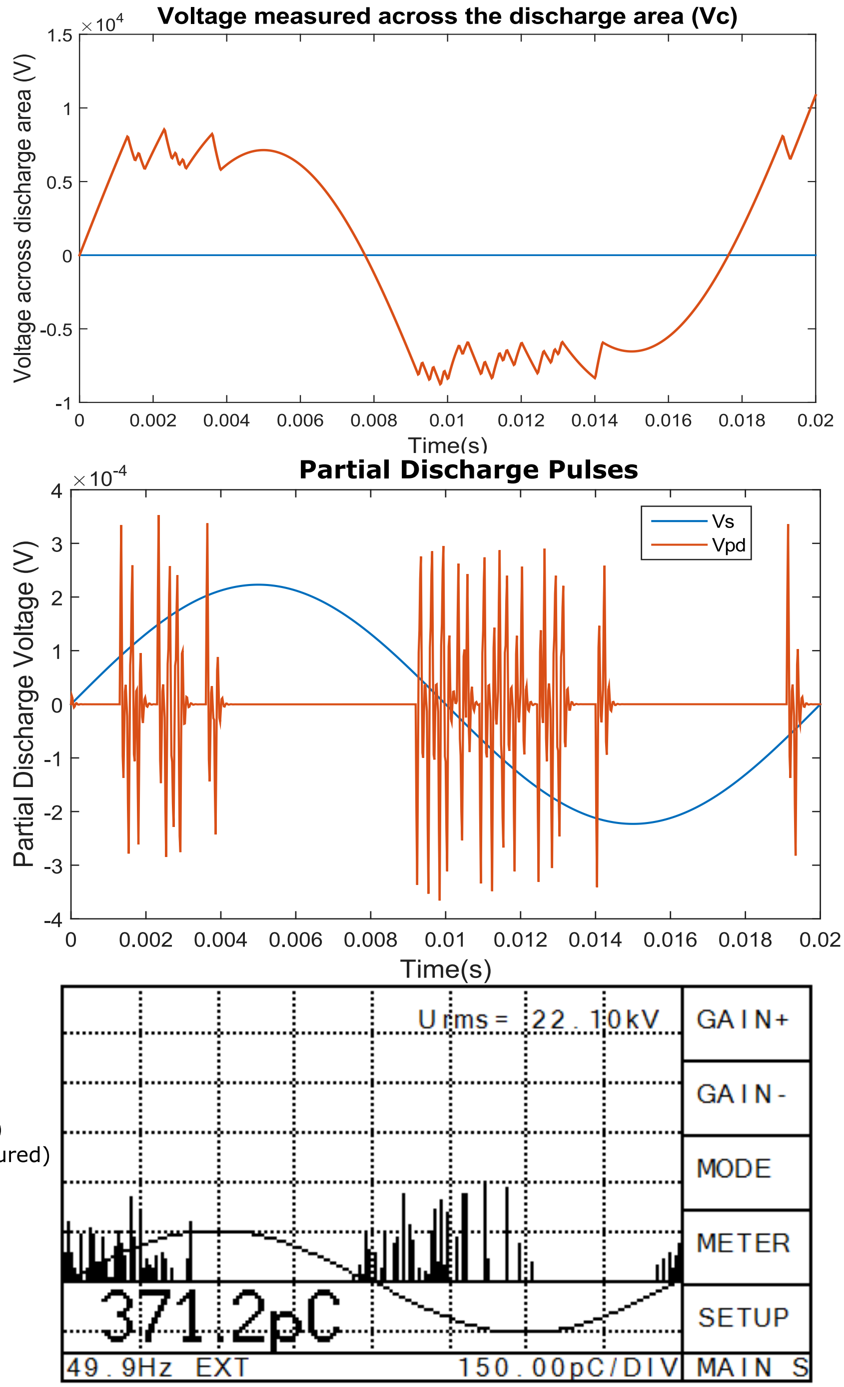

Figure 5.6: PRPDP of the cavity defect during first ageing stage, a) Simulation results of voltage across the cavity, b) Simulation results of detected voltage across the measuring impedance, c) Typical similar experimental results

To model the moderately aged condition, the void resistivity was set to the order 10^{10} ohm, and the PDIV set to 15 kV and PDEV to 12 kV. Figure 5.7 shows the moderately aged stage which is comparable to a typical measured experimental result. As seen in Figure 5.7, the PRR is lower while PD magnitudes are higher than in the unaged stage. Furthermore, large PD magnitudes occur at the rising edge of the applied voltage waveform.

5.4.1.3 Simulated Severely Aged Cavity Defect PD

When the cavity is severely aged, the discharge by-products (such as oxalic acids and acetic acids) are deposited on the cavity surface, increasing the surface conductivity further and causing the discharge area surface to erode and become inhomogeneous. The tips of the eroded surface create localised electric field enhanced regions with several local breakdowns occurring in parallel. This manifests as PD with a high pulse repetition rate of small magnitude PDs. The PRPDP is said to transition from rabbit ear to turtle like, appearing more bulgy. The parameters used to represent the explained phenomena were surface conductance of the order 10^{-8} S, a PDIV of 1 kV and a PDEV of 0.5 kV. Figure 5.8 shows the experimental PRPDP in agreement with the simulation result obtained. Literature [50, 61, 62, 69] reports the PRPDP to appearing more turtle like at the severely aged stage.

a)
(Simulated)

b)
(Simulated)

c)
(Measured)

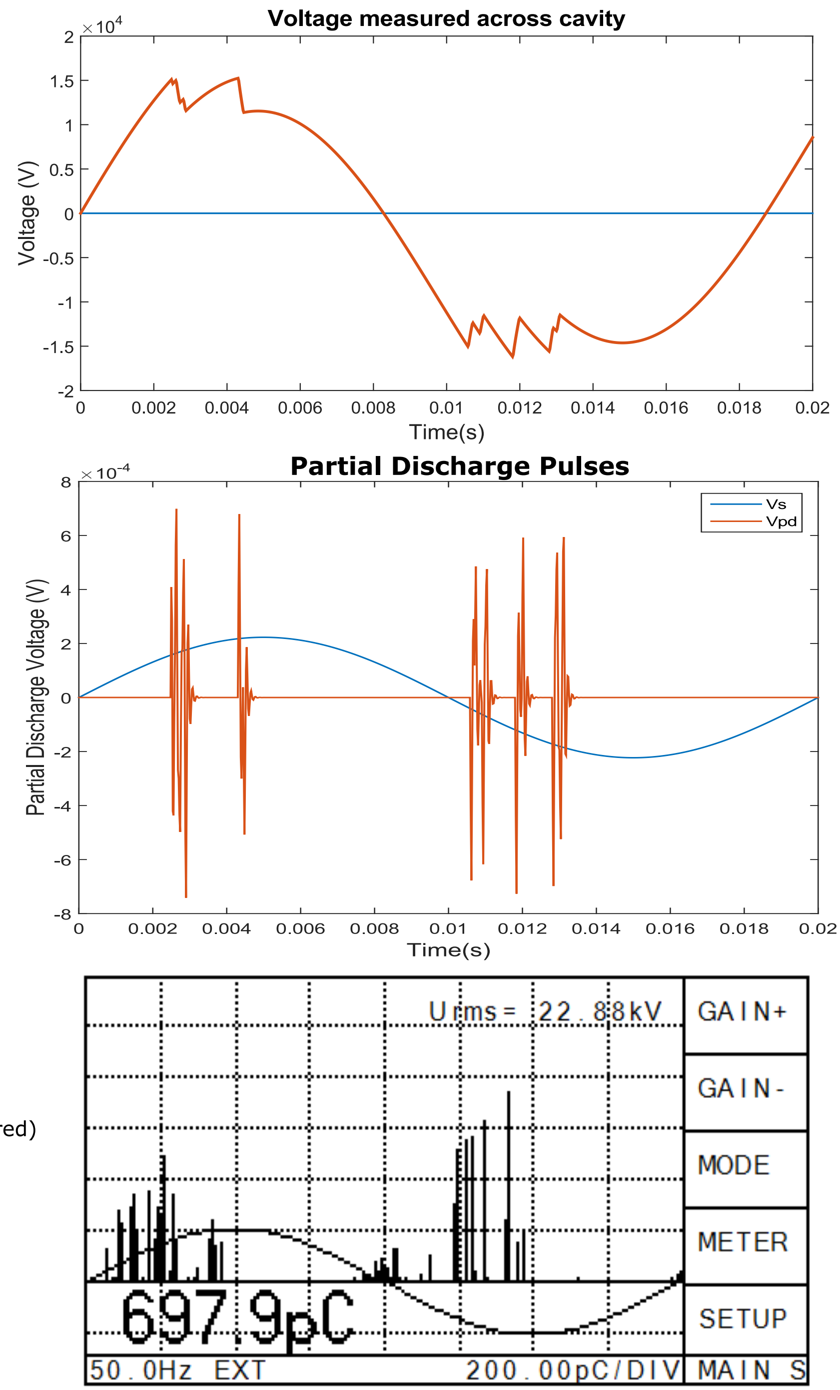

Figure 5.7: PRPDP of the cavity defect during second ageing stage, a) Simulation results of voltage across the cavity, b) Simulation results of detected voltage across the measuring impedance, c) Typical similar experimental results

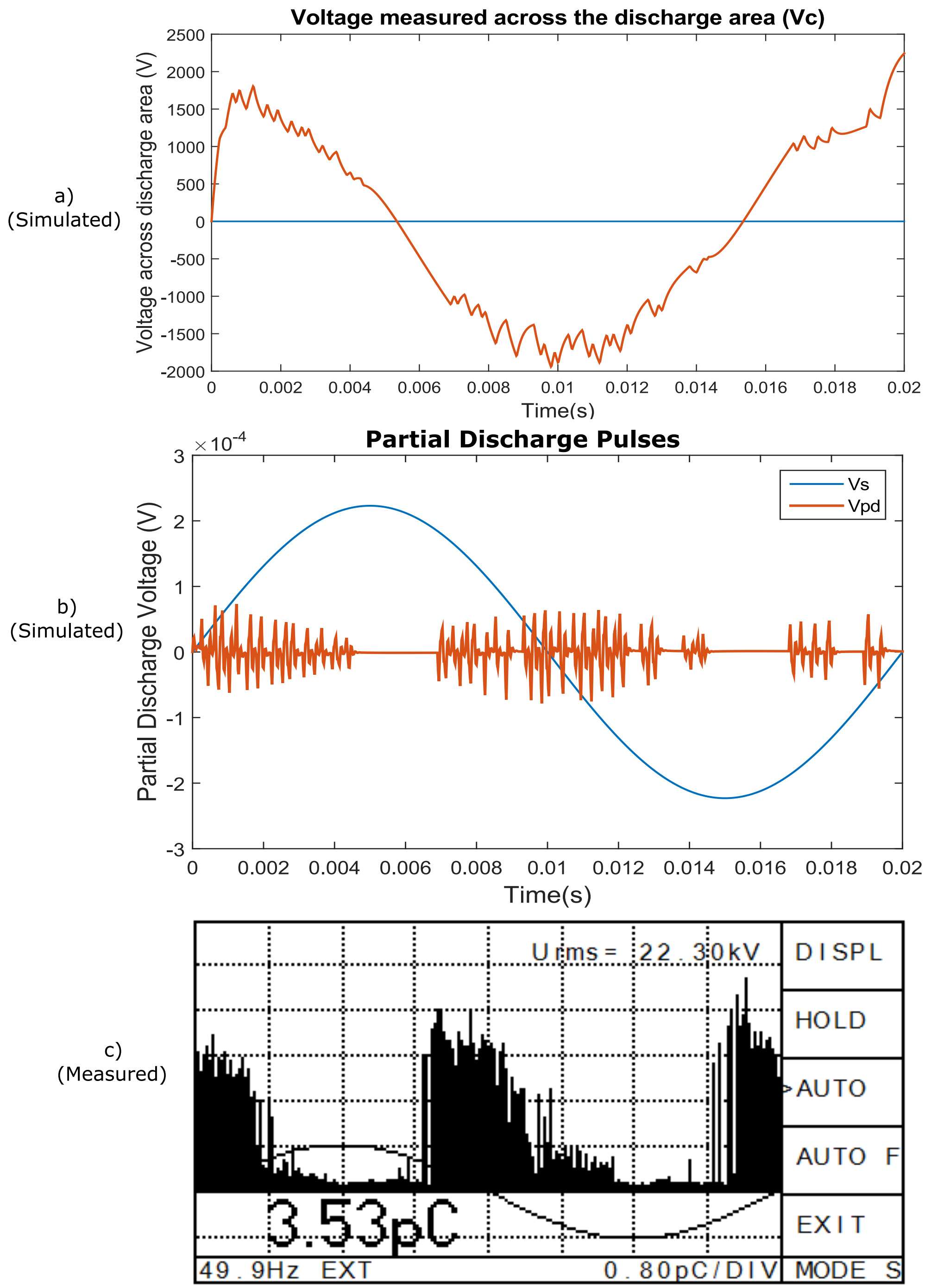

Figure 5.8: PRPDP of the cavity defect during third ageing stage,a) Simulation results of voltage across the cavity, b) Simulation results of detected voltage across the measuring impedance, c) Typical similar experimental results

5.4.1.4 PD Evanescence

Instances of PD evanescence were realised in the model to be an influence of the cavity surface resistivity. When the equivalent resistance component of the cavity surface is very low below orders of 10^6 ohm, it prevents a voltage build-up across the cavity that is sufficient to exceed the PDIV of the void. However this effect is not self-healing as it is degrading to the insulation. This low resistive path now conducts more leakage current; hence thermally degrading the insulation [43]. The heated up surface regions may evaporate, creating several small ditches on the surface.

5.4.2 Simulated Surface-Corona like Discharge vis-a-vis Semicon Feather Defect PD

The PRPDP of the semicon feather appeared with both features of corona and partly surface discharges. As discussed in Figure 4.1, regarding the electric field interplay in a defect region, due to the absence of significant residual charge, corona PD tends to cluster near the peak of the applied voltage. In the simulation, this type of PD pattern was achieved by making the impedance in series with the defect to be as small as possible. The impedance was reduced based on the concept shown in Figure 5.10, whereby R_c is the discharge area resistivity, while R_s is the resistivity of the area in series with the discharging area. Due to the nature of the semicon feather, R_s sector is only the surface thin layer of the XLPE leading to the cable end; hence allocated a smaller value of the order 10^8 ohm as opposed to the original value of 10^{19} ohm order. As a result, the PD shifted towards the peak and the PD magnitudes became larger too as shown in Figure 5.9.

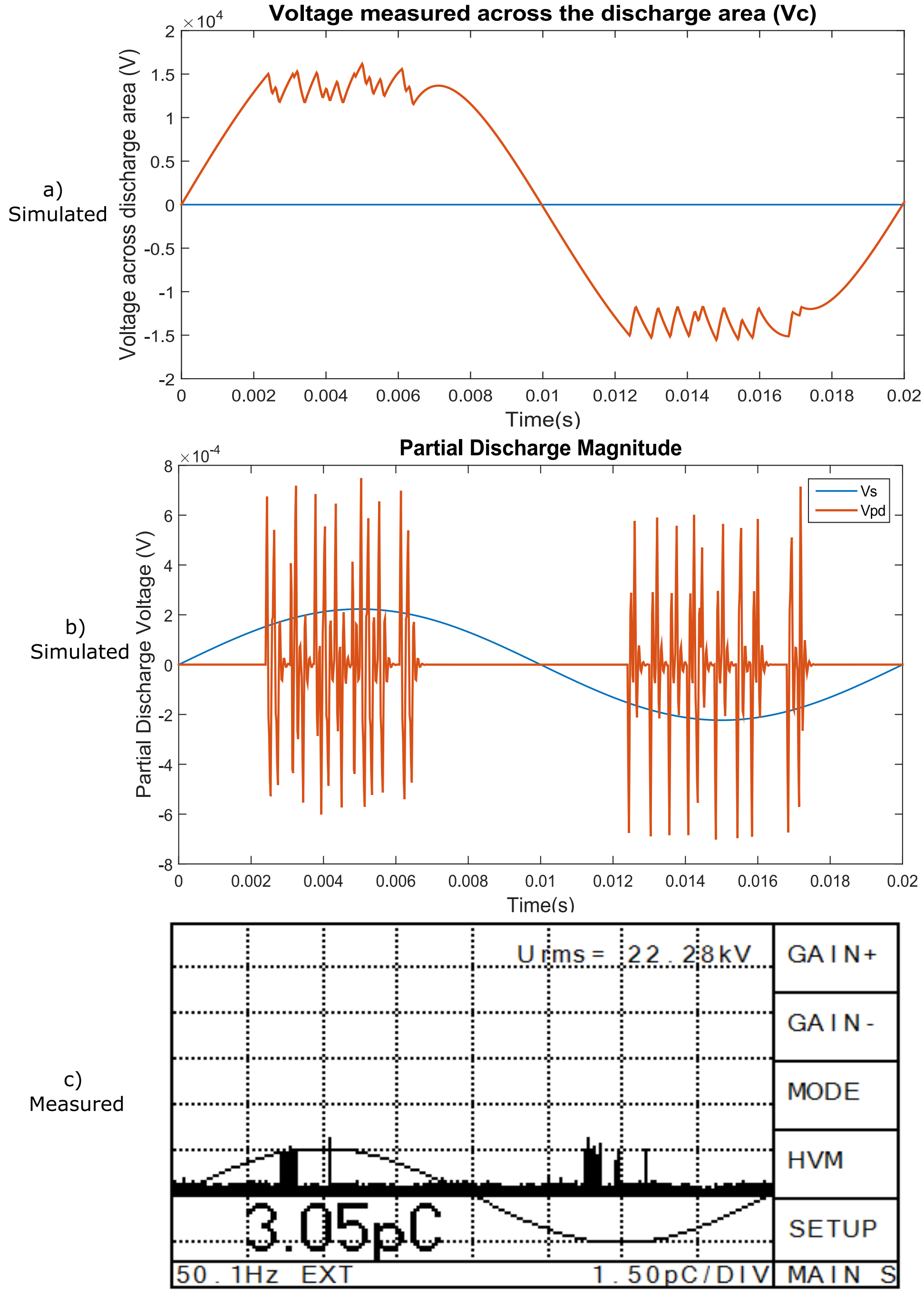

Figure 5.9: Surface Discharge and Corona-like PRPDP Simulation and Experimental Measured Results

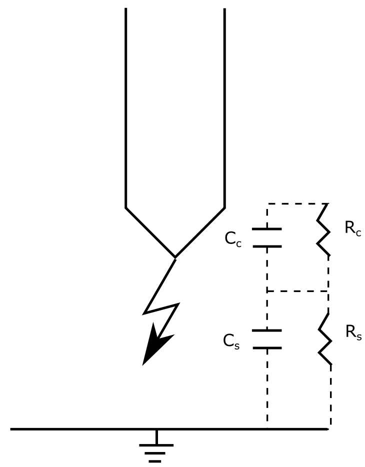

Figure 5.10: Illustration of the surface discharge modelling concept

5.5 Summary and Conclusion

The comprehensive 3-capacitor PD model was implemented in Simulink® using circuit parameters computed and derived for each defect under study. Model outputs were then discussed both for the void discharge and surface-corona like discharge by varying surface conductivity and PDIV based on experimental observed changes with PD ageing. The overview of experimental and simulation results is shown in C. The simulation results show good agreement with the experimentally obtained PD trends. A distinct observation in modelling a void discharge and a corona-surface type of discharge is the insulation regarded to be in series with the defect region as shown in Figure 5.1. It is noted that for a discharge other than the void, the dielectric (air) or outer thin insulation layer contributes to the phase position of the PD on the applied voltage waveform, by shifting it to the peak. The slight differences observed between the simulation results and the experimental results is attributed to the stochastic nature of PD which is challenging to replicate accurately.

Chapter 6

Conclusion

Accelerated PD induced ageing has been conducted on a semicon feather, tram line and ring cut defects made in XLPE power cable terminations. The PD parameters namely maximum apparent PD magnitude (Q_{max}), Pulse Repetition Rate (PRR) and Partial Discharge Inception Voltage (PDIV) were observed as they evolved with increase in ageing time. The research questions posed earlier in this study probed what are the time-evolution characteristics of PDs in typical installation defects in MV XLPE cable terminations. It was also further probed as to what is the explanation of the experimentally observed time-evolution behaviour of the PD and how can the mechanisms be validated through modelling. The following conclusions address the research questions:

1. The general trend observed across the semicon, ring cut and tram line is that of a decreasing maximum apparent PD magnitude from the beginning towards the time the tests were ended. With on-line condition monitoring, observation of such a behaviour should therefore not necessarily be interpreted as a self-healing behaviour, since the defects are still present and PD ageing continues despite the decrease or absence of measurable PD magnitude that is observed.

2. A sudden increase in PRR was also observed in the last ageing stage near the end of the test for the semicon and tram line defects. However, it could not be established if this behaviour would have been signalling imminent failure.

3. For all defects, the last ageing stage identified was the longest, it lasted nearly 43% of the total ageing time. This stage also had the least fluctuations in PD magnitude and PRR. PD ageing can take a significant length of time prior to failure. The last ageing stage observed was prolonged and was not eventful as the other stages. For on-line condition monitoring such a behaviour can be anticipated for PD that has been ageing for a long period of time.

4. The tram line had the least overall PRR. This could be useful in terms of finding a distinction between defects, the low PRR could be a sign of a defect occurring in a region further away from high electric fields, such as the semicon and XLPE insulation interface.

5. For the semicon, the PRPDP appeared one of a mixture of cavity PD and corona PD, with a "body part" in addition to the "rabbit ears". The PRPDP was shifted towards the peak of the applied voltage cycle.

6. For the ring cut and tram line, the PRPDP showed prominent PD at the zero crossing of the supply voltage waveform, and no PD at the peak of the applied voltage waveform. The PRPDP of this nature could therefore be regarded as a signatory feature of such defects in comparison to semicon feather defects.

7. The distinct appearance of the PRPDP per defect was present throughout ageing time. Therefore, the PRPDP can be regarded as a signatory feature distinguishing different defects and at any time instance of the ageing period.

8. The PDIV behavior of all defects remained fairly constant. However, the largest defect size gave the smallest PDIV and the largest maximum apparent PD magnitude throughout the ageing time. In comparison of defects, a lower PDIV is a symptom of a severe defect, and therefore a higher risk for the PDIV to fall within a voltage level as that of the operating level.

The above mentioned conclusions drawn from the study with respect to the PD evolution of the unique defects could be suggested as flags for identifying a defect and the extent of PD ageing in on-line condition monitoring.

From the simulations of the PD model implemented in Matlab® Simulink®, the factors that influenced the observed PD ageing behaviour were understood. The uniquely evolving PD behaviour was attributed to the effect of breakdown voltage and cavity surface resistivity. Both breakdown voltage and surface resistivity changed over time with ageing as the conductivity of the cavity surface changes which inherently also affected the build up of residual charge. This was established through iterative simulations of different breakdown voltages and different cavity surface resistivity based on the known characteristics that accompany the virgin stage, the moderately stage and the severely aged stage according to existing literature. The simulation results were resonant of the experimental obtained results.

One of the concerns was regarding what could be a reliable reference point between identifying the extent of PD degradation and possibly relating that as well to the defect type. The PDIV, Q_{max} and PRR trends show a similar evolution behaviour with ageing for all defects. This could provide a good reference point in terms of the state of progression of the deterioration of the dielectric. However, since the behaviour variation between the defects under study was closely similar, solely monitoring trends of PDIV, PRR or Q_{max} would not allow distinction of defects. Therefore, it is suggested that the PRPDP would serve as a more informative reference in terms of identifying unique defects and at the same time indicate the deterioration effect on the appearance of the PRPDP. Overall, tracing of the PDIV, PD magnitude and PRR simultaneously with the capturing the PRPDP form a more reliable approach to effectively monitor the dielectric condition.

As understood from literature, when it comes to field application for PD measurements on equipment that are in-service or in an environment with other operating equipment, the time domain measurements are easily jeopardised by electrical noise posing a challenge in filtering out the noise. Therefore, future recommendations are to conduct similar tests on the semicon, tram line and ring cut defect, electrically age the defects and monitor the signatures both in the time domain and the frequency domain simultaneously. It could be useful if the time domain and frequency domain signatures are monitored simultaneously and the best option considered.

The comprehensive capacitance PD model implemented served the purpose of identifying the different factors that contribute to the dynamics of the PD mechanism in the defect types studied. Further improvements on the model can be done to model the arc decay of the discharge in order to understand how its dynamic influences the PRPDP appearance if any.

Bibliography

[1] R. Bartnikas and K. Srivastava, *Power Cable Engineering*. Waterloo, Ontario: Standford Educational Press, 1st ed., 1986.

[2] W. A. Thue, ed., *Electrical Power Cable Engineering*. USA: CRC Press, 3 ed., 2011.

[3] J. Paoletti and A. Golubev, "Partial Discharge Theory and Technologies Related to Medium-Voltage Electrical Equipment," *IEEE Transactions on Industry Applications*, vol. 37, no. 1, pp. 90–103, 2001.

[4] A. Eigner and K. Rethmeier, "An Overview on the Current Status of Partial Discharge Measurements on AC High Voltage Cable Accessories," *IEEE Electrical Insulation Magazine*, vol. 32, pp. 48–55, 2016.

[5] "SANS-1339 South African National Standard Electric cables Cross-linked polyethylene (XLPE) insulated cables for rated voltages 3.8/6.6 kV to 19/33 kV," 2010.

[6] R. Strobl, W. Haverkamp, G. Malin, and F. Fitzgerald, "Evolution of stress control systems in medium voltage cable accessories," in *IEEE Transmission and*

Distribution Conference and Exposition, 2001 IEEE/PES, vol. 2, pp. 843–848, 2001.

[7] Y. Zhou, Y. Qin, and P. Chappell, "Cost-effective on-line partial discharge measurements for cables," *IEEE Electrical Insulation Magazine*, vol. 22, no. 2, pp. 31–38, 2006.

[8] Y. Jiang, H. Min, J. Luo, Y. Li, X. Jiang, R. Xia, and W. Li, "Partial Discharge Pattern Characteristic of HV Cable Joints with Typical Artificial Defect," in *Asia-Pacific Power and Energy Engineering Conference (APPEEC)*, (Chengdu, China), pp. 1–4, 2010.

[9] S. A. Boggs, "Partial Discharge: Overview and Signal Generation," *IEEE Electrical Insulation Magazine*, vol. 6, no. 4, pp. 33–39, 1990.

[10] R. Bartnikas, "Partial Discharges, Their Mechanism, Detection and Measurement," *IEEE Transactions on Dielectrics and Electrical Insulation*, vol. 9, no. 5, pp. 763–808, 2002.

[11] L. Renforth, R. R. Mackinlay, M. Seltzer-Grant, and R. Shuttleworth, "Online Partial Discharge (PD) Spot Testing and Monitoring HV Cable Sealing Ends," in *Cigre Session 2008*, (Paris), pp. B1–205, CIGRE.

[12] Aberdare Cables, "Vultex XLPE Medium Voltage Electric Cable - 6,6kV to 33kV," (Brochure. URL: http://www.aberdare.co.za/product-categories/building-construction-non-residential/ [Last Accessed Mar.03, 2018]).

[13] "SANS 60270 : 2000 South African National Standard High-voltage test techniques Partial discharge measurements," 2000.

[14] G. Stone, "Partial Discharge Diagnostics and Electrical Equipment Insulation Condition Assessment," *IEEE Transactions on Electrical Insulation*, vol. 12, no. 5, pp. 89 –904, 2005.

[15] P. H. F. Morshuis, "Partial discharge mechanisms leading to breakdown, analyzed by fast electrical and optical measurement," Ph.D. Thesis, Delf University, 1993.

[16] R. Bartnikas, "A comment concerning the rise times of partial discharge pulses," *IEEE Transactions on Dielectrics and Electrical Insulation*, vol. 12, no. 2, pp. 196–202, 2005.

[17] L. Niemeyer, "A Generalized Approach to Partial Discharge Modeling," *IEEE Transactions on Dielectrics and Electrical Insulation*, vol. 2, no. 4, pp. 510–528, 1995.

[18] S. Boggs, "Partial discharge. III. Cavity-Induced PD in Solid Dielectrics," *IEEE Electrical Insulation Magazine*, vol. 6, no. 6, pp. 11–20, 1990.

[19] C. Nyamupangedengu, "Time-varying partial discharge spectral characteristics in solid polymer insulation," *IET Science, Measurement and Technology*, vol. 6, no. 2, pp. 85–95, 2012.

[20] G. Mazzanti, G. C. Montanari, and L. A. Dissado, "Electrical aging and life models: The role of space charge," *IEEE Transactions on Dielectrics and Electrical Insulation*, vol. 12, no. 5, pp. 876–890, 2005.

[21] G. Mazzanti, G. C. Montanari, and F. Civenni, "Model of inception and growth of damage from microvoids in polyethylene-based materials for HVDC cables part 1: Theoretical approach," *IEEE Transactions on Dielectrics and Electrical Insulation*, vol. 14, no. 5, pp. 1242–1254, 2007.

[22] W. Le, "Physical Model of Pd Behavior and Relevant Damage Growth From Micro-Cavities in Polyethylene-Based," Ph.D. Thesis, University of Bologna, 2011.

[23] G. Mazzanti, G. C. Montanari, and L. A. Dissado, "Electrical aging and life models: The role of space charge," *IEEE Transactions on Dielectrics and Electrical Insulation*, vol. 12, no. 5, pp. 876–890, 2005.

[24] J. Densley, "Ageing Mechanisms and Diagnostics for Power Cables - An Overview," *IEEE Electrical Insulation Magazine*, vol. 17, no. 1, pp. 14–22, 2001.

[25] L. A. Dissado and K. Wu, "Percolation Model for Electrical Breakdown in Insulating Polymers," in *Annual Report Conference on Electrical Insulation and Dielectric Phenomena*, no. 1, (Colorado, USA), pp. 514–518, 2004.

[26] D. R. Cornish, "Msc Engineering Dissertation Nanocomposite Epoxy-Resin Using Partial Discharge Detection Methods," pp. 6–35, MSc. Dissertation, University of the Witwatersrand, 2014.

[27] N. Ahmed and N. Srinivas, "On-line versus off-line Partial Discharge Testing in Power Cables," in *2001 IEEE/PES Transmission and Distribution Conference and Exposition. Developing New Perspectives (Cat. No.01CH37294)*, vol. 2, (Atlanta, Georgia), pp. 865–870, 2001.

[28] N. Ahmed and N. Srinivas, "On-Line Partial Discharge Detection in Cables," in *IEEE Annual Report - Conference on Electrical Insulation and Dielectric Phenomena*, (Minneapolis, USA), pp. 214 – 217, 1997.

[29] E. David, J.-L. Parpal, and J.-P. Crine, "Aging of XLPE cable insulation under combined electrical and mechanical stresses," in *Conference Record of the 1996*

IEEE International Symposium on Electrical Insulation, vol. 2, (Montreal, Quebec, Canada), pp. 716–719, 1996.

[30] D. Fynes-clinton and C. Nyamupangedengu, "Partial Discharge Characterization of Cross-Linked Polyethylene Medium Voltage Power Cable Termination Defects at Very Low Frequency (0 . 1 Hz) and Power Frequency Test Voltages," *IEEE Electrical Insulation Magazine*, vol. 32, no. 4, pp. 15–23, 2016.

[31] D. Fynes-Clinton, "PD Characteristics of Typical MV XLPE Power Cable Termination Defects at VLF and Power Frequency Test Voltages," pp. 1–79, MSc. Dissertation, University of Witwatersrand, 2016.

[32] N. Ahmed and N. Srinivas, "PD Types and their Detection Possibilities by PD Test Methods," in *Annual Report Conference on Electrical Insulation and Dielectric Phenomena*, (Canada), pp. 307–310, 2001.

[33] M. S. Mashikian and A. Szatkowski, "Medium voltage cable defects revealed by off-line partial discharge testing at power frequency," *IEEE Electrical Insulation Magazine*, vol. 22, no. 4, pp. 24–32, 2006.

[34] T. Munih and D. Miljavec, "A method for accelerated ageing of electric machine insulation," in *16th International Conference on Mechatronics*, (Brno, Czech Republic), pp. 65–70, 2014.

[35] G. Mazzanti and G. C. Montanari, "A comparison between XLPE and EPR as insulating materials for HV cables," *IEEE Transactions on Power Delivery*, vol. 12, no. 1, pp. 15–26, 1997.

[36] R. J. Densley, R. Bartnikas, and B. Bernstein, "Multiple stress aging of solid-dielectric extruded dry-cured insulation systems for power transmission cables," *IEEE Transactions on Power Delivery*, vol. 9, no. 1, pp. 559–571, 1994.

[37] R. Bartnikas, R. J. Densley, and R. M. Eichhorn, "Long term accelerated aging tests on distribution cables under wet conditions," *IEEE Transactions on Power Delivery*, vol. 11, no. 4, pp. 1695–1699, 1996.

[38] R. Lyle and J. W. Kirkland, "An Accelerated Life Test For Evaluating Power Cable Insulation," *IEEE Transactions on Power Apparatus and Systems*, vol. PAS-100, no. 8, pp. 3764–3774, 1981.

[39] C. Nyamupangedengu and I. R. Jandrell, "Influence of supply voltage frequency and magnitude on PD pulse parameters," *IEEE Transactions on Dielectrics and Electrical Insulation*, vol. 15, no. 6, pp. 1590–1600, 2008.

[40] C. Nyamupangedengu and I. R. Jandrell, "Partial discharge spectral response to variations in the supply voltage frequency," *IEEE Transactions on Dielectrics and Electrical Insulation*, vol. 19, no. 2, pp. 521–532, 2012.

[41] R. Bartnikas, H. Doepken, G. Eichhorn, G. Rittmann, and W. Wilkens, "Accelerated Life Testing of Wet Cable Specimens at Frequencies above 60 Hz," *IEEE Transactions on Power Apparatus and Systems*, vol. PAS-99, no. 4, pp. 1575–1585, 1980.

[42] IEEE Std1407.(2008), "IEEE Guide for Accelerated Aging Tests for Medium-Voltage (5 kV35 kV) Extruded Electric Power Cables Using Water-Filled Tanks," 2008.

[43] G. Paoletti and A. Golubev, "Partial discharge theory and applications to electrical systems," in *Conference Record of 1999 Annual Pulp and Paper Industry Technical Conference*, (Seattle, Washington), pp. 124–138, 1999.

[44] A. Mor, P. Morshuis, P. Llovera, V. Fuster, and A. Quijano, "Localization techniques of partial discharges at cable ends in off-line single-sided partial discharge cable measurements," *IEEE Transactions on Dielectrics and Electrical Insulation*, vol. 23, no. 1, pp. 428–434, 2016.

[45] "IEEE Guide for Partial Discharge Testing of Shielded Power Cable Systems in a Field Environment," 2007.

[46] M. Pompili, C. Mazzetti, M. Libotte, and E. O. Forster, "The Effect of the Definition Used in Measuring Partial Discharge Inception Voltages," *IEEE Transactions on Electrical Insulation*, vol. 28, no. 6, pp. 1002–1006, 1993.

[47] C. Nyamupangedengu, *Pd-Type-Dependent Spectral Bandwidth in Solid Polymer*. PhD thesis, University of Witwatersrand, 2011.

[48] E. Gulski and F. Kreuger, "Computer-aided Recognition of Discharge Sources," *IEEE Transactions on Electrical Insulation*, vol. 27, no. 1, pp. 82–92, 1992.

[49] E. Kuffel, W. S. Zaengl, and J. Kuffel, *High Voltage Engineering: Fundamentals*. 2nd ed. Newnes: Butterworth-Heinemann, 2000.

[50] J. Li, W. Si, X. Yao, and Y. Li, "Measurement and simulation of partial discharge in oil impregnated pressboard with an electrical aging process," *IET Measurement Science and Technology*, vol. 20, no. 10, pp. 105701(1–7), 2009.

[51] K. Temmen, "Evaluation of surface changes in flat cavities due to ageing by means of phase-angle resolved partial discharge measurement," *Journal of Physics D: Applied Physics*, vol. 33, no. 6, pp. 603–608, 2000.

[52] P. V. Glahn, R. Van Brunt, and T. Las, "Nonstationary behaviour of partial discharge during discharge induced ageing of dielectrics," in *IEE Proceeding-Science Measurement Technology*, vol. 124, pp. 37–45, 1995.

[53] H. A. Illias, G. Chen, and P. L. Lewin, "Partial discharge within a spherical cavity in a dielectric material as a function of cavity size and material temperature," *Science, Measurement & Technology, IET*, vol. 6, no. 2, pp. 52–62, 2012.

[54] J. C. Devins, "The physics of partial discharges in solid dielectrics," *IEEE Transactions on Electrical Insulation*, vol. EI-19, no. 5, pp. 475–495, 1984.

[55] T. Tanaka, "Internal partial discharge and material degradation," *IEEE Transactions on Electrical Insulation*, vol. EI-21, no. 6, pp. 899–905, 1986.

[56] R. Van Brunt, "Physics and Chemistry of Partial Discharge and Corona Recent Advances and Future Challenges," *IEEE transactions on Dielectrics and Electrical Insulation*, vol. 1, no. 5, pp. 761–784, 1994.

[57] L. Wang, A. Cavallini, G. C. Montanari, A. Vaughan, and N. Freebody, "PD-induced surface degradation of insulation- embedded cavities : microscopic investigation," in *Conference Proceedings of ISEIM2011*, (Kyoto, Japan), pp. 121–124, 2011.

[58] A. Gjaerde and J. Sletbak, "Influence of partial discharges on void gas pressure," in *International Conference on Partial Discharge*, (Canterbury), pp. 119–120, 1993.

[59] P. Morshuis, "Assessment of Dielectric Degradation by Ultrawide-band PD Detection," *IEEE Transactions on Dielectrics and Electrical Insulation*, vol. 2, no. 5, pp. 744–760, 1995.

[60] Y. Feng, X. Chen, Y. Xu, and X. Cau, "Electrical Trees and Partial Discharges Degradation Characteristics in XLPE Cable Insulation at High Temperature," in *8th International Conference on Insulated Power Cables*, (Paris), pp. 508–512, 2011.

[61] C. S. Kim, T. Kondo, and T. Mizutani, "Change in PD Pattern with Aging," *IEEE Transactions on Dielectrics and Electrical Insulation*, vol. 11, no. 1, pp. 13–18, 2004.

[62] Y. Z. Arief, H. Ahmad, and M. Hikita, "Partial discharge characteristics of XLPE cable joint and interfacial phenomena with artificial defects," in *2nd IEEE International Conference on Power and Energy*, no. PECon 08, (Malaysia), pp. 1518–1523, 2008.

[63] S. Ilhan and A. Ozdemir, "Partial Discharge Amplitude Distribution for the Evaluation of Insulation Ageing," in *5th International Conference on Electrical and Electronics Engineering*, (Bursa), pp. 251–254, 1988.

[64] Z. Ahmed, G. A. Hussain, L. Varacka, J. Kudelcik, and M. Lehtonen, "Analysis Of Partial Discharge Signals In Medium Voltage XLPE Cables," in *17th International Scientific Conference on Electric Power Engineering (EPE)*, (Prague), pp. 1–6, 2016.

[65] S. Tokunaga, T. Tsurusaki, Y. Arief, S. Ohtsuka, T. Mizuno, and M. Hikita, "Partial discharge characteristics till breakdown for XLPE cable joint with an

artificial defect," in *2nd IEEE International Conference on Power and Energy*, vol. PECon 08, (Nagoya), pp. 1518–1523, 2008.

[66] F. Gutfleisch, "Measurement and Simulation of PD in Epoxy Voids," *IEEE Transactions on Dielectrics and Electrical Insulation*, vol. 2, no. 5, pp. 729 – 743, 1995.

[67] M. I. Qureshi, A. Al-Arainy, and N. H. Malik, "Effect of accelerated laboratory aging on selected electrical properties of medium-voltage heat shrink cable joints," *Taylor & Francis*, vol. 42, no. 5, pp. 496–506, 2014.

[68] J. Pihera, P. Martinek, J. Klasna, and B. Paslavsky, "Partial discharges of thermally aged insulation," in *Electrical Insulation and Dielectric Phenomena Conference*, no. 82, (Virginia Beach), pp. 147–151, 2009.

[69] H. Yoshida, Z. Tian, M. Hikita, H. Miyata, M. Reseamh, and F. Ud, "Study of the time evolution of partial discharge characteristics and interfacial phenomena of simulated XLPE cable joint," in *International Symposium on Electrical Insulating Materials*, (Toyohashi), pp. 501–504, 1998.

[70] M. G. Danikas, "On the Damage of Insulating Materials Below Inception Voltage," *Journal of Electrical Engineering*, vol. 52, no. 11, pp. 367–371, 2001.

[71] H. A. Illias, *Measurement and Simulation of Partial Discharges within a Spherical Cavity in a Solid Dielectric Material*. PhD thesis, University of Southampton, 2011.

[72] G. Bahder, T. Garrity, M. Sosnowski, R. Eaton, and C. Katz, "Physical Model of Electric Aging and Breakdown of Extruded Polymeric Insulated Power Cables," *IEEE Transactions on Power Apparatus and Systems,*, vol. PAS-101, no. 6, pp. 1379–1390, 1982.

[73] H. Illias, Low Tau Jian, A. H. A. Bakar, and H. Mokhlis, “Partial discharge simulation under various applied voltage waveforms,” in *PECon 2012 - IEEE International Conference on Power and Energy*, no. December, (Kota Kinabalu, Malaysia), pp. 967–972, 2012.

[74] D. Götz and H. T. Putter, “UHF PD-diagnosis at high voltage cable terminations-international case studies,” in *13nth International Electrical Insulation Conference(INSUCON)*, (Birmingham), pp. 1–5, 2017.

[75] H. Illias, Y. Teo Soon, A. A. Bakar, H. Mokhlis, G. Chen, and P. L. Lewin, “Partial Discharge Patterns in High Voltage Insulation,” in *Power and Energy (PECon), 2012 IEEE International Conference in*, (Kota Kinabalu), pp. 750–755, 2012.

[76] M. Tozzi, T. Srl, A. Cavallini, and G. Montanari, “On-line Screening of MV Cable Network Grid Through Partial Discharge Measurements,” in *8th International Conference on Insulated Power Cables*, (Paris), pp. 376–379, 2011.

[77] X. Zhang, L. Pan, J. Luo, W. Li, and R. Xia, “Partial Discharge Pattern Characteristics of 220 kV XLPE Power Cable Joints with Artificial Defect,” in *8th International Conference on Insulated Power Cables*, (Paris), pp. 490–492, 2011.

[78] P. Arnold and F. Janicek, “Modelling of partial discharge activity,” in *2016 Diagnostic of Electrical Machines and Insulating Systems in Electrical Engineering (DEMISEE)*, (Papradno), pp. 34–37, 2016.

[79] Z. Achillides, G. Georghiou, and E. Kyriakides, “Partial discharges and associated transients: The induced charge concept versus capacitive modeling,” *IEEE Transactions on Dielectrics and Electrical Insulation*, vol. 15, no. 6, pp. 1507–1516, 2008.

[80] I. W. McAllister, "Electric field theory and the fallacy of void capacitance," *IEEE transactions on electrical insulation*, vol. 26, no. 3, pp. 458–459, 1991.

[81] D. Agoris and N. Hatziargyriou, "Approach to partial discharge development in closely coupled cavities embedded in solid dielectrics by the lumped capacitance model," in *IEE Proceedings A: Science Measurement and Technology*, vol. 140, pp. 131–134, 1993.

[82] N. P. Kolev, E. D. Gadjeva, M. G. Danikas, and N. R. Gourov, "Development of Partial Discharge Model, Simulation and Measurement," in *1999 Conference on Electrical Insulation and Dielectric Phenomena*, (Austin, Texas), pp. 214–217, 1999.

[83] M. Toader and D. Mariana, "Electrical insulation study using partial discharge model," in *10th Meditemean Electrotechnical Conference*, vol. 111, (Limassol), pp. 1060–1063, 2000.

[84] D. Gowda and Anandraj, "Modeling ofPartial Discharge (PD) for Solid Insulation with V oid and Building a Hardware setup to Measure Partial Discharge," in *2016 Biennial International Conference on Power and Energy Systems:Towards Sustainable Energy (PESTSE) Modeling*, (Bangalore), pp. 1–7, 2016.

[85] F. Haghjoo, E. Khanahmadloo, and S. Shahrtash, "Comprehensive 3-capacitors model for partial discharge in power cables," *The International Journal for Computation and Mathematics in Electrical and Electronic Engineering*, vol. 31, no. 2, pp. 346–368, 2012.

[86] H. V. Jaarsveldt and R. Gouws, "Partial Discharge Simulations Used for the Design of a Non-Intrusive Cable Condition Monitoring Technique," *Journal of Energy and Power Engineering*, vol. 7, pp. 2193–2201, 2013.

[87] R. Candela, G. F. Scimemi, P. Romano, and E. R. Sanseverino, "Analysis of Partial Discharge activity at different temperatures through an Heuristic Algorithm," in *1999 Conference on Electrical Insulation and Dielectric Phenomena*, (Austin, Texas), pp. 202–205, 1999.

[88] C. Forssén and H. Edin, "Field Model of Partial Discharges at Variable Frequency of the Applied Voltage," in *Nordic Insulation Symposium*, no. 2, (Trondheim, Norway,), pp. 121–124, 2005.

[89] C. Forssén and H. Edin, "Modeling Partial Discharges in a Cavity at Different Applied Frequencies," in *2007 Annual Report Conference on Electrical Insulation and Dielectric Phenomena Modeling*, (Atlanta, Georgia), pp. 132–135, 2007.

[90] J. Jaarsveldt, "Non-intrusive condition monitoring of power cables within the industrial sector," MSc. Dissertation, North-West University, 2014.

Appendices

Appendix A

Appendix A: Summary of Average Partial Discharge Measurement Results for the Semicon Feather, Ring Cut and Tram Line Defects

Summary of Measured PD Parameters per stage for the semicon feather, ring cut and tram line defect															
PDIV	**Stage 1**			**Stage2**			**Stage3**			**Stage4**			**Stage 5**		
PD Parameter	**PDIV (kV)**	**Qmax (pC)**	**PRR (N)**	**PDIV (kV)**	**Qmax (pC)**	**PRR (N)**	**PDIV (kV)**	**Qmax (pC)**	**PRR (N)**	**PDIV (kV)**	**Qmax (pC)**	**PRR (N)**	**PDIV (kV)**	**Qmax (pC)**	**PRR (N)**
Semicon 1&2	17.97	457.32	1062.20	20.93	249.95	1426.12	16.53	426.55	1549.10	16.60	378.39	1631.15	19.93	133.84	1354.90
Semicon 3	18.04	39.95	1515.09	19.14	13.70	1813.12	17.95	12.53	1572.09	17.42	8.75	1123.23	19.98	74.37	1015.06
Ring Cut 1&2	17.89	289.57	1427.50	18.01	378.50	1223.03	19.80	279.94	1523.46	19.14	545.42	974.51	19.39	21.58	1332.30
Ring Cut 3	14.41	397.36	1664.10	14.57	526.03	1041.77	15.59	628.19	806.09	16.27	520.75	939.19	19.41	275.82	966.67
Tram Line 1&2	17.03	138.12	1900.98	20.46	110.78	1888.96	-	52.32	1700.92	-	270.40	1051.55	-	101.66	1233.34
Tram Line 3	11.52	556.28	1254.06	17.95	1520.08	677.49	21.13	1265.66	695.78	17.97	1590.98	1189.49	14.48	758.64	950.75

Appendix B

Appendix B: Matlab® Code

In this Appendix, the matlab® code for calculating passive circuit elements and modelling the PD phenomena is presented

```
%%...........................................................................

%                 DEFINITION OF INITIAL MODEL PARAMETERS

%%...........................................................................

% Length in m
% Specific conductance in mho/m
% Resistance in ohm
% Pressure in kPa

% Inner Semicon Thickness
d_InSemicon = 1.2E-3;

% Outer Semicon Thickness
d_OutSemicon = 1.5E-3;

% Radius of the conductor core
r_cond = 3.34E-3;

% Insulation thickness from core end to outer insulation
d_insu = 3.4E-3 + d_InSemicon;

% Length of the cable with the defect
L = 1;

%% l_c = Length of the void arc
%% d_c = Distance between the core end and the middle of the void
%% r_c = Thickness of the void (size of the void
%% t_c =  Width of the void


% SEMICON FEATHER %
d_c = d_insu;
r_c = d_OutSemicon;

% SEMICON FEATHER: CORE 1 AND 2
l_c = abs(((2 * asin(10E-3 / (2 * d_insu)) / 360) * 2 * pi * d_insu));
t_c = 10E-3;

% SEMICON FEATHER: CORE 3
l_c = abs(((2 * asin(25E-3/ (2 * d_insu)) / 360) * 2 * pi * d_insu));
t_c = 5E-3;



% TRAM LINE %
t_c = 20E-3;

% TRAM LINE: CORE 1 AND 2
d_c = d_insu - (1.4E-3 /2);
l_c = abs(((2 * asin(0.4E-3/ (2 * d_insu)) / 360) * 2 * pi * d_c));
r_c = 1.4e-3;
```

```
% TRAM LINE : CORE 3
d_c = d_insu - (2E-3 /2);
l_c = abs(((2 * asin(0.8E-3/ (2 * d_insu)) / 360) * 2 * pi * d_c));
r_c = 2e-3;


% RING CUT %

% RING CUT: CORE 1 AND 2
d_c = d_insu - (1E-3 / 2);
r_c = 1e-3;
t_c = 0.6E-3;
l_c = 2 * pi * d_c;

% RING CUT: CORE 3
d_c = d_insu - (2E-3 / 2);
r_c = 2e-3;
t_c = 0.8E-3;
l_c = 2 * pi * d_c;



% Relative permittivity of XLPE insulation material
er_XLPE = 2.645;

% Permittivity of air trapped in the void
eo_Air = 8.85E-12;

% Measures how well water conducts electricity, when compounds are broken
down and dissolved in water, they produce charged particles.
SpecificConductance_Insu = 7e-17;


% Measures how well conductive is the air contained in the void (Gives an
idea on the dissolved compounds in the medium and the water content or
presence)
SpecificConductance_VoidAir = 1e-8;


% The pressure of the air in the void 20
Pres_void = 0.2;


% Temperature in the void/cavity
Temp_void = 315;

% Correction factor for humidity which is 1 for small voids (IET Tech group
1989)
k_h = 1;
```

```
%%...........................................................................

%                        CALCULATION OF CIRCUIT ELEMENT VALUES

%%...........................................................................

%............................................................................
                         CAPACITANCE VALUE CALCULATIONS
%............................................................................


% Capacitance for insulation space between void and HV electrode (core)
C_a = ((e_XLPE / log((r_cond + d_c - (r_c/2)) / r_cond)* ((l_c*t_c)/(r_cond +
d_c))));


% Capacitance for insulation between void and ground
C_b = ((e_XLPE / (log((r_cond + d_insu) / (r_cond + d_c + (r_c/2))))*
((l_c*t_c)/(r_cond + d_c))));


% Combined capacitance value for insulation in the same sector as the void
C_s = (C_a * C_b) / (C_a + C_b);


% Capacitance of the cavity
C_c = (eo_Air / (log((r_cond + d_c + (r_c/2))/(r_cond + d_c - (r_c/2)))) *
((l_c*t_c)/(r_cond + d_c)));


% Capacitance of the rest of the healthy insulation
C_p = (2 * pi * e_XLPE * L) / (log ((r_cond + d_insu) / r_cond));


%...........................................................................
%                        RESISTANCE VALUE CALCULATIONS
%...........................................................................


% Resistance for insulation below cavity
R_a = ((1 / SpecificConductance_Insu) * ((r_cond + d_c)/(l_c * t_c)) * log
((r_cond + d_c - (r_c / 2))/ (r_cond )));


% Resistance for insulation above cavity
R_b = (1 / SpecificConductance_Insu) * ((r_cond + d_c)/(l_c * t_c)) * log
((r_cond + d_insu) / (r_cond + d_c + (r_c /2)));

% Total resistance of insulation in same sector/column as the cavity
R_s = R_a + R_b;
```

```
% Resistance of the void
R_c = (1 / SpecificConductance_VoidAir) * ((r_cond + d_c)/(l_c * t_c)) * log
((r_cond + d_c + (r_c /2)) / ((r_cond + d_c - (r_c /2))));


%  Resistance of the rest of the healthy insulation
R_p = (1 / ( 2 * pi * L * SpecificConductance_Insu) * log ((r_cond + d_insu)
/ r_cond));


%.............................................................................
%                  CORRECTIONAL FACTOR FOR FIELD ENHANCEMENT
%              IN THE INSULATION DUE TO THE PRESENCE OF THE CAVITY
%.............................................................................


% Function to be used to calculate the Area of the void
A_function = @(s)1./((r_c.^2 + 4*s).^ (3./2) .* (t_c.^2 + 4*s).^ (1./2) .*
(l_c.^2 + 4*s).^ (1./2));


% Area of the void
A = integral(A_function,0,Inf);


% Field enhancement factor due to presence of void in the insulation
k_ef = er_XLPE / ((er_XLPE + 2 * ((1 - er_XLPE) * l_c * t_c * r_c * A)));


% Corrected capacitance of the void with field enhancement factor
C_c_cor = (1 / k_ef) * er_XLPE * C_c;


% Corrected capacacitance of insulation in same sector with the void
C_s_cor = k_ef * C_s;

% Corrected resistance of insulation in same sector with the void
R_s_cor = (1 / k_ef) * R_s;
```

```
%.............................................................................
%                                  PLOTS
%.............................................................................


% Transpose t step array to match Vc
t1 = 0:2.0000e-05:0.02;
t = t1';


% Plot Vc measured across cavity, sent to workspace from Simulink
Vin_new = Vin * 1E-8;
Vin_plot = plot(t, Vin_new);
set(Vin_plot, 'LineWidth',1.2);
xlabel ('Time(s)', 'FontSize', x_size);
ylabel ('Voltage across discharge area (V)', 'FontSize', y_size);
title ('Voltage measured across the discharge area (Vc)', 'FontSize',
title_size);
xt = get(gca, 'XTick');
set(gca, 'FontSize', 12)
yt = get(gca, 'YTick');
set(gca, 'FontSize', 12);
hold;
Vdetected_plot = plot(t, Vc);
set(Vdetected_plot, 'LineWidth',1.6);
saveas(gcf,'Vdetected.pdf');


% Plot the Voltage measured across the measuring impedance
Vin_new = Vin * 1E-8;
Vin_plot = plot(t, Vin_new);
set(Vin_plot, 'LineWidth',1.2);
xlabel ('Time(s)', 'FontSize', x_size);
ylabel ('Partial Discharge Voltage (V)', 'FontSize', y_size);
title ('Partial Discharge Magnitude', 'FontSize', title_size);
xt = get(gca, 'XTick');
set(gca, 'FontSize', 12)
yt = get(gca, 'YTick');
set(gca, 'FontSize', 12);
hold;
Vdetected_plot = plot(t, Vdetected);
set(Vdetected_plot, 'LineWidth',1.6);
legend ('Vs','Vpd');
saveas(gcf,'SuperimposedVin_Vdetected.pdf');
```

Appendix C

Appendix C: Overview summary of Experimental and Simulation Results of Cavity and Surface Discharge Type of Defects

Defect Type	Stage 1	Stage 2	Stage 3
Ring Cut and Tram Line Defects: Experimental Results	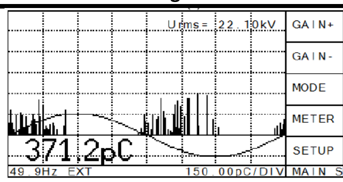	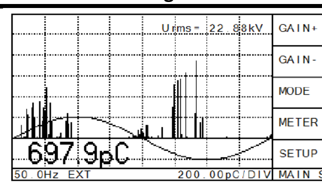	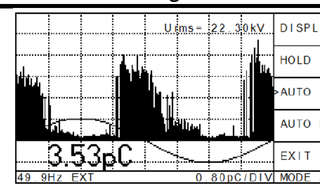
Ring Cut and Tram Line Defects: Simulation Results	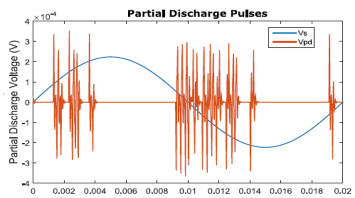	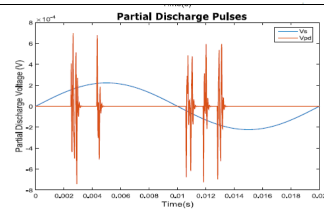	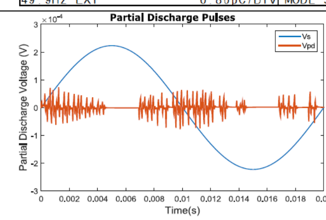
Semicon Feather Defect: Experimental Results	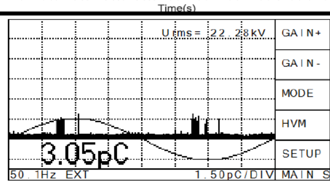	No Distinct Changes	No Distinct Changes
Semicon Feather Defect: Simulation Results	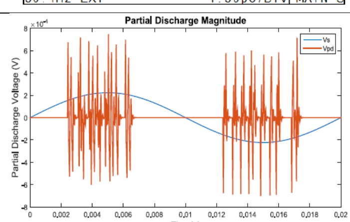	No Distinct Changes	No Distinct Changes

Appendix D

Appendix D: 3-Capacitance Model Layout Configuration in Simulink®

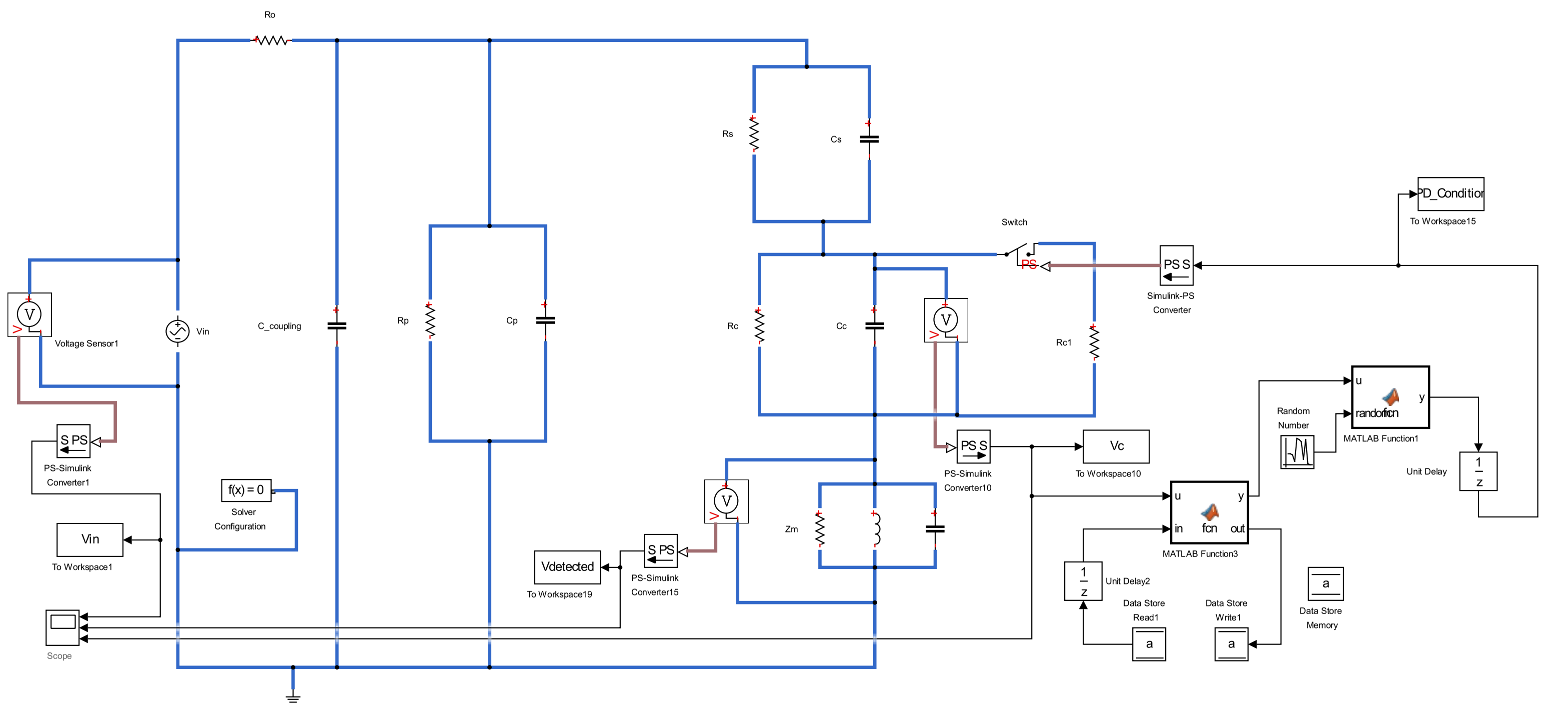
Ro
Rs
Cs
Switch
PS S
Simulink-PS
Converter
PD_Conditio
To Workspace15
V
Voltage Sensor1
Vin
C_coupling
Rp
Cp
Rc
Cc
V
Rc1
S PS
PS-Simulink
Converter1
Vin
To Workspace1
f(x) = 0
Solver
Configuration
PS S
PS-Simulink
Converter10
Vc
To Workspace10
Random
Number
u
y
randomfcn
MATLAB Function1
Unit Delay
V
Zm
S PS
PS-Simulink
Converter15
Vdetected
To Workspace19
u
y
in
fcn
out
MATLAB Function3
Unit Delay2
Data Store
Read1
Data Store
Write1
a
Data Store
Memory
Scope

Appendix E

Appendix E: Partial Discharges, The 'Cancer' of Power Cables

This Appendix presents the paper covering the initial PD characterizing basis work of the study that was submitted and published in the ESI Africa's Power Journal, 4th issue, in 2016.

PARTIAL DISCHARGES, THE 'CANCER' OF POWER CABLES

Power cable related faults are among the major causes of outages in medium voltage (MV) power distribution networks. Modern power cable technologies now use solid extruded insulation. In such cables most failure modes are associated with partial discharge (PD) activity. The most vulnerable parts of the cable systems are the joints and terminations (cable accessories). Partial discharges are therefore often regarded as both symptoms and agencies of power cable degradation. Like cancer in human beings, 'the holy grail' in PD technology is the ability to predict the occurrence, mitigate the presence and more importantly accurately predict time-to-failure (death). In this article, the knowledge on PD technology (especially in the context of power cables) is reviewed, highlighting what is known and what is still to be known. Insights into the work currently being pursued by the authors in trying to shed light on the time-evolution phenomena of partial discharges in XLPE power cables are presented. As cancer is being fought from all possible angles, so should be the partial discharges in power cables in our pursuit for improved reliability in electricity supply systems.

The origin of partial discharges in power cables

In built-up environments such as urban areas as well as in generally space restricted situations, electric power is conveyed through underground power cables. The essence of power cable engineering is the ability to restrict the electric field within very confined (shielded) space. The insulation part of the cable plays this role and has dimensions in the order of a couple of millimetres in distribution voltages. In modern power cable technology the insulation is normally comprised of Cross-linked-Polyethylene (XLPE). A typical cross-sectional structure of an MV XLPE power cable is as shown in Figure 1.

The electric field gradient has to be below the breakdown strength of the insulation and therefore the cable is designed to satisfy this condition. In power cable accessories (joints and terminations), it is a complex process to ensure that the electric field gradient remains within the strength of the insulation. In Figure 2, the behaviour of the electric field lines on a terminal end of a cable is illustrated. If not appropriately intervened (stressed graded), there are regions of stress enhancement, which may cause localised electrical breakdown of the insulation. Such a localised electrical breakdown or micro-spark is termed a partial discharge (PD)[1].

A PD event generates energy in various forms as illustrated in Figure 3. Some of the energy, such as UV radiation, causes localised degradation of the insulation in the discharge area. While the presence of PD energy is an indication of PD activity, the energy itself also further degrades the insulation such that partial discharges are often regarded as both symptoms and agencies of insulation degradation.

Sustained PD activity continuously degrades the insulation and over time

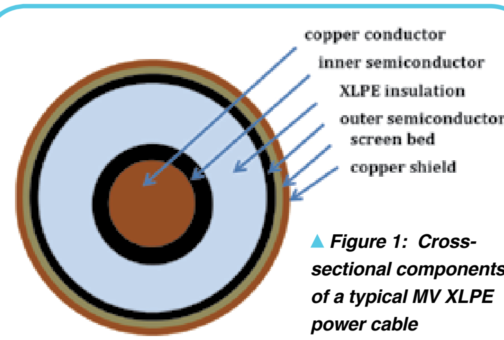

▲ *Figure 1: Cross-sectional components of a typical MV XLPE power cable*

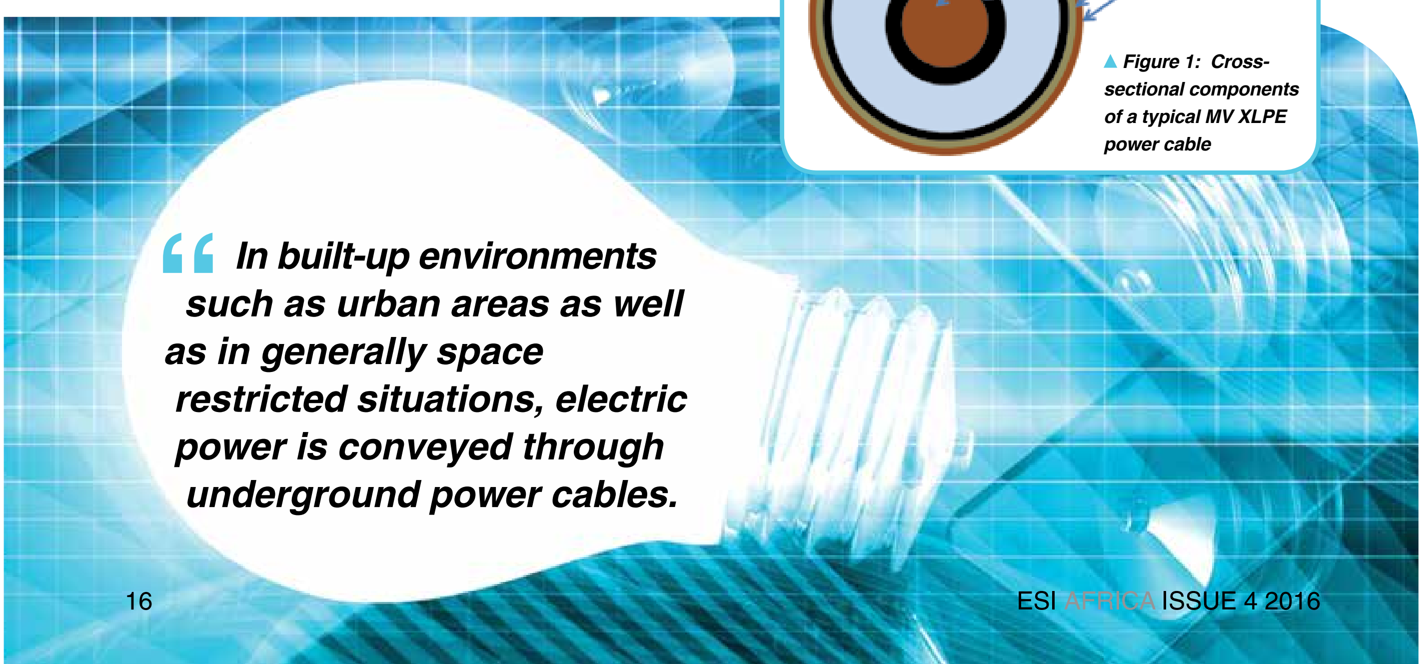

> ***"In built-up environments such as urban areas as well as in generally space restricted situations, electric power is conveyed through underground power cables.***

will initiate a short circuit across the insulation, leading to catastrophic power failures.

Power cable failures account for most of power distribution system failures[3]. Most of the failures are percussed by partial discharge activity in power cable accessories[3]. Challenges associated with power cable faults are that location of the faulty part of the cable and fixing it is a relatively costly and time consuming process as the cables are normally buried underground.

Improved reliability of power cable systems entails early detection and mitigation of incipient PD faults. It is for this reason that for many decades researchers have consistently sought to understand PD phenomena and develop means of detecting and interpreting the presence of PD activity in the power cables.

PD detection and diagnosis?

Detection and interpretation of the energy emitted from a PD source can give information about the defect. PD detection techniques are based on the principle of sensing and processing any of the forms of energy emitted by a PD event[4]. Various PD detection techniques are illustrated in Figure 4. Each type of PD detection technique is characterised by the nature of the PD energy being detected.

A major challenge is that PD energy quantities are usually minute compared to the ambience. As an example, if PD current is the parameter being measured, a typical PD event involves a couple of tens of pico-Coulomb (pC) charge transfer in tens of microseconds. It therefore implies that PD current pulse magnitude can be in the order of one microampere. Measurement of such a minute current in an environment of typical power system load currents and electromagnetic interferences is similar to the proverbial search for a needle in a haystack! It is for this reason that extraction of PD signals from the noisy environment is a major frontier of research in PD technology especially in on-line PD detection. Significant progress, however, has been achieved in developing effective techniques of noise mitigation in PD diagnosis. In that regard most commercial PD measurement technologies have state-of-the-art PD noise management techniques although there is still room for improvement.

Detection of cancerous cells in a human body is an important beginning of a diagnosis and prognosis process; such is the case with partial discharges. Once a PD has been detected the implication thereof on the insulation integrity and life of the cable has to be determined through informed interpretation of the PD signal. The ability to locate the PD defect and especially in lengthy power cables

“ PD detection techniques are based on the principle of sensing and processing any of the forms of energy emitted by a PD event[4].

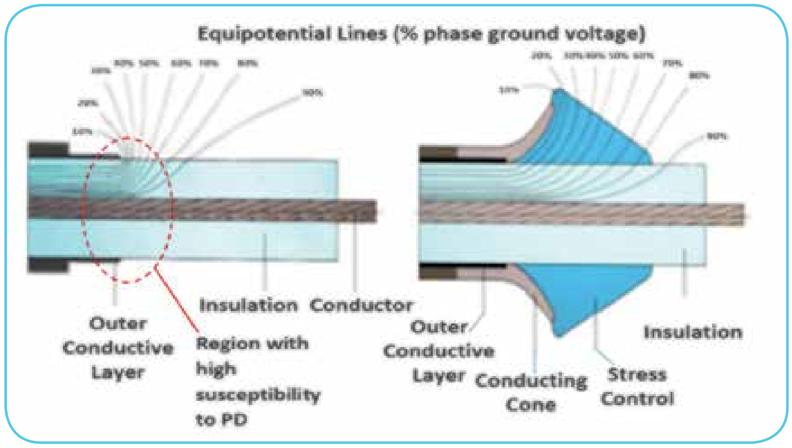

▲ *Figure 2: Electrical stress at cable termination[2]*

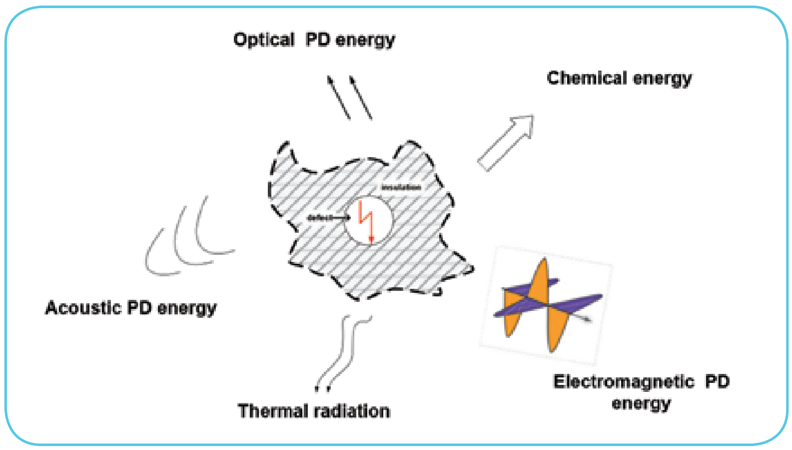

▲ *Figure 3: Different forms of energy released by a PD event[4]*

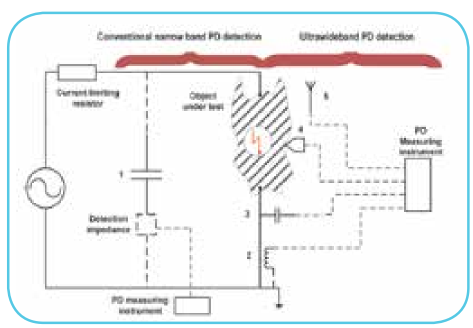

▲ *Figure 4: PD detection techniques where: (1) is PD current detected through a coupling capacitor, (2) is detection of the PD current magnetic field through an inductive probe, (3) is detection of PD transient electric field using a capacitive probe, (4) is detection of the PD event acoustic energy through an acoustic sensor and (5) is detection of PD electromagnetic radiation through an antenna[4].*

Figure 5: Power cable terminations with PD defects under laboratory-based long term ageing experiment.

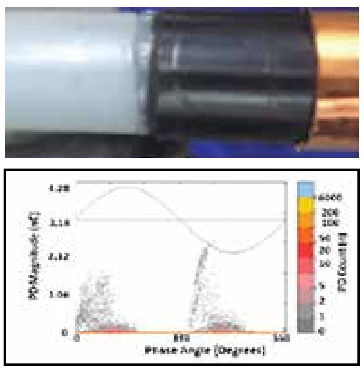

Ring cut defect and corresponding PDPRP

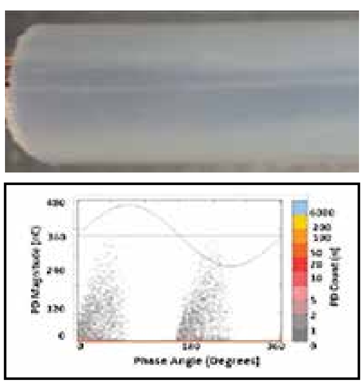

Tram line defect and corresponding PDPRP

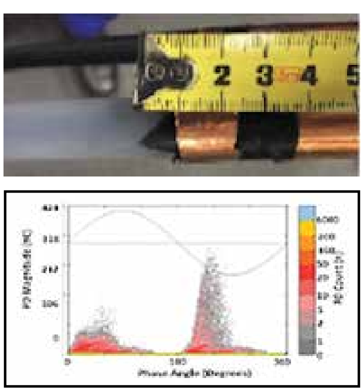

Semicon feather defect and corresponding PDPRP

Figure 6: The defects and the PDPRP[2]

buried underground is critical and again this is a major area of research. Once located, the nature of the PD defect has to be determined. There are different types of PD defects such as corona in air, air-filled cavities embedded in the insulation, surface discharges and electrical trees in the insulation. Different types of PDs have different severity effects on insulation. As an example corona in air would normally not be of a major concern in power cables compared to air cavities in the insulation.

The ability to recognise and classify PD defects is therefore cardinal in PD diagnosis. This requirement has and is still a major preoccupation of many researchers. Significant knowledge in that regard has been accumulated thus far from various research efforts around the world. In some equipment under known conditions, PD signals can be considered as signatures for typical known defects. Off-the-shelf PD diagnosis equipment is now available that is able to automatically locate and recognise partial discharge sources but the technology is not yet mature. The ideal goal of PD diagnosis is to be able to accurately predict the remaining life of equipment. However, for anyone with the slightest knowledge of PD phenomena, this is still a 'holy grail'!

For medical doctors to reasonably predict the remaining life of a terminal cancer patient, the various time-tagged phases of cancer progression in the body have to be known. Similarly, in PD technology, researchers are obsessed with the search for an understanding of how different types of partial discharges evolve from inception to complete insulation failure. It is hoped that such knowledge will be a firm springboard for efforts in predicting the equipment's remaining life based on PD diagnosis.

PD evolution

PD mechanisms in solid polymeric insulation such as XLPE are now known to evolve through different physiochemical processes as the insulation degradation progresses towards complete failure under continuous exposure to PD activity. In broad terms, the evolution stages are: virgin, moderately aged and severely aged. At every stage, certain defect types such as air-filled cavities in solid polymeric insulation have signatory features such as PD current (voltage) pulses shape, pulse repetition rate or frequency spectrum or phase-resolved-pattern (PDPRP). How PD signatures vary as a function of insulation type, equipment type, environmental conditions such as temperature and many other factors is still very much a subject of research. Only when those phenomena are fully understood will prospects of predicting the remaining life of equipment based on PD diagnosis be realistic. It is in this context that the authors of this article have on-going research in studying time-evolution behaviour of typical PD defects in MV XLPE power cable terminations installation defects. The terminations under experiment are as shown in Figure 5.

Experimental results obtained thus far show that each PD type in the cable terminations gives distinct PDPRP signatures as shown in Figure 6.

Although the experiment is ongoing until cable failure, the initial results as presented in Figure 7 show the following:

- The PD intensity generally increased with time.
- The PD magnitude of the semi-con feather increased initially and then decreased.
- The PD magnitude of the tram-line and ring-cut defects decreased after 2 hours then increased in the next 4 hours.

The presence of discharge near the zero crossings of the voltage wave indicates the influence of residual charge in the discharge area. On the other hand, the observed changes within the 4 hours of ageing time could merely be the initial unstable transitions of PD at virgin stage, which would later on stabilise. It is acknowledged that at this stage of the on-going research, the PD data sets are not sufficient to enable deriving conclusive information. Therefore, as the measurement data accumulates, comprehensive statistical analyses of the PDPRP would be implemented to extract more information about the trends.

Conclusion

Partial discharges can be regarded as the 'cancer' of power cable insulation and therefore need to be managed effectively for better reliability of MV distribution power systems. Although significant knowledge on PD has accumulated over the years resulting in availability of commercial PD

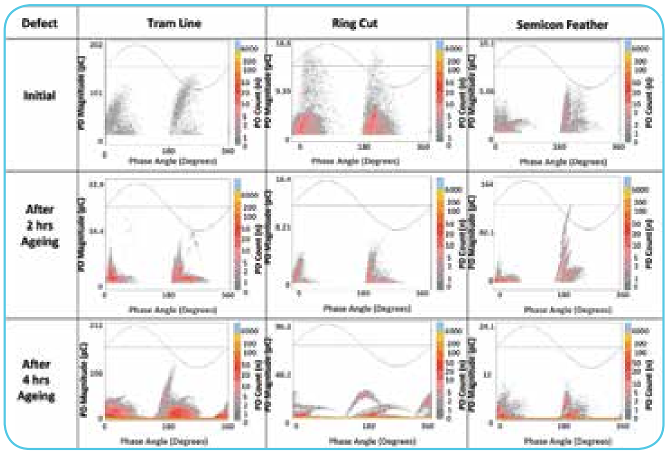

▲ ***Figure 7: Four hour ageing PDPRP results***

diagnosis equipment, there are still challenges related to prediction of remaining life of equipment. There is, however, hope that current research thrusts in the understanding of PD evolution phenomena in specific equipment like power cables will shed light on the possibilities of predicting equipment time-to-failure. ESI

ABOUT THE AUTHORS:

Cuthbert Nyamupangedengu is an associate professor in the School of Electrical & Information Engineering at the University of the Witwatersrand (Wits), Johannesburg. He received a B.Sc. (Hons.) in Electrical Engineering from the University of Zimbabwe in 1994. At Wits, in 2004, he was awarded the M.Sc. in Engineering (with distinction) and in 2011, the Ph.D. Cuthbert was an engineer in the Zimbabwe Electricity Supply Authority from 1995 to 2005 in various capacities.

Elizabeth Haikali obtained a B.Sc. (Hons.) degree in Electrical Engineering from the University of Namibia in 2013 and is currently pursuing an M.Sc. in Engineering in the field of high voltage insulation at the University of the Witwatersrand, Johannesburg, South Africa. She is also employed as an Assistant Engineer at NamPower, Namibia's state-owned utility.

REFERENCES

[1] High Voltage Test Techniques - Partial Discharge Measurements, IEC Standard 60270, 2000.
[2] D. Fynes-Clinton, "PD Characteristics of Typical MV XLPE Power Cable Termination Defects at VLF and Power Frequency Test Voltages," MSc Dissertation, University of Witwatersrand, 2016.
[3] M. Stotzel, M. Zdrallek, and W. H. Wellssow, "Reliability calculation of MV-distribution networks with regard to ageing in XLPE-insulated cables," IEE Proceedings-Generation Transmission Distribution, 2001, no. 6, pp. 597 – 602.
[4] C. Nyamupangedengu, "PD-Type-Dependent Spectral Bandwidth in Solid Polymer," PhD Thesis, University of Witwatersrand, 2011.

Appendix F

Appendix F: PD Evolution of Artificial Defects Introduced in MV XLPE Power Cable Terminations - Preliminary Results

A paper that looked at preliminary results of the accelerated ageing results is presented in this Appendix. The paper was accepted and published in the 25^{th} South African Universities Power Engineering Conference (SAUPEC)proceedings. The SAUPEC conference was held in January 2017 at the University of Stellenbosch, South Africa. The paper also had a power point component that was presented by E. Haikali.

PD EVOLUTION OF ARTIFICAL DEFECTS INTRODUCED IN MV XLPE POWER CABLE TERMINATIONS - PRELIMINARY RESULTS

E. Haikali*, C. Nyamupangedengu**

School of Electrical and Information Engineering, University of the Witwatersrand 2050, South Africa
*Email: *Elizabeth.haikali@students.wits.ac.za **Cuthbert.nyamupangedengu@wits.ac.za*

Abstract: Power cable terminations and joints are the most vulnerable parts of a power cable system, causing the most power cable failures. This problem can be better understood by investigating the Partial Discharge (PD) phenomena in common cable termination defects. The present work investigates changes in PD behaviour up to time of failure. Artificial defects were created in cable terminations and investigated using an accelerated ageing test setup. Preliminary results show that Partial Discharge Inception Voltage (PDIV) is a function of defect severity. PD magnitudes of the surface type of discharge decreased consistently over time while that of cavities fluctuated significantly. The first 100 hours showed instability in PD mechanism which can be an indication that effective diagnosis should consider this transition time. At this stage of the work, it may be possible to conclude that PD indeed changes with ageing time and the changes are a function of the defect type.

Key words: accelerated ageing, partial discharge, cable defects, termination defects, MV cable, PD signatures

1. INTRODUCTION

Most failures in power cables have been attributed to cable joints and terminations which are most susceptible to installation defects [1]. Partial Discharge (PD) testing has been recognised as one of the most effective insulation condition diagnostic methods [2]. It has been reported in the literature that different defects give distinct PD signatures and this includes the work by Fynes-Clinton [3]. However, how these signatures evolve with ageing time during service is not known. The study presented in this paper focuses on defects in Cross-Linked Polyethylene (XLPE), Medium Voltage (MV) power cable terminations under induced PD ageing. Focus is on how these unique PD signatures in artificial defects on the cable terminations evolve from the point of inception up to breakdown. In practice, this would help in categorising different levels of PD severity and possibly provide insight on the remaining operating life time.

The specimens under study are 3 m lengths of XLPE 6.35/11 kV heat shrink terminated cables with artificial defects. The defects as shown in Table 1 are a ring cut and a tram line in the XLPE and a semiconductor screen feather extending over the XLPE.

The rest of the paper is structured as follows: Section 2 gives a review on PD evolution, followed by experimental methodology. The results are then discussed before concluding the work.

2. PD EVOLUTION - A LITERATURE REVIEW

Insulation is normally known to be the most vulnerable part of a High Voltage (HV) electrical equipment [4]. Therefore, insulation is an integral part of system reliability philosophies. Despite improved cable production measures that ensure good quality insulation [5], power cables remain susceptible to defects during installation. For this reason, power cable failures account for most of power system failures [6, 7], and these are specifically in cable accessories [1]. The vulnerability of cable accessories is due to the abrupt change in the cable surface geometry that distorts the normally uniform electrical field distribution at the semi conductor end and insulation interface [1]. The stress control measures such as stress cones or tubes help to deflect the electric fields away from the sensitive region [1]. The regions however, remain of high risk as the presence of a defect in a high intense electric field may ignite PD leading to insulation degradation.

Various researchers have studied different PD manifestations in order to discern distinct changes in PD until failure. Most have studied PD by monitoring charge, radiation (using fast detecting optical cameras) and chemical reactions (temperature, pressure, gas, volume and discharge area surface morphology). The degradation process have been categorised into several stages; some five [5], others three [8], with Morshuis [9] proving a good summary of the three stages.

Table 1: Typical Termination defects that were introduced on the cable samples in the study

Defect Type	Description	Dimensions
Semi-conductor feather	The outer semi-conductor screen was not stripped off the XLPE insulation uniformly. An extending triangular feather was left with a base and height denoted by B and H respectively. For core 1 and core 2 (B = 10 mm, H = 10 mm). The feather for core 3 was made sharper (B = 5 mm, H = 25 mm).	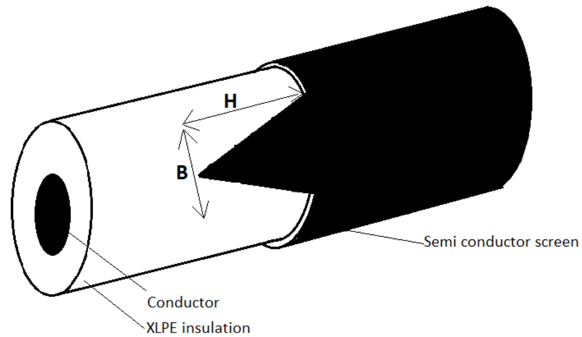
Tram Line	The tram line represents a cut prone to occur when a sharp object is used to strip off the semicon screen. The cavity runs along the XLPE with a depth H, and a thickness T. For core 1 and core 2 (H = 1 mm, T = 0.4 mm). Core 3 was made deeper (H = 2 mm and T = 0.8 mm).	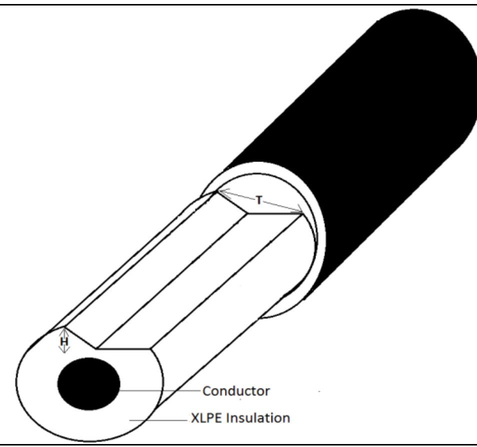
Ring Cut	The ring cut similarly to the tram line represents a cavity in the XLPE likely to occur when establishing the semicon screen end. The cut forms a complete ring in the XLPE with a width denoted as W and a depth R. For core 1 and core 2 (W = 0.6 mm, R = 1 mm). The cut for core 3 was (W = 0.8 mm, R = 2 mm).	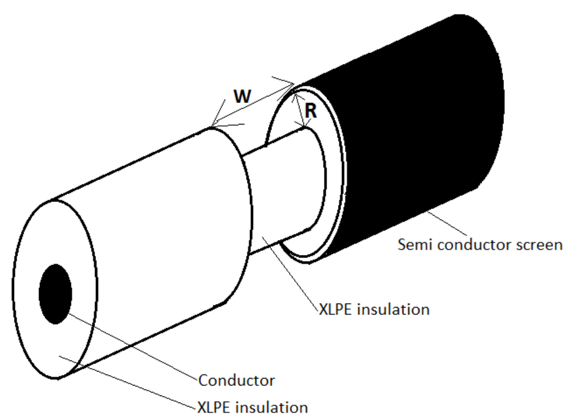

PD pulse time characteristics have been used to observe some changes that occur with ageing. The changes reflect the ion and electron dynamics at the discharge site. Kim *et al*. [5] measured PD by obtaining both the Phase Resolved Partial Discharge Pattern (PRPDP) and PD pulse characteristics while monitoring the cavity gas volume. They concluded that the variations in PD were due to the changes in the gas composition, pressure and the physiochemical properties of the cavity surface. In the previous work by the authors [10], it has been reported that at inception, both surface and cavity discharges had high spectral bandwidth which decreased over time. The spectral bandwidth scatter plots had two distinct clusters. These clusters could signify two distinct ageing stages over the defect lifetime.

According to the review by Morshuis [9], PD evolve through three stages towards failure. The three main stages are: virgin, moderately aged and severely aged in the order of occurrence. PD characteristics are distinct in each of these stages and this knowledge informs diagnosis. The virgin stage is characterised by a "streamer like" discharge of large PD magnitudes, with a steep front and a short pulse width [9, 10]. This is a result of the gap over-voltage due to a prolonged statistical time lag. The time lag is defined as the time duration from when the threshold stress of the cavity is exceeded to when the seed electron becomes available. The seed electron availability at this stage is largely dependent on background radiation.

The moderately aged stage is associated with smaller PD magnitudes, higher repetition rate, longer rise time, longer pulse width and longer fall time [9]. This is because residual charge supplies the seed electrons, hence less gap over-voltage conditions. Additionally, the discharge site surface undergoes physiochemical changes that result in an increase in surface conductivity and roughness. The changes are due to the discharge by-products such as carboxylic acids [9].

At the severely aged stage, discharge by-products crystallize on the site surface, therefore causing small pulsating "corona like" discharges at crystal tips [11]. Due to the high conductivity of the surface at this stage, the electric field intensity weakens which extinguishes PDs [11]. The absence of PD at this stage can be mistaken for healthy condition of the insulation, and yet the insulation is undergoing electrical treeing induced failure.

Due to the above outlined time dependent behaviour of PD as it ages, it is of interest to know how the initially unique identified signatures evolve with time from the point of inception up to the point of breakdown. The current work therefore presents results of an investigation on how PD of typical XLPE termination defects evolve over time.

3. EXPERIMENTAL SET UP AND PROCEDURE

The test samples used in this study comprised of 3 m long, three core, 6.35/11 kV XLPE cables with heat shrink terminations on each core. During termination, three typical defects were introduced per cable as shown in Table 1. Identical defects were created on two cores for test repeatability, while on the third core, the defect dimensions were increased to check on the effect of severity.

The cable samples were connected in parallel for aging as shown in Figure 1. The un-terminated end of each cable sample was immersed in insulation oil to prevent unwanted discharges. A voltage of 9.5 kV at 350 Hz was applied continuously for 10 hours after which each core would be tested for PD using the test set up shown in Figure 2.

PD measurements were conducted in accordance with the SANS 60270, SANS 1339 and IEEE 400.3 using the Power Diagnostix ICM Compact^{TM}. The test voltage was increased in steps of 2 kV per 30 seconds up to $2.5U_o$ where it was maintained for 1 minute then decreased to $1.73U_o$. PRPDP were recorded for 1 minute both at $2.5U_o$ and $1.73U_o$. PDIV and PDEV were also noted. The ageing and PD testing procedures were repeated until failure or until no significant changes in PD. The elevated voltage and frequency were decided upon based on the common best practice [12, 13]. The tests were conducted in a double screened Faraday Cage laboratory, and the average noise level recorded was 0.4 pC.

Figure 1: The cable test specimens connected in parallel for accelerated PD induced aging.

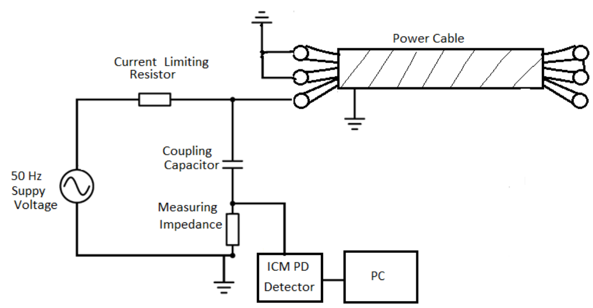

Figure 2: The test set up used for PD testing at 50 Hz

4. RESULTS AND ANALYSIS

The PD parameters monitored were the Phase Resolved Partial Discharge Patterns (PRPDP), the maximum apparent PD magnitude, the Partial Discharge Inception Voltage (PDIV), Partial Discharge Extinction Voltage (PDEV) as discussed in detail in the following sections. The maximum voltage applied during PD testing was 23 kV. Therefore, no data was recorded for voltages above 23 kV.

4.1. Semicon Feather (PDIV and PD magnitude)

For all the defects, the PDIV varied randomly between 10 and 22 kV in the first 150 hours as shown in Figure 3 for the semicon feather. The corresponding PD magnitude shown in Figure 4 depict a continuous decreasing trend.

An un-aged defect have a longer statistical time lag for the free electron to be available. The discharge therefore initiates at a higher voltage. This explains the increment in PDIV for the semicon for the first 100 hours. Despite subsequent discharge events, the time lag can remain long due to the high ionization potential of an un-aged cavity [9]. Later, a decrement in PDIV for the semicon occurred between 125 and 255 hours. This could be due to the reduction in the time lag hence less gap over-voltage conditions. The free electrons become easily available from the residual charge built up on the cavity surface.

For the semicon feather, the most severely defected core initially (up to 100 hours) had the least PDIV as expected. Subsequently however, the PDIV increased above the other two cores. It is also notable that core 3 which has the most severe defect gave the least PD magnitude throughout as shown in Figure 4. After 150 hours, there was no PD in the most severely defected core. The semicon had the least incidences of PD disappearance, although when these incidences occurred, they lasted for long time periods.

The behaviour of the most severely defected core could be a sign that the triangular feather of the semicon screen which had a sharper edge burnt out due to the intense discharge. The intense discharge is caused by the enhanced electric field on the thin feather tip. This could possibly be a self healing process, however it can only be concluded if the most severely defected core fails last.

The continuous decrease in PD magnitudes in the other cores is due to the increase in surface conductivity. The gaseous by-products of the discharge react with the insulation giving off conductive by-products such as oxalic acid [9]. The electric field at the discharge site collapses, reducing the build up of gap over-voltages which in turn decrease PD magnitudes.

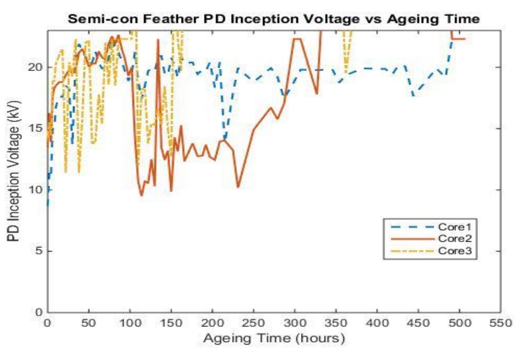

Figure 3: PDIV of three cores of the semicon feather over time

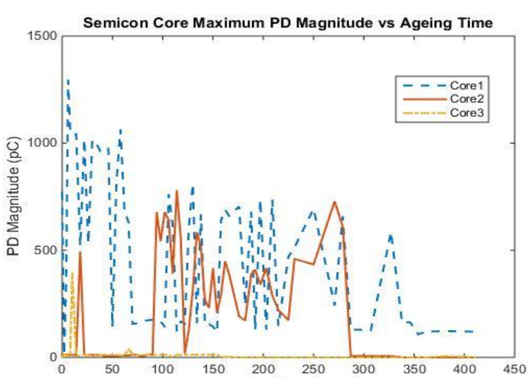

Figure 4: PD magnitude of three cores of the semicon feather over time

4.2. Ring Cut (PDIV and PD magnitude)

Generally, for the ring cut defects as shown in Figure 5, the most severely defected core had the least PDIV throughout the ageing period as expected. There are alternating periods of sustained presence and absence of PD for all the three cores. In the most severely defected core whenever there was PD activity, the magnitudes were generally consistent as shown in Figure 6. The largest maximum apparent PD magnitudes were recorded in the initial period of ageing especially for core 1 and 2. This behaviour is consistent with the effect of ageing on PD magnitudes as explained in section 2.

The fluctuations in PD magnitudes over time can be attributed to the changes in gas content and pressure in the discharge cavity. The ring cut defect is more of a dielectric bounded cavity, and therefore susceptible to gas pressure changes. Oxygen would be exhausted, while other electronegative gasses such as CO and CO_2 are produced. The gas pressure constantly fluctuates depending on the consumption and production of gasses at the discharge site. These findings are consistent with those found by Qureshi et al. [7, 14] who observed a significant increase and later decrement of PD magnitude in aged 15 kV XLPE cables.

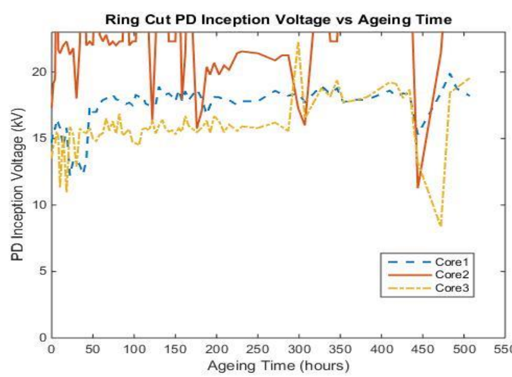

Figure 5: PDIV of three cores of the ring cut over time

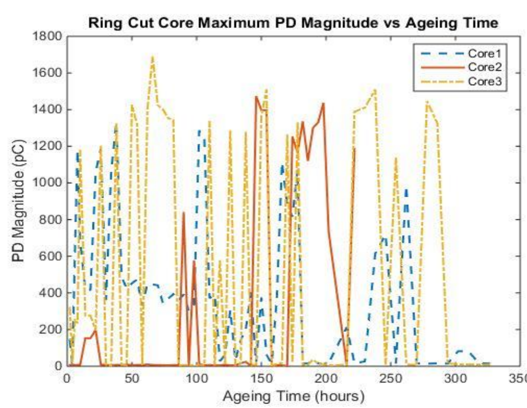

Figure 6: PD magnitude of three cores of the ring cut over time

4.3. Tram Line (PDIV and PD magnitudes)

As with the ring cut, the most severely defected core with a tram line defect had the lowest PDIV compared to the other cores as shown in Figure 7. Similarly the corresponding magnitudes show a similar characteristic trend as in the ring cut. It is however notable that the PD magnitude of the core with the most severe defect as shown in Figure 8 is much bigger than the other cores. The reason for this behaviour is as explained in section 4.2.

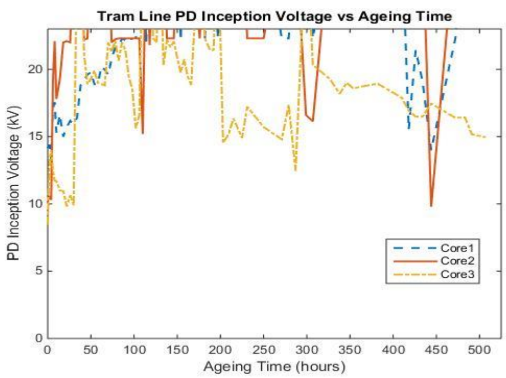

Figure 7: PDIV of three cores of the tram line over time

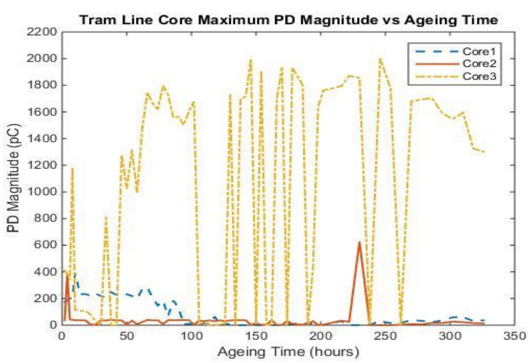

Figure 8: PD magnitude of three cores of the tram line over time

5. CONCLUSION

With regard to ageing time, there is a marked instability in PD in the first 100 hours for all the defect types. In tram line and ring cut, the severity translates to more PD induced ageing while the opposite would be true for the semicon feather. The findings further suggest that a significantly fluctuating PD behaviour with ageing might imply the source to be a cavity type of defect in the insulation.

ACKNOWLEDGEMENTS

The authors would like to thank Eskom for their support of the High Voltage Engineering Research Group through the Tertiary Education Support Programme (TESP). They would also like to thank the Department of Trade and Industry (DTI) for THRIP funding and to thank the National Research Foundation (NRF) for direct funding of the research group. Further gratitude is dedicated to NamPower for their funding through the bursary scheme.

REFERENCES

[1] R. Strobl, W. Haverkamp, G. Malin, and F. Fitzgerald, "Evolution of stress control systems in medium voltage cable accessories," in *IEEE Transmission and Distribution Conference and Exposition, 2001 IEEE/PES*, 2001, vol. 2, pp. 843–848.

[2] W. A. Thue, Ed., *Electrical Power Cable Engineering*, 3rd ed. USA: CRC Press, 2011.

[3] D. Fynes-clinton, "PD Characteristics of Typical MV XLPE Power Cable Termination Defects at VLF and Power Frequency Test Voltages," University of Witwatersrand, 2016.

[4] G. C. Montanari, "Envisaging Links between Fundamental Research in Electrical Insulation and Electrical Asset Management," *IEEE Electrical Insulation Magazine*, vol. 24, no. 6, pp. 7–21, 2008.

[5] C. S. Kim, T. Kondo, and T. Mizutani, "Change in PD Pattern with Aging," *IEEE Trans. Dielectr. Electr. Insul.*, vol. 11, no. 1, pp. 13–18, 2004.

[6] M. Stotzel, M. Zdrallek, and W. H. Wellssow, "Reliability calculation of MV-distribution networks with regard to ageing in XLPE-insulated cables," in *IEE Proceeding-Generation Transmission Distribution*, 2001, no. 6, pp. 597–602.

[7] M. I. Qureshi, A. Al-Arainy, and N. H. Malik, "Effect of accelerated laboratory aging on selected electrical properties of medium-voltage heat shrink cable joints," *Taylor Fr.*, vol. 42, no. 5, pp. 496–506, 2014.

[8] S. M. Shahrtash and T. Shahsavarian, "Modelling of aged cavities for partial discharge in power cable insulation," *IET Sci. Meas. Technol.*, vol. 9, no. 6, pp. 661–670, 2015.

[9] P. F. Morshuis, "Assessment of Dielectric Degradation by Ultrawide-band PD Detection," *IEEE Trans. Dielectr. Electr. Insul.*, vol. 2, no. 5, pp. 744–760, 1995.

[10] C. Nyamupangedengu, "Time-varying partial discharge spectral characteristics in solid polymer insulation," *IET Sci. Meas. Technol.*, vol. 6, no. 2, pp. 85–95, 2012.

[11] E. Gulski and F. . Kreuger, "Computer-aided recognition of Discharge Sources," *IEEE Trans. Electr. Insul.*, vol. 27, no. 1, pp. 82–92, 1992.

[12] R. Bartnikas, R. J. Densley, and R. M. Eichhorn, "Long term accelerated aging tests on distribution cables under wet conditions," *IEEE Trans. Power Deliv.*, vol. 11, no. 4, pp. 1695–1699, 1996.

[13] R. Lyle and J. W. Kirkland, "An Accelerated Life Test For Evaluating Power Cable Insulation," *IEEE Trans. Power Appar. Syst.*, vol. PAS-100, no. 8, pp. 3764–3774, 1981.

[14] A. A. Al-Arainy, N. H. Malik, M. I. Qureshi, and M. N. Al-Saati, “The performance of strippable and bonded screened medium-voltage XLPE-insulated cables under long-term accelerated aging,” *IEEE Trans. Power Deliv.*, vol. 22, no. 2, pp. 744–751, 2007.

Appendix G

Appendix G: The Unique PD 'Signatures' of Artificial Installation Defects Introduced in MV XLPE Power Cable Terminations

This Appendix presents the paper covering unique PD characteristic according to defect that was received and published in the 26th South African Universities Power Engineering Conference (SAUPEC) proceedings. A power point was presented by E. Haikali.

THE UNIQUE PD 'SIGNATURES' OF ARTIFICIAL INSTALLATION DEFECTS INTRODUCED IN MV XLPE POWER CABLE TERMINATIONS

E. Haikali*, C. Nyamupangedengu**

School of Electrical and Information Engineering, University of the Witwatersrand 2050, South Africa
*Email: *Elizabeth.haikali@students.wits.ac.za **Cuthbert.nyamupangedengu@wits.ac.za*

Abstract: Most power cable failures have been traced to originate from cable joints and terminations. This work studies the Partial Discharge (PD) characteristics of three common defects likely to occur during cable installation with the aim of identifying if there is a unique pattern to each defect. The results show that all defects have unique Phase-Resolved-Partial-Discharge-Patterns (PRPDP). The PRPDPs were further analysed using statistical operators. The semicon feather defect had the flattest kurtosis with the most symmetry between the positive PD and the negative PD. The tram line was most skewed, while the ring cut had the sharpest kurtosis. With these distinct observations unique across specific defects, it is postulated that a collection of such data bases can help with identifying unknown defects by cross comparison.

Key words: partial discharge, cable defects, termination defects, MV cable, PD signatures, statistical operators

1. INTRODUCTION

Partial Discharge (PD) is a phenomenon that causes partial bridging of insulation in shielded power cables. PD is brought about by the presence of voids, scissions, contaminants, or protrusions in the insulation [1]. The presence of defects in the insulation causes an enhancement in the electric field in the local region as shown in Figure 1 and Figure 2.

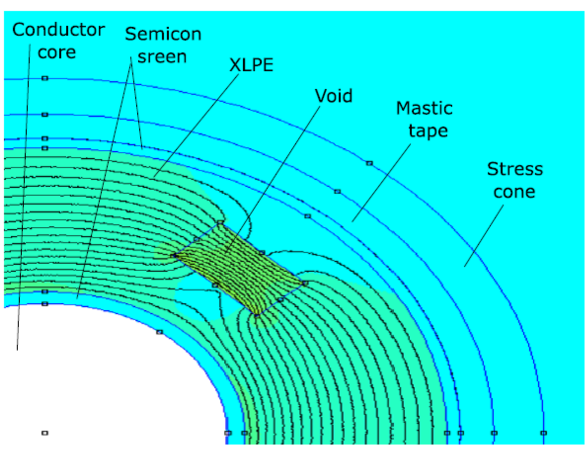

Figure 1: FEM simulation of a void in XLPE

Figure 1 and 2 shows the localised electric field enhancement in the air-filled cavity. After pro-longed re-occurrence of PD, the partial bridging may develop into a permanent bridging and eminent failure. PD measurements is one of the reliable diagnosis methods for electrical equipment [1]. Researchers have also found that certain PD characteristic features are uniquely relatable to classified types of defects [2-4].

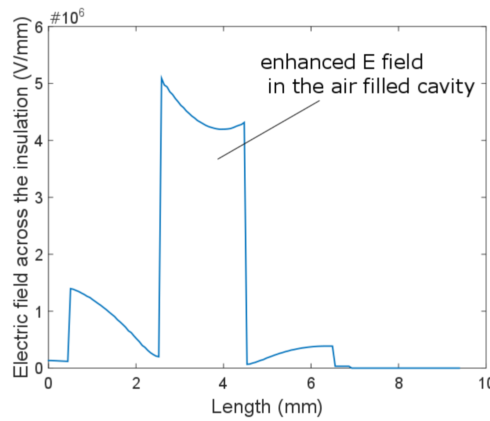

Figure 2: The electric field plot across the XLPE layer in the power cable

The present study seeks to determine the PD features that uniquely relate to each of the three typical defect types. The study deals with three 3 m long, 3 core, 6.6/11 kV XLPE sample cables terminated with heat shrink terminations. The typical cable termination defects under study are those likely to occur due to poor installation workmanship as illustrated in Table 1. The third core of each cable sample was intentionally made more severe to investigate the influence of defect severity to the unique 'signatures'.

2. EXPERIMENTAL SETUP AND PROCEDURE

The cables were tested at 50 Hz, at 22.3 kV AC using the test circuit shown in Figure 3. The voltage was increased in steps of 2 kV per 30 seconds. At 22.3 kV, a waiting

Table 1: Typical termination defects that were introduced on cable samples in the study [5]

Defect Type	Description	Dimensions
Semi-conductor feather	The outer semi-conductor screen was not stripped off the XLPE insulation uniformly. An extending triangular feather was left. with a base (B) and height (H) denoted by B and H respectively. For core 1 and core 2 (B = 10 mm, H = 10 mm). The feather for core 3 was made sharper (B = 5 mm, H = 25 mm).	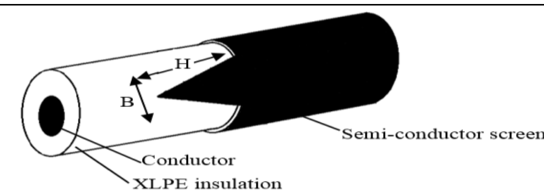
Tram Line	The tram line represents a cut prone to occur when a sharp object is used to strip off the semicon screen. The cavity runs along the XLPE with a depth (D), and a thickness (T). For core 1 and core 2 (D = 1 mm, T = 0.4 mm). Core 3 was made deeper (D = 2 mm and T = 0.8 mm).	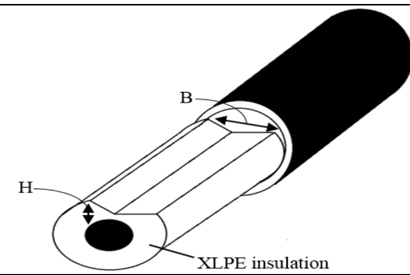
Ring Cut	The ring cut similarly to the tram line represents a cavity in the XLPE likely to occur when establishing the semicon screen end. The cut forms a complete ring in the XLPE with a width (W) and a depth (D). For core 1 and core 2 (W = 0.6 mm, D = 1 mm). The cut for core 3 was (W = 0.8 mm, D = 2 mm).	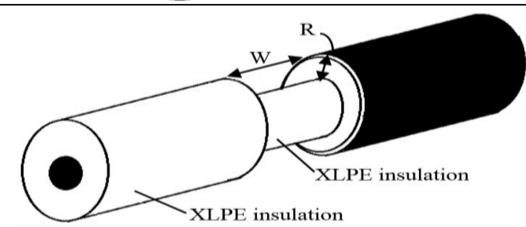

time of 1 minute was allowed to let PD to ignite, thereafter, the PRPDP was recorded for 1 minute.

3. PHASE-RESOLVED-PARTIAL-DISCHARGE-PATTERN-ANALYSIS

A Phase-Resolved-Partial-Discharge-Pattern (PRPDP) is a three dimensional representation of the PD parameters namely PD magnitude and Pulse Repetition Rate with respect to the phase angle of the applied voltage. The statistical operators of the PRPDP distributions were computed per half cycle. Attention was mainly focused on Height Phase Distribution Hqn (ϕ) and the Pulse Count Phase Distribution Hn (ϕ). These were analysed u sing the statistical operators namely Skewness (Sk), Kurtosis (Ku) and Cross-correlational factor (cc) shown in Table 2.

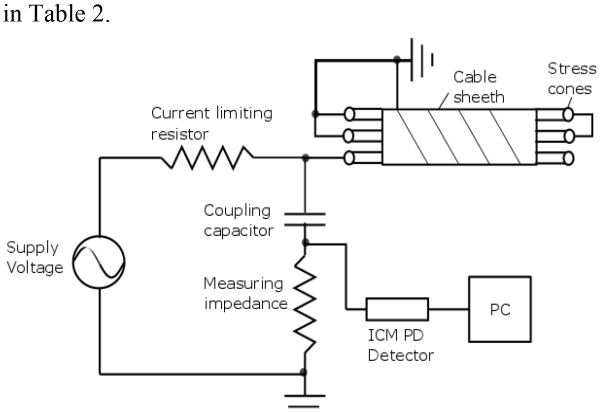

Figure 3: PD testing circuit [5]

3.1. Semicon Feather Defect

Figure 5 shows the PRPDP defect signature of the semicon feather that was obtained in the study. The pattern resembled the 'rabbit ears' widely reported in the literature [6-8]. The right ear was more pronounced than the left ear. During the negative half cycle, the insulation acts as the source of electrons causing larger avalanches build up hence larger PDs in the negative half cycle [9]. Positive PD occurred between 0 degree and shortly after 120 degree phase angle. Meanwhile, the negative PD occurred between 180 degrees and 300 degrees. The semicon feather resembled corona to some extent with PD spanning at the voltage peak (manifesting an absence of counteracting space charge). The nature of a semicon feather PD has similarities with corona in terms of unrestricted/unconfined area for PD activity and a presence of a projecting sharp tip which could bring the corona effect. The Kurtosis for both Hqn (ϕ) and Hn (ϕ) are negative as shown in Table 1, meaning the distribution historian is flatter than the normal distribution. The Semicon feather is the flattest of all the defects and also is skewed towards the left of the normal distribution. The semicon feather defect however showed the most symmetrical amongst all the defects.

3.2. Tram Line Defect

The unique PRPDP of the tram line is shown in Figure 6 with a skewness visibly towards the right for all the cores. PD span between 0 degrees and 100 degrees, while the

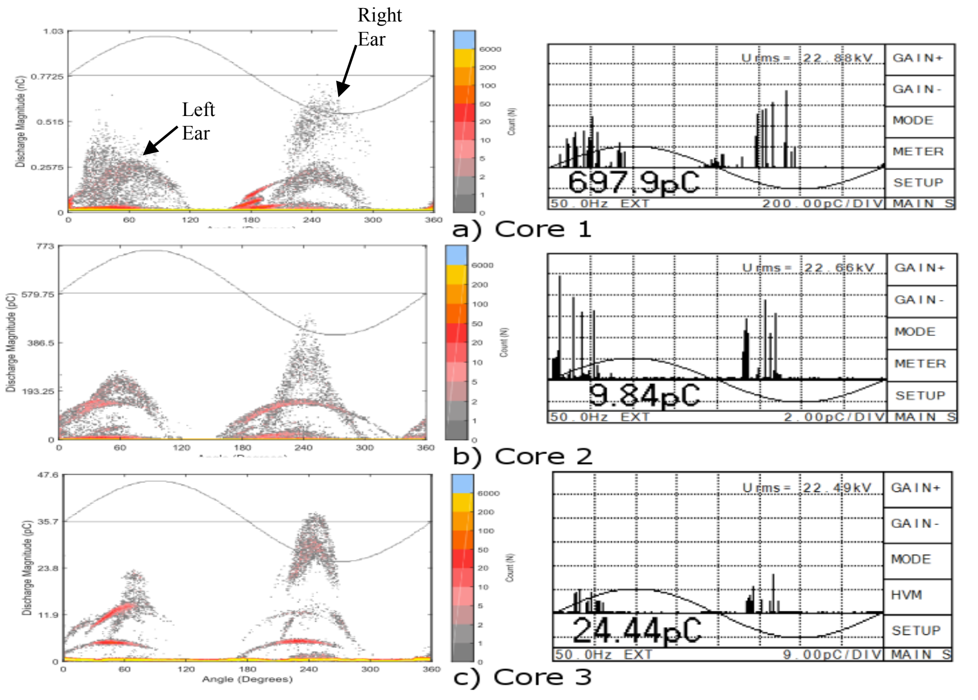

Figure 5: PRPDP for the semicon feather defect

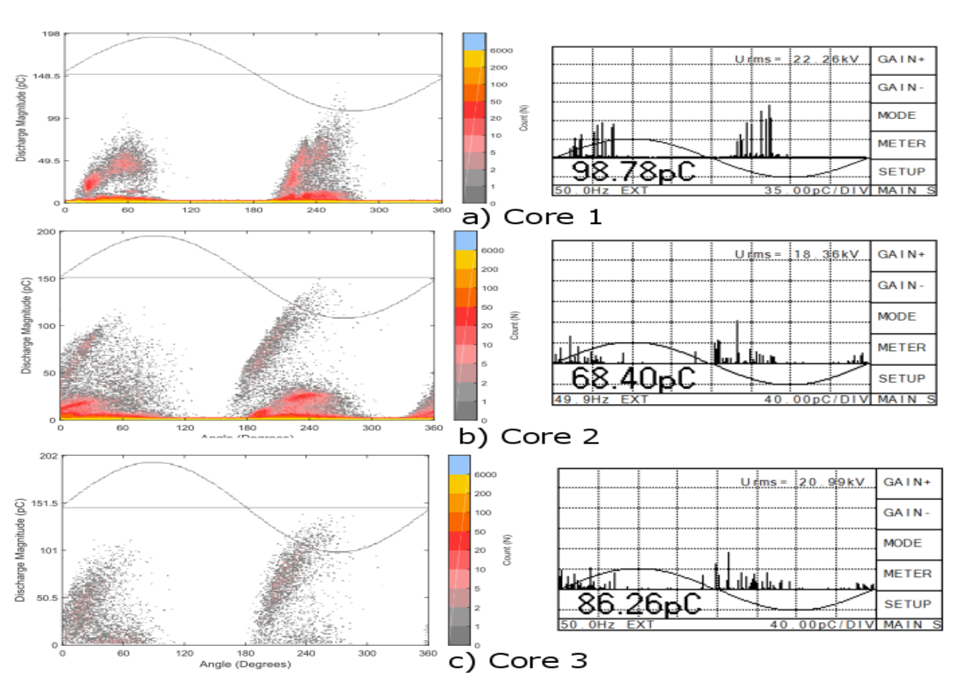

Figure 6: PRPDP for the tram line defect

negative phase PD occurred between 180 degrees and 280 degrees. The PRPDP peak occurred at the rising edge of the applied voltage and extends to just before the peak or trough. The distinct PD features that stood out was that the tram line was most skewed leaning towards the left of the normal distribution as shown in Table 2.

3.3. Ring Cut

PD of the ring cut defects resembled the “rabbit ears” commonly reported in the literature as shown in Figure 7 [6-8]. The rabbit ears are known as the result of residual space charge effect which seemed to be most pronounced in the ring cut defect.

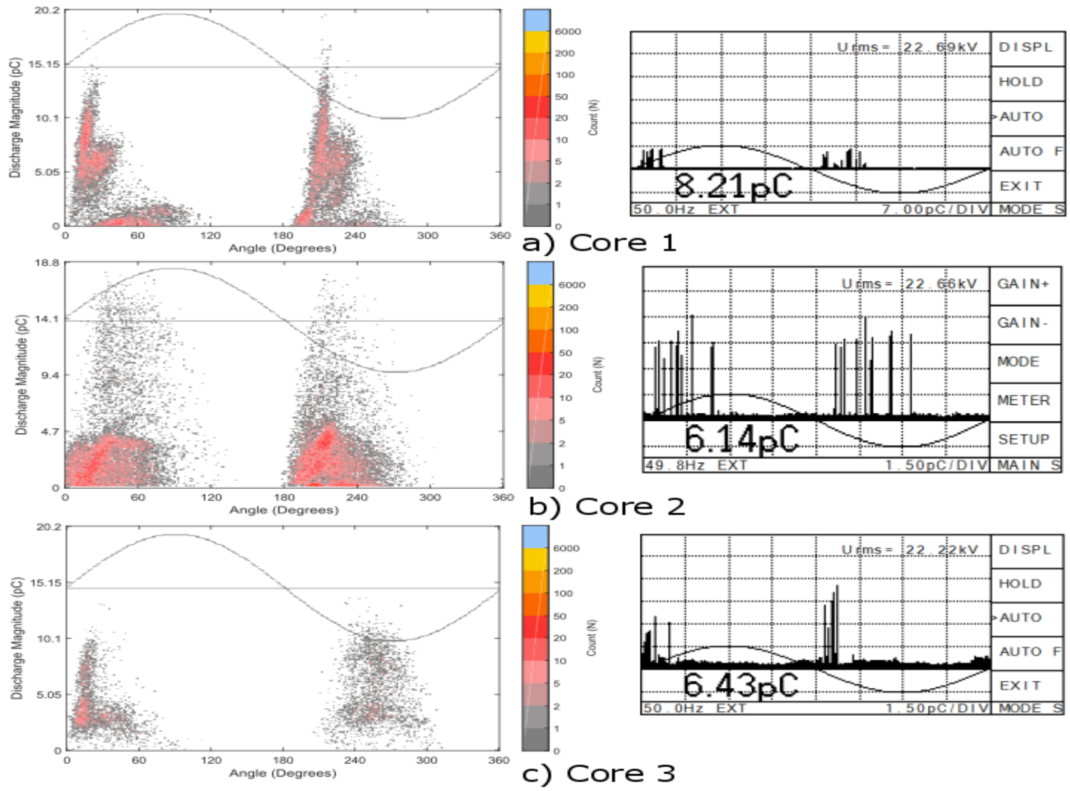

Figure 7: PRPDP for the ring cut defect

Table 2: Statistical operators of PD phase distribution functions of the PRPDP under discussion

Defects		Statistical operators								
		Hqn +ve half cycle Ku	Hqn -ve half cycle Ku	Hqn +ve half cycle Sk	Hqn -ve half cycle Sk	Hn +ve half cycle Ku	Hn -ve half cycle Ku	Hn +ve half cycle Sk	Hn -ve half cycle Sk	Hqn cc
Semicon feather	Core1	-1.79	-1.46	0.04	0.52	-1.25	-1.27	0.05	0.02	0.90
	Core 2	-0.98	-1.16	0.28	0.34	-1.19	-1.21	0.00	0.01	0.88
	Core3	-1.16	-1.19	0.04	0.12	-1.20	-1.21	0.00	0.01	0.93
Tram Line	Core1	0.80	0.78	1.18	1.22	-1.20	-1.21	0.04	0.04	0.95
	Core 2	-0.69	-0.90	0.66	0.51	-1.21	-1.22	0.01	0.02	0.86
	Core3	1.95	0.84	1.61	1.39	-1.21	-1.21	0.03	0.03	0.77
Ring Cut	Core1	1.12	1.25	1.32	1.38	-1.04	-1.12	0.45	0.39	0.86
	Core 2	-1.10	-1.20	0.09	0.19	-1.20	-1.20	0.00	0.01	0.92
	Core3	0.89	2.75	0.80	1.50	-1.02	-1.11	0.26	0.33	0.46

The nature of the ring cut provides a curved discharge surface area convenient for retaining space charge after a PD event. The phase degree of occurrence was between 0 degrees and 90 degrees and from 180 degrees to 270 degrees. The Peaks of the PRPDP occur at the rising edge of the applied voltage. This pattern is similar in shape to that observed in [4] who studied the PRPDP of a XLPE incision defect. The ring cut was the sharpest, its kurtosis was greater than that of the normal distribution and that of all two other defects as indicated in Table 2.

4. DISCUSSION

Figure 8 shows the electric fields interplay in a cavity at different points of the applied voltage cycles according to Neimeyer's model [10]. The shape of the PRPDP is a complex function of several factors, of which some are unique based on the nature of the defect and geometry of discharge area. The factors affecting the PRPDP are namely space charge, space charge relaxation time constant, surface conductivity and seed electron availability [10-11].

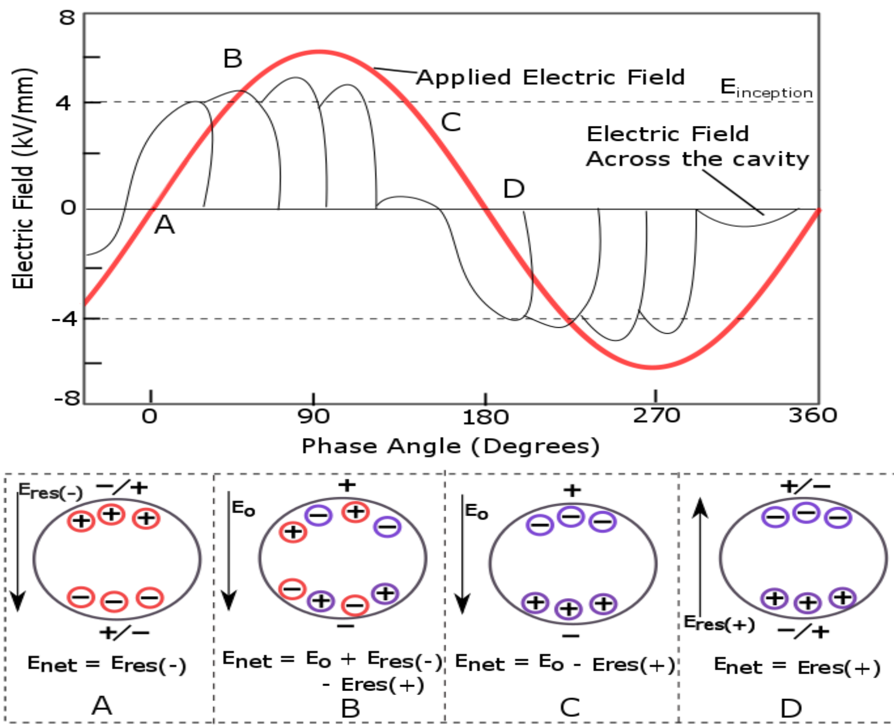

Figure 8: The influence of space charge on Electric field in a cavity [9-10]

As illustrated in Figure 8, the presence of space charge changes the electric field in the cavity and inevitably affects the shape of the PRPDP, which is more significant when dealing with PD under AC [12]. Space charge under AC conditions is more likely to have an influence due to the likelihood of the applied voltage period (depending on the frequency) being competitive with the residual decay time. Preceding discharges will therefore have an effect on the succeeding discharges [12].

A discharge occurs when the overall electric field across the cavity exceeds the PD inception electric field when a seed electron is available to begin an avalanche. The generation of a seed electron is a random process, however can be through volume production (radiative ionization of medium gas) or surface production [10]. Electron generation by volume production refers to radiative ionization of medium gas at insulation-gas interface. Meanwhile, surface production is achieved by means of cathodic emissions of electrons, de-trapping of electrons from insulation surface traps, ion impact and photo effect on electrodes or insulation surface [10]. The phenomenon that supports electron generation amongst other factors is a function of the nature of the defect, surface polarity and micro-roughness.

In Figure 8, the region labelled (A) denotes the zero crossing point of the applied voltage transitioning from the negative half cycle to the positive half cycle. The applied background field is therefore zero, and hence the net electric field across the defect is solely from the residual charge of previous discharges. PRPDP that show PD at the zero crossing therefore gives an indication of the presence of residual charge. The tram line and the ring cut defects gave the most significant PD magnitudes over the zero crossing.

The region marked (B) in Figure 8 shows the rising edge of the positive half cycle. In this region, the net electric field is a sum of the background field, the in-phase electric field of the residual charge from negative PD and the out-of-phase electric field of the residual charge from positive PD occurring at the rising edge. The ring cut shows a peak in the PRPDP at this point. The presence of the peak at this point could be an indication of a significant residual charge retained from the negative half cycle. The PRPDP peak of the tram line appear later shortly after the rising edge.

Region C denotes the falling edge of the positive half cycle. The net electric field in this region is a sum of the background field and the out-of-phase electric field from the positive PD residual charge. Depending on the charge decay constant, the residual charge from the negative half cycle often has decayed to zero at point C. The net electric field is therefore likely to be minimal and hence a reduced likelihood for the inception electric field to be exceeded. The semicon feather has a PRPDP peak at this point, an indication of the absence of opposing residual charge from the positive half cycle and merely a response to the high electric field at the applied voltage peak.

Region (D) indicates the zero crossing transitioning from the positive half cycle to the negative half cycle. The background electric field is zero at this point hence the net electric field is again solely dependent on the residual charge of proceeding discharge events that occurred in the positive half cycle. Region (D) is similar to region (A).

Overall at all points, when the net electric field exceeded the inception electric field in the presence of a seed electron, a discharge event is guaranteed to occur. The smaller the net electric field, the less the likelihood of this condition to be met. The semicon feather showed PRPDP peaks around the peak and trough of the applied voltage, a sign of absent residual charge. Both the tram line and the ring cut showed peaks of the PRPDP on the rising edges, a sign of a constructive effect of residual charge from the previous half cycle.

According to [9], since the tram line and the ring cut are located within the insulation, the electric field is expected to be symmetrical. The symmetrical electric field will be visible if both the tram line and the ring cut were more symmetrical Hqn (ϕ) (than the semicon feather). However, that is not the case, in fact, the semicon was most symmetrical, followed by the tram line, and lastly the ring cut. The tram line and the ring cut were rather most symmetrical in terms of magnitude which can be an indication of a similar defect interface at either anode or cathode which then also gives an indication of defect location.

The only observed pattern that could be associated with the severity of the defect was that the most severely defected core had the least PD intensity, common across all defects. Illias [6] also reported a reduction in pulse repetition rates in larger defects. A reduced repetition rate in larger defects is suspected to be due to a shorter charge decay time and therefore a reduced chance to harvest a seed electron from the defect surface. Additionally, the residual charge has lesser time to superimpose on background field for the inception field to be exceeded.

5. CONCLUSION

Unique PRPDP signatures of three defects in 6.6/11 kV XLPE cable terminations have been presented and discussed. The distinction in PRPDP depends on the influence of the nature of the defect to the retaining of space charge. The distinct features observed can aid with a more accurate diagnosis of unknown defects. This would contribute towards automated diagnosis with reference to a pool of known defect signatures.

ACKNOWLEDGEMENTS

The authors would like to thank Eskom for their support of the High Voltage Engineering Research Group through the Tertiary Education Support Programme (TESP). They would also like to thank the Department of Trade and Industry (DTI) for THRIP funding and to thank the National Research Foundation (NRF) for direct funding of the research group. Further gratitude is dedicated to NamPower for their funding through the bursary scheme.

6. REFERENCES

[1] J. Densley, “Ageing Mechanisms and Diagnostics for Power Cables - An Overview,” *IEEE Electrical Insulation Magazine*, vol. 17, no. 1, pp. 14–22, 2001.

[2] E. Gulski and F. . Kreuger, “Computer-aided Recognition of Discharge Sources,” *IEEE Trans. Electr. Insul.*, vol. 27, no. 1, pp. 82–92, 1992.

[3] (CigreWorkingGroup21.03), “Recognition of Discharges,” Paris, 1969.

[4] Y. Jiang, H. Min, J. Luo, Y. Li, X. Jiang, R. Xia, and W. Li, “Partial Discharge Pattern Characteristic of HV Cable Joints with Typical Artificial Defect,” in *Asia-Pacific Power and Energy Engineering Conference (APPEEC)*, 2010, pp. 1–4.

[5] H. Elizabeth NN and N. Cuthbert, “PD Evolution of Artificial Defects Introduced in MV XLPE Power Cable Terminations - Preliminary Results,” in *Proceedings of the 25th South African Universities Power Engineering Conference (SAUPEC)*, 2017.

[6] H. A. Illias, “Measurement and Simulation of Partial Discharges within a Spherical Cavity in a Solid Dielectric Material,” PhD thesis, University of SouthAmpton, 2011.

[7] C. S. Kim, T. Kondo, and T. Mizutani, “Change in PD Pattern with Aging,” *IEEE Trans. Dielectr. Electr. Insul.*, vol. 11, no. 1, pp. 13–18, 2004.

[8] J. Li, W. Si, X. Yao, and Y. Li, “Measurement and simulation of partial discharge in oil impregnated pressboard with an electrical aging process,” *Meas. Sci. Technol.*, vol. 20, no. 10, p. 105701, 2009.

[9] H. Illias, Y. Teo Soon, A. A. Bakar, H. Mokhlis, G. Chen, and P. L. Lewin, “Partial Discharge Patterns in High Voltage Insulation,” *Power Energy (PECon), 2012 IEEE Int. Conf.*, no. December, pp. 750–755, 2012.

[10] L. Niemeyer, “A Generalized Approach to Partial Discharge Modeling,” *IEEE Trans. Dielectr. Electr. Insul.*, vol. 2, no. 4, pp. 510–528, 1995.

[11] F. Gutfleisch, “Measurement and Simulation of PD in Epoxy Voids,” *IEEE Trans. Dielectr. Electr. Insul.*, vol. 2, no. 5, pp. 729–743, 1995.

[12] G. C. Montanari, “Bringing an insulation to failure: The role of space charge,” *IEEE Trans. Dielectr. Electr. Insul.*, vol. 18, no. 2, pp. 339–364, 2011.